Master's thesis

NTNU
Norwegian University of Science and Technology
Faculty of Engineering
Department of Energy and Process Engineering

Vilde Jakobsen Svortevik

Modelling and Simulation of Combined Cooling, Heating, and Power System for a Multi-Renewable Energy Supply in Low-Carbon Buildings

Master's thesis in Energy and Environment
Supervisor: Vojislav Novakovic
June 2021

NTNU
Kunnskap for en bedre verden

Vilde Jakobsen Svortevik

Modelling and Simulation of Combined Cooling, Heating, and Power System for a Multi-Renewable Energy Supply in Low-Carbon Buildings

Master's thesis in Energy and Environment
Supervisor: Vojislav Novakovic
June 2021

Norwegian University of Science and Technology
Faculty of Engineering
Department of Energy and Process Engineering

NTNU
Norwegian University of
Science and Technology

Preface

This master thesis has been completed within the field of Energy and Process Engineering at the Norwegian University of Science and Technology (NTNU). Specifically, the thesis makes out 30 study points and is completed during the spring of 2021. The thesis is a part of the ongoing research project «*Key technologies and demonstration of combined cooling, heating, and power generation for low-carbon neighbourhoods/buildings with clean energy (ChiNoZEN)*» a collaboration between Chinese and Norwegian scientists. In addition, it is a continuation of the project report, prepared as a preliminary project for this master thesis.

I would like to thank postdoctoral researcher Dejene Assefa Hagos for all the academic guidance and follow-up throughout the process. I would also like to thank my internal supervisor Vojislav Novakovic for great counselling and assistance. In addition, I would like to thank the Chinese project partners in the ChiNoZEN project for providing relevant information and follow-up. It has been educational and exciting to be a part of the project. At least, I would like to thank all my friends at NTNU for their support during the process.

In general, it has been exciting to work with the investigation of a CCHP system based on a multi-renewable energy supply. It has also given me insight and knowledge that I am sure will sustain my future career.

Abstract

There is a significant and growing concern associated with anthropogenic emission of greenhouse gasses (GHG), including CO_2 emissions from fossil fuel-fired power plants and conventional heating plants. Sustainable energy production and utilization are essential for achieving energy and climate goals at all levels and for global sustainable development. One of the cutting-edge environmentally friendly energy solutions that could reduce the emission of GHG and mitigate climate challenges is the combined cooling, heating, and power (CCHP) systems.

This thesis aimed at investigating some of the research objectives in the ongoing ChiNoZEN project on low-carbon neighbourhoods and buildings, a collaboration between Chinese and Norwegian scientists. The assumed specific CCHP system configuration and case building are based on the Chinese project partners' idea.

In this thesis, the energy and environmental performance of a specific CCHP system developed under the framework of the ChiNoZEN project have been evaluated. The CCHP system is designed to provide energy for a low-carbon neighbourhood based on a multi-renewable energy supply. The system configuration is mainly consisting of a heat pump (air-to-water), a biogas internal combustion engine (ICE), photovoltaic thermal collectors (PV/T), a biomass fermenter, a heat storage tank, and two wind turbines. To ensure that the energy production and supply are matched with the specific demands, potential control strategies and operation strategies are implemented and validated. The state-of-the-art of key CCHP technologies, CCHP applications, and existing CCHP simulation tools have been reviewed. Using TRNSYS as the selected simulation tool, the dynamic performance of the CCHP system and implemented control strategies and operation strategies have been investigated. Due to the lack of suitable experimental data for the implemented specific component models, the simulation model is verified based on existing mathematical references.

The results showed that annual electricity production from wind energy and solar energy is 18.7% higher than the annual electricity demand. As a result of daily fluctuations in both energy demand and energy production, wind energy and solar energy are still only able to cover 37.5% of the annual electricity demand. Consequently, an operation strategy where biomass energy is combined with wind energy and solar energy is implemented. The biogas internal combustion engine (ICE) is assumed to cover the total hourly electricity demand when electricity production from wind energy and solar energy is insufficient. The renewable energy share in total energy consumption for wind energy, solar energy, and biomass energy is by this reason equal to 30.0%, 7.5%, and 62.5%, respectively. Furthermore, calculations confirmed that the fermenter has the capacity to cover the required annual biogas consumption. The calculations showed that the maximum annual produced biogas in the fermenter is 58.7% higher than the annual biogas consumption by the biogas internal combustion engine (ICE).

The seasonal heating mix distribution by technology showed that the heat production is in balance with the corresponding monthly demand/consumption. The results further showed that the seasonal heat production of the main heating components is lower than the assumed auxiliary heater. Measures such as increasing the assumed maximum capacity of the main heating components should be considered.

From the performed analysis, it is concluded that the CCHP system has the basic prerequisites to cover the space heating, space cooling, domestic hot water (DHW), and electricity-specific appliances demand, based on a multi-renewable energy supply. Nevertheless, for a robust and dynamic system, some of the system component capacities and the proposed operation strategy should be further improved and optimized.

The assumed control strategies regarding building load demands are validated by dynamic simulations. It was confirmed that the annual energy production and supply are in match with the specific demands.

Finally, the environmental benefits or impacts, if any, of the proposed CCHP system were assessed. The results showed that the proposed system could reduce the annual CO_2 emissions by 88.0% compared to a conventional system entirely based on grid electricity.

Sammendrag

Det er en økende bekymring knyttet til menneskeskapte CO_2 utslipp, blant annet fra fossile kraftverk og konvensjonelle varmeanlegg. Økte utslipp bidrar til en global oppvarming. Bærekraftig energiproduksjon, og utvikling av miljøvennlige energiløsninger, regnes som en viktig faktor for å snu den negative utviklingen. En av de nye energiløsningene som kan bidra til å redusere CO_2 utslippene er kombinerte kjøle, varme, og strømforsynings (CCHP) anlegg.

Denne oppgaven vil undersøke forskningsspørsmål tilknyttet det pågående ChiNoZEN forskningsprosjektet, som primært omhandler lavutslippsnabolag og lavutslippsbygg. Prosjektet er ett samarbeid mellom kinesiske og norske forskere. Den antatte systemkonfigurasjonen med tilhørende komponentkapasiteter er anbefalt og utviklet av de kinesiske samarbeidspartnerne i prosjektet.

I oppgaven er det spesifikke CCHP systemet hovedsakelig vurdert på bakgrunn av energiproduksjon og utslipp av CO_2. Systemet er utviklet for å dekke energibehovet til ett spesifikt lavutslippsnabolag, og er basert på fornybare energikilder. Systemkonfigurasjonen består hovedsakelig av en varmepumpe (luft-til-vann), forbrenningsmotor (biogass som drivstoff), fotovoltaiske termiske solfangere, en biogass-komponent, varmtvannsbereder, og to vindturbiner. For å sikre at energiproduksjon og energiforsyning i systemet korresponderer med nabolagets energiforbruk, er kontrollstrategier implementert og validert. Det er videre gjennomført en litteraturstudie for å avdekke kunnskapsstatus på området, og blant annet er det gjort vurderinger av CCHP teknologier, CCHP applikasjoner og eksiterende dynamiske simuleringsverktøy. Ved å bruke TRNSYS som simuleringsverktøy, har den dynamiske ytelsen til CCHP systemet og implementerte kontrollstrategier og driftsstrategier blitt undersøkt. På grunn av manglende eksperimentelle data, er simuleringsmodellen validert basert på eksisterende matematiske referanser for de implementerte komponentmodellene.

Resultatene fra analysene viste at samlet elektrisitetsproduksjon fra vindenergi og solenergi er 18.7% høyere enn det totale årlige elektrisitetsbehovet for systemet og for el-spesifikt utstyr og belysning. Det er imidlertid betydelige variasjoner i behov og i produksjon av elektrisitet i løpet av døgnets timer. Når man tar høyde for disse svingningene, dekker vindenergi og solenergi 37.5% av det totale behovet. Følgelig må det anvendes en driftsstrategi der vindenergi og solenergi kombineres med bioenergi for å dekke det totale årlige elektrisitetsbehovet. I de timene av døgnet hvor elektrisitetsproduksjonen fra vindenergi og solenergi ikke er tilstrekkelig må altså en forbrenningsmotor, med biogass som drivstoff, anvendes. Andelen fornybar energi i det totale energiforbruket er dermed henholdsvis 30.0%, 7.5% og 62.5% for vindenergi, solenergi og bioenergi. Videre bekrefter beregninger også at den spesifikke biogass-komponenten har kapasitet til å dekke det samlede årlige energibehovet til forbrenningsmotoren. Beregninger viste at maksimal årlig produksjon av biogass fra denne komponenten er 58.7% høyere enn det årlige behovet til forbrenningsmotoren.

Analysen av månedlig varmebehov og varmeproduksjon fra de ulike systemkomponentene viste at produksjonen i systemet korresponderer med behovet knyttet til romoppvarming og varmtvann. Videre viste resultatene at månedlig varmeproduksjon fra hovedkomponentene i systemet er lavere enn produksjonen fra den antatte elektriske tilleggsvarmeren, som ideelt sett bare skal fungere som spisslast og dekke det ekstra oppvarmingsbehovet. Basert på dette funnet bør kapasiteten til hovedkomponentene økes.

På bakgrunn av resultatene konkluderes det med at det foreslåtte CCHP systemet er i stand til å dekke behovet for romoppvarming og romkjøling, varmtvann, og el-spesifikt utstyr og belysning, med fornybare energikilder. For at systemet skal være robust og dynamisk, må imidlertid spesifiserte kapasiteter for aktuelle hovedkomponenter og driftsstrategier forbedres og optimaliseres ytterlige.

Validering av implementerte kontrollstrategier bekrefter at energiproduksjonen i systemet korresponderer med spesifiserte lasteprofiler for henholdsvis romoppvarming og romkjøling, varmtvann, og el-spesifikt utstyr og belysning, for det aktuelle nabolaget.

Til slutt viste miljøanalysen at det foreslåtte CCHP systemet kan redusere årlig utslipp av CO_2 med 88.0%, sammenlignet med ett konvensjonelt system basert på elektrisitet fra strømnettet.

Table of contents

Abbreviations

ATC	Annual total cost
AUX	Auxiliary heater/cooler
CCHP	Combined cooling, heating, and power
CHP	Combined heating, and power
CDE	Carbon dioxide emissions
COP	Coefficient of performance
DHW	Domestic hot water
EES	Engineering equation solver
FEL	Following the electrical load
FTL	Following the thermal load
GHG	Greenhouse gasses
HP	Heat pump
HRSG	Heat recovery steam generator
HRT	Hydraulic retention time
HU	Heating unit
ICE	Internal combustion engine
LHV	Lower heating value
nZEB	Nearly zero-emission building
nZEN	Nearly zero-emission neighbourhood
ORC	Organic Rankine Cycle
PEC	Primary energy consumption
PGU	Power generation unit
PLR	Part load ratio
PV	Photovoltaic
PV/T	Photovoltaic thermal

SP	Separate production
TRNSYS	Transient system simulation program
ZEB	Zero-emission building
ZEN	Zero-emission neighbourhood

Nomenclature

COP_{hp}	Coefficient of performance [-]
ϕ_{hp}	Heating capacity of heat pump [kJ/hr]
$P_{el,hp}$	Effective electrical power input heat pump [kJ/hr]
C_p	Power coefficient [-]
$P_{me,out}$	Actual wind power produced [kW]
P_w	Wind power into turbine [kW]
A_{swept}	Wind turbine blade swept area [m^2]
ρ	Fluid density [kg/m^3]
n_t	Total wind power conversion efficiency [%]
n_{gear}	Wind turbine gearbox efficiency [%]
n_{gen}	Wind turbine generator efficiency [%]
n_{ele}	Wind turbine electrical efficiency [%]
PLR_{des}	Desired part load ratio [kW]
$\dot{P}_{des}$	Ratio of desired electrical load [kW]
$\dot{P}_{rtd}$	Rated power of the device [kW]
n_{mech}	Mechanical efficiency [%]
n_{elec}	Electrical efficiency [%]
$\dot{P}_{shaft}$	The total mechanical shaft power [kW]
$\dot{q}_{required}$	Total energy input required by the engine/generator [kW]
$\dot{q}_{JW}$	Energy transferred to the jacket water steam [kW]
$\dot{q}_{OC}$	Energy transferred to the oil cooler steam [kW]
$\dot{q}_{AC}$	Energy transferred to the aftercooler coolant steam [kW]
$f_{jacketWater}$	Heat fraction rate jacket water [%]
$f_{oilCooler}$	Heat fraction rate oil cooler [%]

$f_{afterCooler}$	Heat fraction rate aftercooler coolant [%]
f_{total}	Total heat fraction rate [%]
$\dot{m}_{jacketWater}$	Mass flow rate jacket water [kg/hr]
$\dot{m}_{oilCooler}$	Mass flow rate oil cooler [kg/hr]
$\dot{m}_{afterCooler}$	Mass flow rate aftercooler coolant [kg/hr]
$Cp_{jacketWater}$	Specific heat jacket water [kJ/kg·K]
$Cp_{oilCooler}$	Specific heat oil cooler [kJ/kg·K]
$Cp_{afterCooler}$	Specific heat aftercooler coolant [kJ/kg·K]
$T_{jacketWater,out}$	Jacket water outlet temperature [°C]
$T_{jacketWater,in}$	Jacket water inlet temperature [°C]
$T_{oilCooler,out}$	Oil cooler outlet temperature [°C]
$T_{oilCooler,in}$	Oil cooler inlet temperature [°C]
$T_{afterCooler,out}$	Aftercooler outlet temperature [°C]
$T_{afterCooler,in}$	Aftercooler outlet temperature [°C]
Q_{el}	Electrical power output PV/T [kW]
IAM	Incident angle modifier PV/T [-]
G_T	Total horizontal radiation upon the collector surface PV/T [kW]
$Area$	Area collector surface PV/T [m^2]
η_{PV}	Efficiency of the PV/T cells [%]
$(\tau\alpha)_n$	Transmittance-absorptance product [%]
Q_{th}	Thermal power output PV/T [kW]
$\dot{m}$	Mass flow rate through the solar collector [kg/hr]
T_{fo}	Outlet fluid temperature PV/T [°C]
T_{fi}	Inlet fluid temperature PV/T [°C]
ε	Emissivity of the top surface of the collector [%]
Θ	Angle of incidence [°]

N_{tubes}	Number of tubes in PV/T collector [-]
L	Length of collector along flow direction [m]
$T_{f,o}$	Initial temperature of fermentation liquid [°C]
$T_{w,in}$	Inlet water temperature from heat storage tank [°C]
$T_{w,out}$	Outlet water temperature from fermenter [°C]
T_a	Outdoor average air temperature [°C]
$T_{f,d}$	Temperature of fermentation liquid [°C]
$\dot{m}_{m,w}$	Mass flow rate of hot water [kg/s]
$\dot{m}_{m,in}$	Mass flow rate of fresh biomass feeding [kg/s]
$\dot{m}_{m,g}$	Mass flow rate of biogas [kg/s]
$C_{p,w}$	Specific heat capacity of fresh water [kJ/kg·K]
-	Plant availability factor [%]
$C_{p,d}$	Specific heat capacity of biomass feeding [kJ/kg·K]
$C_{p,g}$	Specific heat capacity of biogas [kJ/kg·K]
A_{top}	Area of the top of the fermenter [m^2]
A_{bottom}	Area of the bottom of the fermenter [m^2]
K_{top}	Average heat transfer coefficient top of fermenter [$W/m^2 \cdot K$]
K_{bottom}	Average heat transfer coefficient bottom of fermenter [$W/m^2 \cdot K$]
r	Inner radius of fermenter [m]
h_1	Heat transfer coefficient of the gas at the top of the fermenter to the fermenter wall [$W/m^2 \cdot K$]
h_2	Heat transfer coefficient between the outer top surface of the insulation layer, and the environment [$W/m^2 \cdot K$]
$h_{1'}$	Heat transfer coefficient of the gas at the bottom of the fermenter to the fermenter wall [$W/m^2 \cdot K$]
$h_{2'}$	Heat transfer coefficient between the outer bottom surface of the insulation layer, and the ground [$W/m^2 \cdot K$]
δ_1	Thickness of the polyurethane insulation layer [m]

δ_2	Thickness of stainless steel on the fermenter top [m]
λ_1	Thermal conductivity of stainless steel [W/m·K]
λ_2	Thermal conductivity of rigid polyurethane insulation layer [W/m·K]
H_s	Height of the inside fermenter liquid [m]
H_b	Heigh of inside fermenter biogas [m]
V_{Liquid}	Liquid fermenter volume [m^3]
V_{Total}	Total fermenter volume [m^3]
δ_1‘	Thickness of 304 stainless steel [m]
h_2”	Heat transfer coefficient between the outside of the fermenter wall, and the environment [$W/m^2 \cdot K$]
A_{wb}	Area of the biogas, in contact with tank wall [m^2]
A_{ws}	Area of the side wall of the fermenter tank. Contact with tank wall [m^2]
K_{ws}	Heat transfer coefficients between the inner liquid of fermenter with the sidewalls of fermenter [$W/m^2 \cdot K$]
K_{wb}	Heat transfer coefficients between the biogas layer in fermenter with the sidewalls of fermenter [$W/m^2 \cdot K$]
h_s	Convective heat transfer coefficients between the inner liquid of fermenter with the sidewalls of fermenter [$W/m^2 \cdot K$]
h_b	Convective heat transfer coefficients between the biogas layer in fermenter with the sidewalls of fermenter [$W/m^2 \cdot K$]
ρ_{CH_4}	Density of methane [kg/m^3]
x_{CH_4}	Mass fraction of methane in biogas [%]
LHV	Lower heating value, biogas [MJ/kg]
HRT	Hydraulic retention time [/day]
S_0	Concentration of influent volatile solids (VS) [kg/m^3]
B	Methane production rate of the organic waste [m^3/kgVS]
B_0	Limiting methane production rate of the organic waste [m^3/kgVS]
K	Dimensionless dynamic parameter

u_m	Maximum growth rate of microorganisms [/day]
Y_v	Biogas production rate [m^3/kgVS]

List of figures

List of tables

1 Introduction

In this chapter, the research background and research objectives will be presented. In addition, the specific research method and plan, limitations, and report structure will be reviewed.

Some parts of this chapter are based on the author's project report, prepared as a preliminary project for this master thesis.

1.1 Background

The level of CO_2 emissions in the atmosphere has increased by approximately 40% since 1750. This in turn contributes to the global warming of the earth, and measurements indicate that the temperature in the atmosphere has increased by approximately 0.85 ℃ from 1880 until 2012 [1]. This development leads to an increased concern related to the emission of GHG, energy dependency, climate changes, and the depletion of fossil fuels [2]. Energy and environmental issues are key challenges for future global sustainable development, and there is a strong need for new environmentally-friendly energy solutions [3].

The building sector energy management plays a significant role towards a clean energy transition. In 2017, the building sector alone accounted for approximately 36% of the global final energy use [4]. Furthermore, the *International Energy Agency* (IEA) reported that global CO_2 emissions reached a preliminary peak in 2019. Considering indirect emissions related to the upstream power generation, the building sector accounted for 28% of the worldwide energy-related CO_2 emissions. Electricity is the primary energy commodity in the building sector and covered about 33% of the global energy use in buildings in 2019. It is further reported that the continued utilization of fossil fuels-based electricity would hamper the transition to a low carbon building sector and energy system at large [5].

In [6], the authors have studied the depletion of fossil fuels and anthropogenic climate changes and concluded that energy production is the primary source of CO_2 emissions and other GHG. It is also stated that approximately 70% of the anthropogenic emission of GHG originates from the energy sector such as the combustion of fossil fuels. *Figure 1* illustrates the emission of CO_2 by sector specifically for Europe between 1990 to 2018 [7]. The power and heating sector are the highest CO_2 emitting sectors. The need for increased integration of more renewable energy sources into the traditional energy system and the power grid is crucial for the decarbonization of these sectors.

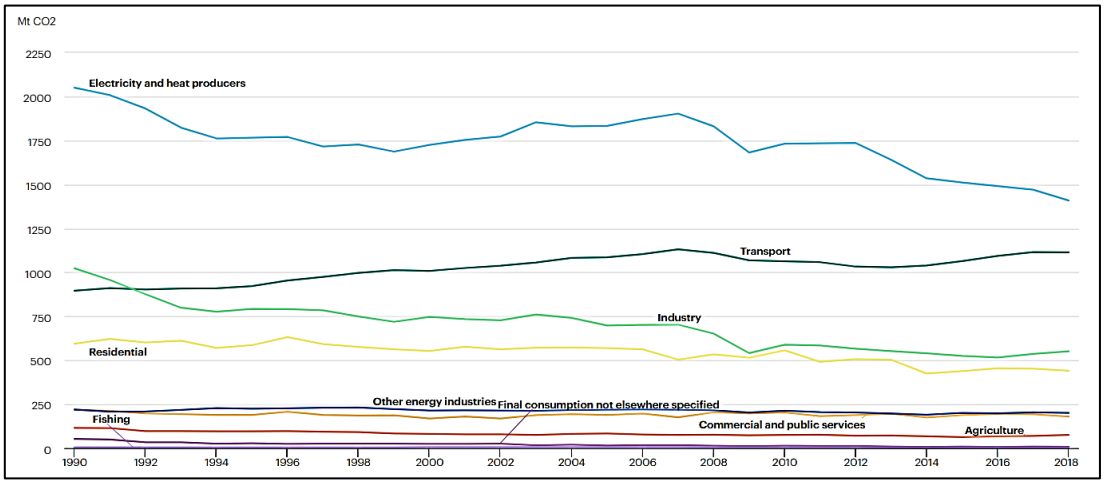

Figure 1: CO_2 emission by sector, Europe 1990-2018 [7].

To overcome and mitigate the aforementioned energy and CO_2 emissions challenges, other energy conversion technologies and the utilization of green renewable fuels are vital. Towards this, the development and application of combined cooling, heating, and power (CCHP) systems in building complex/neighbourhood/district level energy systems is a well-proven solution. This is based on the technology being able to reduce global primary consumption concerning the emission of GHG [4]. A report published by the IEA states that a typical CCHP system has a 75-80% overall energy efficiency. In comparison to this, the overall energy efficiency of a stand-alone conventional system is about 60% [8]. Furthermore, it should be possible to achieve an even higher advantage by feeding the system with renewable energy sources, such as biomass, solar radiation, and wind [9].

Biomass is CO_2-neutral but limited in availability and needs to be used in an optimized CCHP system. In addition to this, it could be used in solid, liquid, and gaseous forms [2]. During its life cycle, biomass is considered to produce no net emissions of CO_2, assuming that it is made sustainable. This has led to biomass being considered one of the most attractive and relevant replacements for fossil fuels in general power generation systems [10]. The development has also led to an increased amount of CCHP systems based on multi-renewable energy supply. Specifically, this involves systems primarily based on biogas but further supported by a photovoltaic thermal (PV/T)- and wind turbine system to transform solar- and wind energy into electrical power [11]. Relevant research is indicating that the utilization of solar energy in a biomass-based CCHP system could contribute to a further reduction in dependency on fossil fuels, and a decreased emission of GHG [12].

1.2 Research objectives and research questions

The objective of this thesis is to evaluate the energy and environmental performance of a specific CCHP system developed under the framework of the ChiNoZEN project. The CCHP system is designed to provide energy for a low-carbon neighbourhood based on a multi-renewable energy supply. The assumed specific CCHP system configuration and case building are based on the Chinese ChiNoZEN project partners' idea. For ensuring that the annual energy production and supply are equivalent to existing load demands, potential control strategies and operation strategies are implemented and validated. In addition, an environmental assessment analysis will be performed for the CCHP system.

The following main research questions will be elaborated:

RQ1. *How can the CCHP system provide the space heating, space cooling, domestic hot water (DHW), and electricity-specific appliances demands, based on a multi-renewable energy supply, for the low-carbon neighbourhood?*

RQ2. *How are the implemented control strategies and operation strategies for the CCHP system able to meet the annual energy consumption load profiles of space heating, space cooling, domestic hot water (DHW), and electricity-specific appliances demands, for the low-carbon neighbourhood?*

RQ3. *How is the environmental performance of the CCHP system?*

1.3 Research method

The state-of-the-art of key CCHP technologies, CCHP applications, and existing CCHP simulation tools have been reviewed. Based on this, a critical analysis of existing simulation tools for investigating the dynamic performance of a proposed CCHP system has been executed. Minor changes have been performed regarding the system configuration of the proposed CCHP system. After choosing TRNSYS as the most suitable simulation tool regarding the overall objective of the analysis, the dynamic performance analysis of the CCHP system has been conducted.

Next, an analysis has been carried out to evaluate if the CCHP system can provide the required energy for a low-carbon neighbourhood, based on a multi-renewable supply. Relevant results are discussed and compared with similar studies for an overall evaluation of how the CCHP system can cover existing case building demands. Potential control strategies and operation strategies have been evaluated theoretically in TRNSYS and validated based on results from the dynamic performance analysis.

For further optimization of the CCHP system, an environmental assessment has been conducted based on considerations from the ZEB research center.

Based on the results and analyses carried out in the report, suggestion for further work on the topic under investigation has been prepared.

1.4 Limitations

The following limited factors and thereby delimitations are existing for this master thesis:

- It has been difficult to obtain crucial and relevant information from the Chinese ChiNoZEN project partners during the work process. This especially applies to data associated with system configuration and case building, with the associated system capacities and equipment capacities. The building case is hypothetical, and there are no measurements for comparison. The dynamic performance analysis is therefore based on theoretical evaluations alone and is not supported by experimental measurements. The Chinese ChiNoZEN project partners have not been able to provide any current data for this purpose. Load profiles for the case building are developed based on simulations carried out for a similar building. Unfortunately, the project partners were not able to provide relevant data in due time.

- Necessary availabilities in TRNSYS were delayed from the supplier, and the simulation process was started later than desired. Due to limited time, it has not been possible to test findings from the basic simulation model. This applies, for example, to the biogas internal combustion engine (ICE) with rated capacity and the proposed operation strategy. In addition, the biogas fermenter is only evaluated by performing static evaluations.

- The system boundary is set to assess the inlet energy flow and outlet energy flow of the CCHP system. No assessment has been made of the energy transmission and delivery in the specific buildings. Simplifications have been made for adapting the system configuration to the TRNSYS environment and for the system configuration provided by the Chinese ChiNoZEN project partners. Implemented control strategies and operation strategies are only evaluated theoretically in TRNSYS.

1.5 Report Structure

The thesis is organized into nine chapters. Chapter one will introduce the background, objectives and research questions, and project limitations of the thesis. In addition, the research method will be presented.

Chapter two will include relevant theory regarding the combined cooling, heating, and power system, including benefits and key-technology options. In addition, possible system configurations, operation strategies and optimization possibilities will be reviewed. Further, the theory associated with dynamic performance analyses, renewable energy sources, and low carbon neighbourhood and buildings will be presented.

Chapter three will present state-of-the-art of combined cooling, heating, and power systems, including existing research and development of key technology options, possible renewable-energy sources, and dynamic performance analyses.

In chapter four, the use case will be presented. This includes a presentation of chosen simulation software, the case building, and the combined cooling, heating, and power system. In addition, associated load profiles and meteorological data are presented.

Chapter five will present all relevant information regarding the transient dynamic simulation performed in the analysis, including the simulation model, implemented component models, and control strategies. In addition, mathematic models connected to the overall analysis are presented.

Chapter six will present all the results considered as relevant for the overall objective of the thesis. This is the electricity production mix by technology and the heating mix by technology. Further, the proposed control strategy, evaluation of required biogas production, and the evaluation of environmental performance will be presented. In addition, implemented control strategies are validated in this section.

Chapter seven will present the discussion and comparison with prior similar studies. The discussion will also highlight the result concerning the main research question of the thesis.

Finally, the conclusion is presented in chapter eight, followed by suggestion for future work in chapter nine.

2 Theory

This chapter presents relevant theory regarding the combined cooling, heating, and power (CCHP) system, including benefits and key-technology options. Possible system configurations, operation strategies, and optimization possibilities are further reviewed. In addition, theory associated with dynamic performance analyses, renewable energy sources, and low carbon building and neighbourhoods are presented.

Some parts of this chapter is based on the author's project report, prepared as a preliminary project for this master thesis.

2.1 The combined cooling, heating, and power system

The combined cooling, heating, and power system, hereafter referred to as the CCHP system, is an extended concept of the combined heat and power (CHP) system. The CHP is a reliable and proven technology, and the technology has been used extensively in large-scale centralized industrial applications and large-scale centralized power plants [13]. For the separate conventional production (SP) system, the provided electricity and heat are typically purchased electricity from the local grid. In contrast to the conventional SP system, the by-product heat in a CHP system is recycled for different uses. A CHP system consists of a power generation unit, a heat recovery system, and a heat storage system.

To develop the conventional CHP system into a CCHP system, it is necessary to integrate additional thermally activated technologies. This allows the system to provide cooling energy. Typical cooling components are absorption chillers and adsorption chillers [14]. Specifically, the thermally activated technology unit utilizes the rejected heat from the power generation unit to provide cooling [15]. It is essential to point out that CHP systems are often referred to as cogeneration, which involves explicitly generating two forms of energy using one single primary energy source. In the context of this concept, CCHP systems are referred to as trigeneration, which further implies the generation of three different forms of useful energy [2].

In summary, a typical CCHP system consists of a power generation unit (PGU), a thermally activated cooling unit, a heat recovery system and storage system, and a heating unit (HU). Most often, the PGU consist of a prime mover and an electricity generator [15]. *Figure 2* illustrates a typical CCHP system. Electricity is provided by the PGU when fuel is being supplied. The heat produced as a by-product in the process is further used to meet the cooling and heating demands in the building through the thermally activated cooling unit and HU.

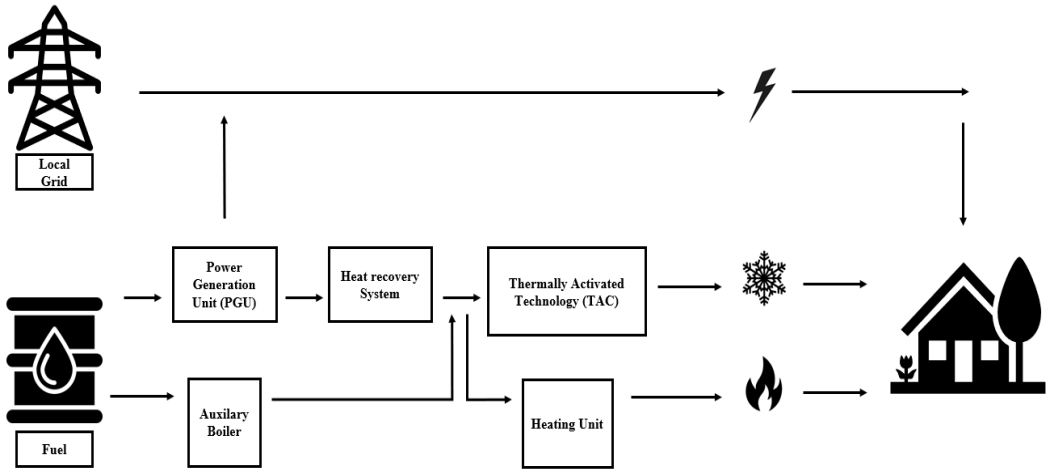

Figure 2: Example of a general CCHP system. Redrawn from [15].

2.2 Trigeneration and benefits

Several studies specify the advantages of both CHP systems and CCHP systems compared to a conventional SP system. In [15], it is pointed out that the main benefits related to a general CCHP system are higher energy efficiency, reduction in emission of GHG, and higher reliability. Furthermore, in [16], a reduction in operating costs, better use of resources, short transmission lines, fewer units, multiple generation options, and minor grid failure are stated as advantages of CCHP systems. In the study, it is also concluded that the biomass-trigeneration system reached the highest trigeneration efficiency.

Most CCHP systems today are fossil-fuelled-based systems [17]. Replacing these non-renewable systems to a renewable-based CCHP system is an obvious alternative to reduce emissions related to fossil-fuelled power generation plants [10]. In [17], a biomass-based CCHP system is studied. It is concluded that it is possible to integrate the required technology in CCHP systems today and achieve a primary energy saving in the process. However, in [18], it is made clear that the actual benefits of CCHP systems over conventional systems in terms of emissions reduction and energy savings are primarily dependent on the plant operation, heating and cooling loads, the specific technology involved, and how the system is structured.

2.3 Key technology options for renewable energy-based trigeneration

In this section, essential technologies that are currently applicable to most renewable energy-based CCHP systems are presented. Specifically, this involves the prime mover of the system and the thermally activating cooling technology.

2.3.1 Prime movers

The prime movers are known as the central device of a CCHP system and ultimately determine the system's overall fuel consumption. Examples of prime movers used in general CCHP systems today are external combustion engines (known as Stirling engines), internal combustion engines (ICE), steam turbines, gas turbines, microturbines, and fuel cells [16]. In addition, the Organic Rankine cycle (ORC) has been referred to as an innovative and promising technology and is therefore also of great interest concerning biomass CCHP systems [19]. *Table 1* is summarizing and comparing CCHP key technologies applicable to biomass [20] [21].

Table 1: Summary and comparison of key CCHP technologies.

CCHP Technology	Advantages	Disadvantages	Available sizes
Internal combustion engines (ICE)	High power efficiency with part-load operational flexibility. Fast start up. Low investment cost. Can be used in Island mode, and have good load following. capability. Can be overhauled on site. Operate on low-pressure gas.	High maintenance costs. Limited to lower temperature cogeneration applications. High air emissions. Must be cooled even if recovered heat is not used. High level of low frequency noise.	1 kW to 10 MW in distributed generation High speed (1200 RPM) ≤ 4MW Low speed (102-514 RPM) 80 MW
Steam turbine	High overall efficiency stream to power.	Slow start up. Low power to heat ratio.	50 kW to 250 MW

	Can be mated to boilers firing a variety of gaseous, liquid, or solid fuels. Ability to meet more than one site heat grade requirement. Long working life and high reliability. Power to heat ratio can be variated.	Requires a boiler or other steam source.	
Gas turbine	High reliability. Low emissions. High grade to heat available. No cooling is required.	Require high pressure gas or in-house gas compressor. Poor efficiency at low loading. Output falls as ambient temperature rises.	500 kW to 250 MW
Microturbine	Small number of moving parts. Compact size and light weight. Low emissions. No cooling required.	High costs. Low mechanical efficiency. Limited to lower temperature applications.	30 kW to 250 kW
Fuel cell	Low emission and nose. High efficiency over load range. Modular design.	High cost. Fuels requires processing unless pure hydrogen is used. Sensitive to fuel impurities. Low power density.	5 kW

Some CCHP systems consist of thermally activating cooling technology to provide cooling energy [13]. Instead of electricity, the utilization of rejected heat is known as one of the most efficient solutions to provide cooling energy. In addition to this, the current process is a critical reason for the CCHP system reaching a low emission of GHG and a high overall energy efficiency [15]. By absorbing or adsorbing the waste heat from the prime mover, shifting the electric load for cooling to the thermal load is possible. This is often referred to as cascade utilization of heat [15]. The current waste heat from the prime mover in the system could be exhaust gas, hot water, or steam. Because of this, the heat energy from different prime movers divides into different temperature ranges [22]. Thermally activated technology includes adsorption chillers, absorption chillers, and desiccant dehumidifiers [13].

2.3.2 Absorption chillers

The working fluid in an absorption refrigeration system is a binary solution consisting of refrigerant and absorbent [23]. The general process connected to an absorption chiller can be divided into two processes. This is the *absorption process* and the *separation process* [15]. *Figure 3* illustrates the general principle behind the two processes. In part A, the left container contains the liquid refrigerant, and the right container has a binary solution (absorbent/refrigerant). The pressure and temperature in the left container will be reduced because the solution in the right container will absorb the refrigerant vapor. This process results in a refrigeration process in the left container (illustrated as Q_L) and a more dilute solution in the right container. This is referred to as the *absorption process*, and because this process is exothermic, heat is rejected to the surrounding for maintenance of the absorption capability (illustrated as Q_I). Part B represents the separation process, which will occur when the absorption process is impossible to continue because of saturation of the refrigerant, and the refrigerant must be separated. Heat is a key factor concerning this process and is typically added to the right container (illustrated as Q_H). In addition to this, the refrigerant vapor will condensate because heat is transferred to the surroundings (illustrated as Q_I). Based on this, the primary refrigeration process is achieved by utilizing heat energy [23].

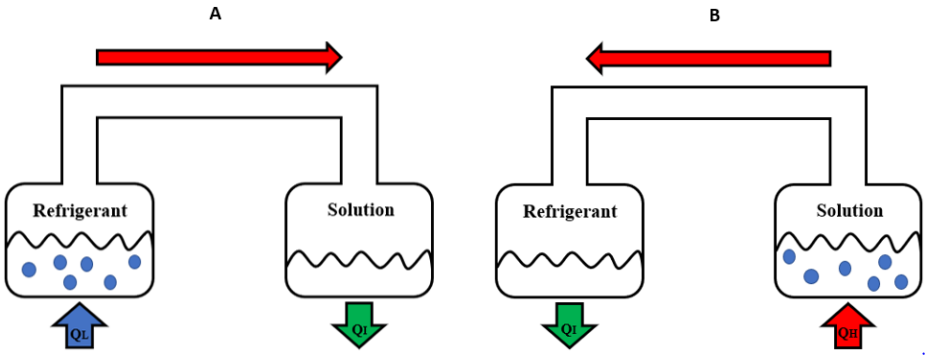

Figure 3: General illustration of absorption process (A) and refrigerant separation process (B). Redrawn from [23].

The general absorption refrigeration cycle combines Part A and Part B, illustrated in *Figure 3*. This is based on the ability to provide cooling energy simultaneously. Usually, it is also necessary to use a circulation pump because the absorption process occurs at a lower pressure than the separation process [23]. *Figure 4* illustrates the general absorption refrigeration cycle, in addition to the circulation pump and necessary valves and pipes.

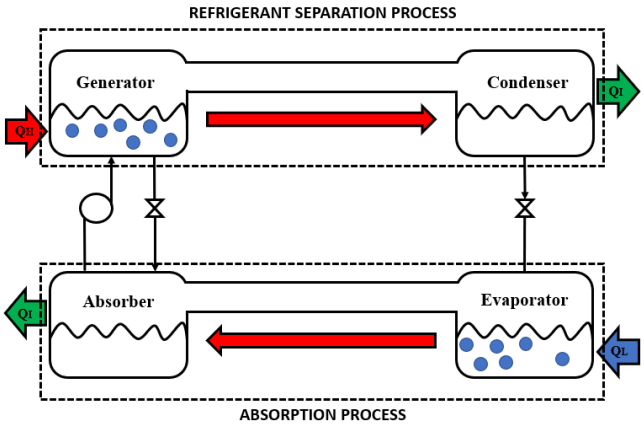

Figure 4: Absorption refrigeration cycle. Combination of Part A and Part B (Figure 3). Redrawn from [23].

2.3.3 Adsorption chillers

Technology related to adsorption cooling is referred to as environmentally friendly and effective. This is mainly because the current systems utilize low-grade heat sources and the exploitation of refrigerants with zero ozone depletion potential [24]. The system has many similarities to a conventional vapor compression system, but instead of using work as an energy provider for compression, the adsorption cooling system utilizes heat energy [13]. *Figure 5* illustrates the thermodynamic phases complementary to the basic adsorption cycle, which consist of four steps. *Figure 6* illustrates an example of a corresponding adsorption refrigeration system associated with the adsorption cycle shown in *Figure 5*.

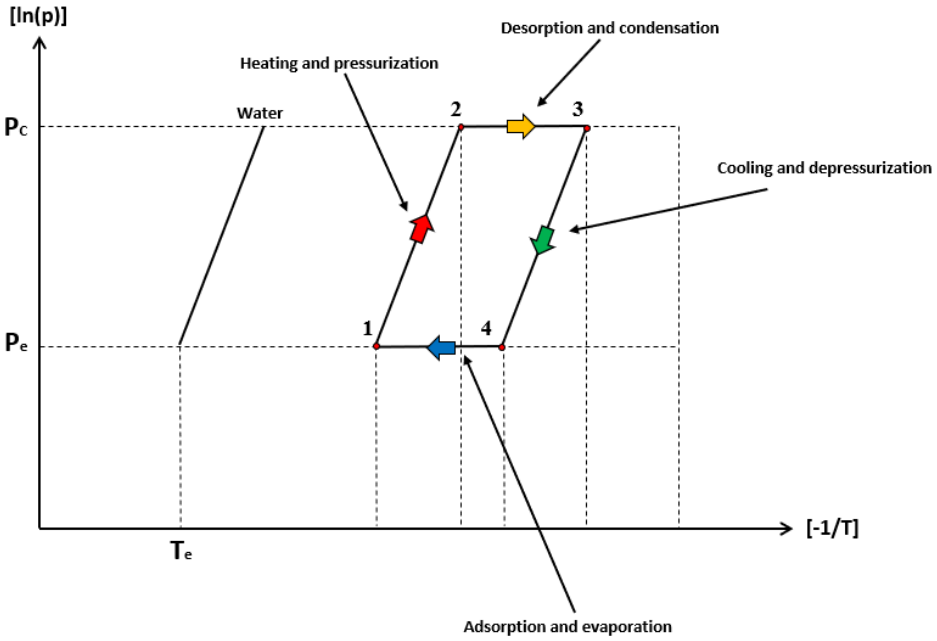

Figure 5: Thermodynamic phases complementary to the basic adsorption cycle. Redrawn from [24].

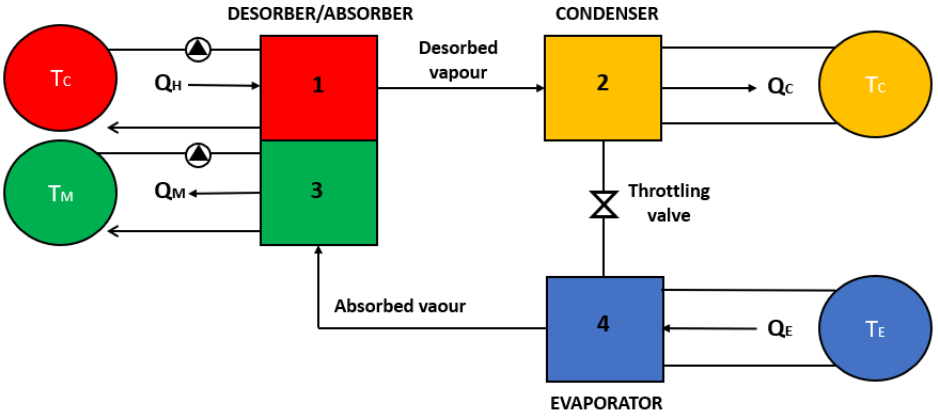

Figure 6: Example of a general adsorption refrigeration system. Redrawn from [24].

In *phase 1-2* (heating and pressurization), heat is supplied by an external heat source, which results in increased pressure and temperature inside the adsorber. In *phase 2-3* (desorption and condensation), desorption of the refrigerant vapor from the adsorbent occurs because of increased temperature in the adsorber. In the condenser, this desorbed vapor will be liquified. This is resulting in a release in condensed heat. In *phase 3-4*, the adsorber is cooled down by a heat transfer fluid, which results in a decrease in pressure (from condensing pressure to evaporating pressure) and temperature. In *phase 4-1*, the refrigerant vapor will be adsorbed from the evaporator by the absorbent because of the decreased temperature. This process is producing the desired refrigeration effect [24].

2.4 System configuration

The system configuration of energy systems involves the overall choice of various components that the system will consist of. The system configuration of the CCHP system should be designed based on energy demands in the specific area, operation strategy, the capacity of chosen key technologies, and the level of

emission of GHG. This is for achieving an energy-efficient, economic, and environmentally friendly system. The design of the specific system configuration is further dependent on the system scale, and available key technologies, like prime movers and thermally activated technology. In addition to this, different areas with different climate conditions will lead to other energy demands. When the CCHP system configuration has been selected, the chosen operation strategy is the key to achieving the most energy-efficient, economical, and environmentally friendly way for the CCHP system to operate [25]. *Table 2* illustrates examples and comparisons of different system configurations.

Table 2: Example and comparison of different system configurations [25].

	Size	**Preference**
Micro	< 20 kW	Distributed energy system
Small	20 kW – 1 MW	Supermarkets, retail stores, hospitals, office buildings, and university campuses
Medium	1 MW – 10 MW	Large factories, hospitals, and schools
Large	> 10 MW	Large industries

2.5 System management, optimization, and sizing

After the specific system configuration has been determined for the CCHP system, the next step is to select appropriate equipment capacities and manage a reasonable energy flow. In a CCHP system, the overall energy performance characteristic is strongly affected by the operational strategy and equipment capacity. Based on this, it is necessary to determine the appropriate capacity of the associated equipment types to realize high economic, environmental, and energetic potentials. This is for the energy supply system to be able to match the customer's load demands.

In [26] it is found that correct sizing of the power generation unit is a key design variable of the CCHP system. This is based on the device determining the capacity of other parts of the system and the total electricity supplement. The control strategy is connected to the chosen operation mode and plays an essential role in the overall system operation. Both electric and thermal demands in buildings have a high variation based on differences in climate and level of activity. Seen in this context, it is challenging to match the existing requirements with the energy produced [27]. Therefore, a proper control system is vital for system efficiency, power generation, and increasing power availability. Furthermore, the control system is essential for decreasing the engine operating hours and dumped power [28]. Today, both conventional and novel operation strategies are used for CCHP systems [25].

2.5.1 Conventional operation strategies

Two traditional operation modes are often used to run the prime mover according to the thermal or electrical demand. This is by following the electrical load (FEL) and by following the thermal load (FTL) [29]. If the FEL strategy is used, the CCHP system will start by providing enough electricity for the building users. Additional fuel should be purchased to the auxiliary heater for increased thermal energy generation if the excess heat is unable to meet the cooling demand and heating demand. If the FTL strategy is used, the system first satisfies the thermal demand, including heating and cooling. If the electricity provided by the PGU is unable to meet the specified electricity demand, additional electricity from the local grid should be purchased [25].

2.5.2 Novel operation strategies

Novel operation strategies are used to reduce the annual total cost (ATC), primary energy consumption (PEC), and emission of GHG. In addition, it is desirable to reduce the total energy waste. This is based on a completely optimal and adapted operating strategy being designed. The literature review shows that there are many different types of novel operation strategies that can be used for a CCHP system today. The strategy should further be adapted to the specific system and the required demands for heating, cooling, and electricity [25].

2.5.3 Optimization strategies

In addition to simulation-based operational strategies, it is further necessary to apply the optimization criteria for the system. This is for ensuring the benefits of CCHP systems, compared to the conventional technologies. Examples of different optimization strategies for CCHP systems today are the reduction of PEC, reduction of ATC, and reducing the emission of GHG [30]. According to the research performed in [31], the system design of the CCHP system is mainly including the two aspects of system configuration design and system operation strategy. It is further pointed out that the system configuration scheme affects both the energy utilization rate, operation effect, and investment running cost. Therefore, optimizing the system configuration is also an essential part of the overall CCHP system research.

2.6 Dynamic performance analyses

As mentioned in chapter 1, the construction sector is responsible for a large proportion of the emission of GHG occurring today. This is again related to increased complexity and technology associated with the built environment, consisting of varying building types with highly demanding user requirements. Based on this information, both researchers and professionals have concluded that well-developed technical tools, like building performance simulation (BPS), are needed to make this problem manageable [32].

Dynamic performance analyses are generally conducted to evaluate different system configurations and operation strategies, in addition to optimization strategies, under the variation of climatic conditions. This is for determining the appropriate capacity and operation mode for the CCHP system, as pointed out in section 2.5.1. Dynamic performance analyses are also conducted for the evaluation of variable renewable energy generation [33]. The analyses can be performed using dynamic simulation tools, and the advantages are that both location and time interval can be changed as desired. General building simulation could be applied in a life cycle perspective, and it could include construction, system design, operation management, and maintenance. The analyses can be based on a steady-state (assumes constant variables with respect to time) or dynamic approach (variables changes with respect to time) [34].

2.7 Renewable energy sources

This chapter presents theory regarding biomass, solar radiation, and wind power as renewable energy sources in CCHP systems. In addition, relevant biomass conversion technologies will be elaborated.

2.7.1 Biomass

The growing need to replace fossil-fired power generation plants with renewable energy-based systems has led to increased biomass-fueled CCHP systems. Biomass is an attractive alternative vis-a-vis other renewable energy sources, partly because, if it is produced sustainably, it is CO_2-neutral and could be used in solid, liquid, and gaseous forms. Nevertheless, its availability is limited and should be used optimally [2]. There

are several technologies associated with heat and electricity production from biomass, such as thermal gasification [35].

Biomass is a renewable energy source because the growth of new trees and plants replenishes the harvest [36]. Therefore, sustainable production and utilization of biomass could reduce the emission of GHG and contributes to energy and climate targets at all levels [37]. *Figure 7* shows the various types of biomass.

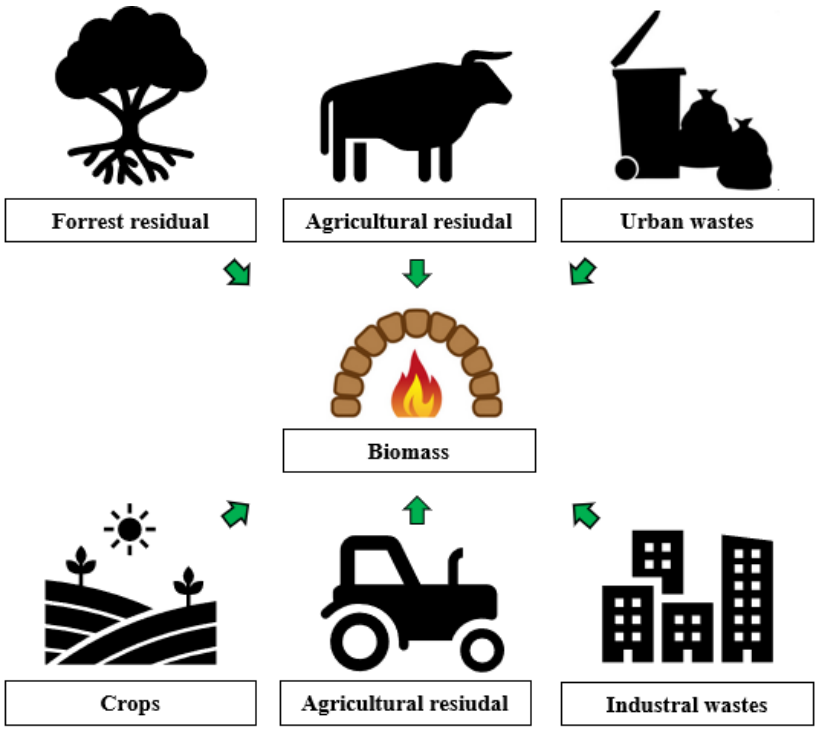

Figure 7: Various types of biomass resources. Redrawn from [38].

The thermochemical transformation of the biomass sources into useful end products can occur through different conversion technologies. Available technologies today are carbonization, liquefaction, co-firing, combustion, pyrolysis, and gasification [39]. In addition to thermochemical transformation technology, the transformation could occur through general bio-conversion (fermentation) and extraction (bio-oil) [40]. *Figure 8* illustrates biomass application pathways conducted today.

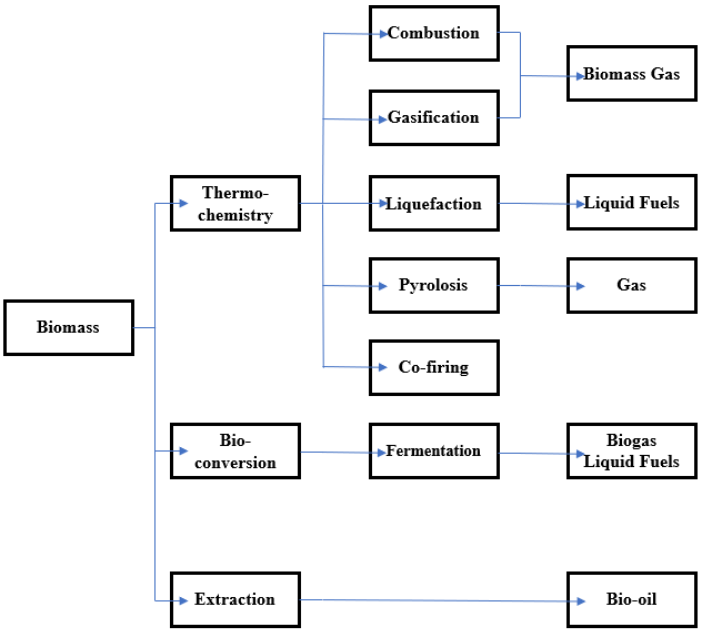

Figure 8: Illustration of possible biomass application pathways. Redrawn from [40].

2.7.2 Solar radiation

Photovoltaic thermal (PV/T) collectors, hereafter referred to as PV/T collectors, convert solar energy into heat and electricity [41]. As mentioned in chapter 1, further development in energy conversion technologies, and greater utilization of green renewable fuels, can be beneficial for overcoming the climate change disorder. This has also led to an increase in energy systems based on multi-renewable energy sources. An example of this is the utilization of biogas in a CCHP system, further consisting of the transformation of solar energy into electrical power and heat by PV/T systems. Relevant research indicates that these biomass-based assisted solar energy CCHP systems can achieve higher overall energy efficiency compared to separate energy production [11].

2.7.3 Wind

In addition to biomass energy and solar energy, wind power is an essential source of environmentally friendly energy. The renewable energy source has become more relevant as a substitute or supplement to traditional fuel in recent years [42]. Wind energy is produced by the nuclear fusion of hydrogen (H) into helium (He) in its core and is generally a converted form of solar energy. The renewable energy form has established itself as an essential player in the global energy market and further represents the mainstream energy source of new power generation [43]. Based on this information, it is also desirable to develop CCHP systems, including wind energy, for renewable power generation. Relevant research indicates that CCHP systems, including wind power generation, results in lower operating costs and higher energy efficiency [44]. In addition to this, researchers also indicate that energy systems, including the combination of different types of renewable energy sources, such as wind and solar energy, can cover approximately 90% of the energy demand with renewable energy [28].

2.7.4 Biomass conversion technologies

Combustion, gasification, pyrolysis, and anaerobic digestion are the most common technologies applied today. This is for converting the solid biomass into energy carriers that are further used in a power generation

unit [45]. *Table 3* identifies the most common biomass conversion technologies, in addition to associated prime mover technologies for CCHP systems today.

Table 3: Summary and commercialization status of available biomass conversion technologies and prime mover technologies for CCHP systems [45].

Energy Conversion Technology	Conversion Technology Commercialization status	Integrated CCHP Technology (Prime mover)
	Anaerobic Digestion	
Anaerobic digester	Commercial technology	ICE Micro- and gas turbine Fuel cell
	Direct Combustion – Boilers	
Fixed bed boiler (stoker)	Commercial technology. Standard technology for biomass, offered by several manufacturers.	Steam turbine
Fluidized bed boilers	Commercial technology. Newer technology, available through several European-based manufacturers.	
Cofiring	Commercial technology	
Modular (direct combustion technology)	Commercial technology. Small number of demonstration projects in CCHP configuration are existing.	Steam turbine ORC
	Gasification	
Fixed bed gasifiers	Emerging technology. The actual number of biomass gasification system in operation are estimated to be below 25.	Gas turbines (simple- and combined cycle) ICE
Fluidized bed gasifiers		
Modular (gasification technology)	Emerging technology. Small number of projects are funded for research and development	ICE Microturbine Fuel cell
Modular (hybrid gasification/combustion)	Emerging technology. Limited commercial demonstration.	Steam turbine ORC

2.8 Low carbon neighbourhoods and buildings

Increasing system energy efficiency and decarbonizing the power system are factors related to achieving a significant reduction in global CO_2 emissions. This transition could be a part of an important transition towards a low-carbon society. Globally, buildings are becoming more power-reducing and energy-efficient. I Norway and China, the focus has been on emission and energy efficiency. This has led to increased research associated with both Zero Emission Buildings (ZEB) and Zero Emission Neighbourhood (ZEB), in addition to nZEB/nZEN (nearly zero-emission buildings) [46].

The Research Centre on ZEN in smart cities is creating solutions for both ZEN and ZEB for contributing to a low carbon society. In the ZEN research center, the following definition is established regarding ZEB [46]:

- "A zero-emission neighbourhood aims to reduce its direct and indirect greenhouse gas emission, towards zero over the analysis period, in line with a chosen ambition level with respect to which life cycle modules and building infrastructure elements to include.

2.8.1 CO_2 emission factors

There has been an ongoing debate on how to consider the electricity from the grid regarding CO_2 emissions within the ZEB Research center. This is mainly related to the methodology considered when calculating the carbon emission credit for electricity generation and use [46]. Further, it is related to how the generation of energy based on renewable generation should be evaluated during the operational phase. In [47], CO_2 emissions from both biofuels and district heating in nZEB are investigated. In addition, the ZEB research center has been employed different CO_2 factors, mainly developed by authors in [48] and [47]. *Table 4* summarizes the specific CO_2 factors which are employed by the ZEB research centre.

Table 4: Specific CO_2 emission factors [46].

Energy carrier	gCO_2/kWh	Reference
Electricity from the grid	130	[49] [48]
Oil (fossil)	285	[48]
Gas (fossil)	210	[48]
Wood chips	4-15	[47]
Pellets/briquettes	7-30	[47]
Biogas from manure	25-30	[47]
Bio-diesel and bio-oil	50	-
Bio-etanol	85	-
Waste incineration (heat only)	185-211	[47]

3 State-of-the-art review of the CCHP system

This chapter will present a state-of-the-art review of the CCHP system. It includes existing research on key CCHP technologies and renewable energy-based CCHP technologies. In addition, existing research on dynamic performance analysis will be presented.

Some parts of this chapter is based on the 'author's project report, prepared as a preliminary project for this master thesis.

3.1 Key CCHP technologies

This section presents the current state-of-the-art in research on key CCHP technologies such as prime movers and thermally activated technology.

3.1.1 Prime movers

In [17], it is pointed out that in biomass-fired CCHP systems, the ORC is proven to be a reliable technology. It is most suited for power supply applications in between 200 kW and 2MW capacity. In addition to this, the authors in [50] completed a techno-economic assessment of biomass-based trigeneration systems, where integrated ORC was considered to be the optimal solution. In their study, it was concluded that the trigeneration system reached a much higher process efficiency in comparison to power only mode. According to this, it is pointed out in [51] that the ICE is the most suitable technology for smaller applications. In [2] ICE has been used in a biomass gasification-based trigeneration system. The choice is argued by several authors recommending this prime mover for the current plant size (small-medium size, 20 kW to 2 MW). For example, this applies to the study in [52] on biomass syngas as a fuel source in an ICE.

The Stirling engines have been referred to as a potential solution in small-scale biomass-based CCHP systems, primarily because they present high system efficiencies. But the solution has high investment costs, in addition to a lack of testing regarding operation and durability. The solution needs to be developed significantly more to compete with other stated technologies [17].

In general, the literature review indicates that most systems based on biomass as a primary fuel source integrate ORC or the ICE as the prime mover in the system.

3.1.2 Thermally activated cooling technology

In [53], an optimization model regarding a biomass-based CCHP and HP system with an integrated absorption chiller has been investigated. It was concluded that the small-scale CCHP system is achieving an overall high energetic efficiency. According to this, the current system can reduce CO_2 emissions by approximately 75%. In addition to this, it was concluded in [54] regarding their research on biomass-fuelled CCHP systems integrated with ORC that the plants combined by adsorption units had a slightly better general performance than the absorption units. It is further elaborated in [22] that it requires the thermally activated technology to be a good match for the specific prime mover for the system to achieve optimal energy cascade utilization.

In general, the literature review indicates that most biomass-fuelled CCHP systems use either absorption chillers or adsorption chillers as thermally activated cooling technology to couple with the system's prime mover.

3.2 Renewable energy sources

This section presents the current state-of-the-art in research on renewable energy sources for CCHP systems, including biomass energy, solar energy, and biomass energy.

3.2.1 Biomass

In [2] research regarding trigeneration modelling, based on biomass gasification is investigated. It is pointed out that few studies examine the possibility of using biomass in trigeneration plants. This can be explained by the fact that many studies focus on biomass in cogeneration systems. Furthermore, it is specified in [2] that the existing studies on biomass in trigeneration systems primarily focus on integrating biomass combustion, ORC, and absorption chillers.

For research regarding biomass gasification trigeneration systems, both [10] and [55] are relevant to mention, in addition to [2]. The research performed in [10] has already been mentioned in section 2.2, without pointing out that a biomass gasifier was used in combination with an ICE and an absorption chiller. It is concluded in the study that the trigeneration system reaches a much higher process efficiency, and a significant reduction in CO_2 emissions, in comparison with a power-only system. In [55], the biomass gasifier is also coupled with an ICE and an absorption chiller. The system reaches an acceptable overall efficiency of 51.42%. In [56], a techno-economic evaluation of two different types of CHP configurations has been performed. This was the ORC integrated with biomass combustion and an ICE integrated with biomass gasification. It was concluded that the ORC-based system has a higher initial investment cost but lower break-even electricity selling price compared with the ICE-based system.

As illustrated in *Figure 8*, it is also possible to use fermentation as a biomass-conversion technology. In general, this process produces high-energy clean fuels by pyrolyzes of biomass materials under anaerobic conditions. According to the research performed in [40], this technology has been spread actively in advanced countries and paid positive attention. However, concerning the utilization of this technology specifically for CCHP systems, the literature review indicates a lack of research regarding this technology. Of the few studies that exist, the authors in [57] conducted a comparison of gas fermentation to thermochemical conversion routes. The study mainly focuses on a hybrid biochemical/thermochemical gas fermentation route (combination of gasification and fermentation). It was concluded that this conversion route reaches a higher carbon to fuel conversion efficiency. Because of this, the technology has lower emissions of GHG, resulting in a more environmentally friendly conversion path.

In summary, the literature review regarding biomass-fuelled CCHP systems indicates that the plant configurations are primarily based on combustion, gasification, and fermentation of biomass as conversion technology.

3.2.2 Solar radiation

In [58], an energy and environmental analysis of a CCHP system with the integration of biogas and a PV system has been performed. Specifically, the system uses biogas for cooling, heating, and power generation, with the support of a PV system. It is also relevant to point out that the system is based on biogas from agricultural waste as a fuel source and a further power generation from an ICE. The results obtained from the energy and environmental analysis showed that the current CCHP system is highly preferable concerning reducing CO_2 emissions.

In [59], the optimal operation of a residential district-level combined photovoltaic/natural gas power and cooling system has been studied. The system is based on a heat recovery steam generator (HRSG) to convert water into superheated steam. In addition to this, an auxiliary heater could be used if the HRSG cannot produce sufficient steam. For providing cooling energy to the residential neighbourhood, a two-stage steam absorption chiller has been used. PV panels are generating electricity, which is further incorporated into the

plant. The specific system was able to meet all requirements regarding heating, cooling, and electricity demands. It is also pointed out that the plant configuration significantly improved the efficiency related to the energy production process.

Overall, the literature review indicates promising results regarding the system performance of biomass-based assisted solar energy CCHP systems.

3.2.3 Wind

As presented in section 2.7.3, existing research on the application of wind power in CCHP systems shows promising results regarding energy efficiency performances. This is further elaborated in [44]. The study was covering an optimal design and operation strategy of renewable-energy-based CCHP systems, including wind power. The results indicated that a combined strategy of electricity purchased at the valley during the night and power generated by the CCHP system during daytime (peak periods) is cost-optimal. This solution is further the most energy-efficient. The authors in [60] additionally performed an energy analysis of a CCHP system integrated with wind turbines and compressed air energy storage systems. The results showed that the proposed system is an excellent candidate for the residential sector, based on providing different kinds of energy from renewable energy sources.

In addition, a CCHP and renewable-energy-based hybrid energy system is studied in [61]. The electricity subsystem consists of solar PV collectors, a wind power plant, and gas turbines. The CCHP system is compared to a CCHP system driven by natural gas. According to the results, the renewable-energy-based CCHP system could reduce the emission of GHG by utilizing wind energy and solar energy. In addition to this, the renewable-energy-based CCHP system is indicating better results regarding operation performance, and both carbon dioxide emission reduction and joint optimization are higher.

In general, the literature review regarding the integration of wind power in CCHP systems indicates promising results. This is both in terms of economy, energy efficiency, and from an environmental perspective.

3.3 Dynamic CCHP performance analysis tools

This section will present existing research regarding transient dynamic simulation tools and evaluations of equipment capacities and operation strategies relevant for the CCHP systems.

3.3.1 Transient dynamic simulation tools

In [62] a research regarding the simulation of CHP systems and CCHP systems has been performed. According to the study, the most used simulation tool regarding modelling and simulation of CCHP systems are TRNSYS and Engineering Equation Solver (EES).

For example, authors in [63] evaluated the potential of integrating renewable energy technological resources for tri-generation application on an island. TRNSYS was considered the most optimal modelling tool for the CCHP system, and both the energetic efficiency, environmental impact, and life cycle costs were evaluated. In addition to this, a modelling approach for the design of biomass-based, solar-assisted CCHP system is studied in [53]. Both the demand model and supply model related to the system were developed in TRNSYS. In the case of EES, authors in [2] modeled all configurations regarding the system in the current simulation tool. The study pointed out that the EES is proven to be suitable for modelling CCHP systems. This is mainly because the program consists of relevant thermodynamic properties and the possibility of defining a user interface, resulting in a user-friendly program.

Nevertheless, it is pointed out in [62] that TRNSYS is most often preferred and recommended regarding dynamic simulations of CCHP systems. This is mainly because it provides a library of built-in components.

The components are most often based on experimental and validated data, and TRNSYS is therefore often used by the academic community. This has led to results associated with work contained by TRNSYS being considered highly reliable.

3.3.2 Control strategies

The optimal control strategy of a hybrid PV/Wind/Engine/Battery system for the providing of electricity and drinkable water to remote applications is studied in [28]. A transient model was implemented in the TRNSYS simulation program to evaluate the system during a one-year operation for two locations. For the system operation strategy, a rule-based algorithm was developed. The main focus of the control strategy was to maximize the energy extraction from renewable energy sources for improving battery performance. The ICE was only used during periods when the renewable sources did not generate enough electricity to cover the load demand (referred to as emergencies). It was concluded that the share of renewable energies is sufficiently high for the energy system, and the results are further emphasizing the importance of power management in energy systems.

An analysis of the optimization of CCHP systems based on energy, economic, and environmental considerations is performed in [30]. The specific system is operated following both the electrical load (FEL) and the thermal load (FTL). The system was further optimized based on operation cost, PEC, and carbon dioxide emissions (CDE). Overall, the results showed that when the CCHP system uses any stated operation criteria during operation, the performance is better than systems without optimization.

4 ChiNoZEN use case description

This chapter presents and describes all relevant information related to the assumed use case study for the dynamic performance analysis. This involves a description of the chosen transient dynamic simulation software, the building complex, and the CCHP system. Building load characteristics and metrological data will further be presented.

Some parts of this chapter is based on the author's project report, prepared as a preliminary project for this master thesis.

4.1 Use case description

In this master thesis, a CCHP system is proposed as a possible energy system solution for a low-carbon neighbourhood. The primary purpose of this analysis is to investigate whether the system can cover the building load demands for space heating, space cooling DHW, and electricity-specific appliances based on a multi-renewable energy supply. Based on this, potential control strategies will be considered.

The system configuration are developed by the Chinese partners in the ChiNoZEN project (further referred to as Chinese ChiNoZEN project partners, between Norway and China. Minor changes have been made to the proposed CCHP system, specified in section 4.3.2. The system was in the early phase developed as a CHP system, and it is desirable to investigate a possible solution for the supplement of air cooling to the building.

The system should be suitable for applications in low-carbon neighbourhoods and buildings. Based on this information, a case study on an existing low-carbon neighbourhood has been performed. The Chinese ChiNoZEN project partners also suggested the case building. A dynamic performance analysis will be performed for evaluating if the system is suitable for application in this specific neighbourhood, based on building energy demands and a multi-renewable energy supply.

Based on the results, a suitable system operation strategy will be proposed. Wind energy and solar energy are unlimited renewable energy sources, while biomass is a limited resource. It is, therefore, desirable to maximize the production of electricity from wind turbines and the PV/T.

4.2 The TRNSYS modelling environment

TRNSYS is an extensible and complete simulation environment mainly used for transient simulation of systems and multi-zoned buildings. It is globally used to validate new and innovative energy concepts by both researchers and engineers [64]. Overall, the TRNSYS simulation software package facilitates the addition of relevant mathematical models and components add-on. It is possible to connect system components with weather data related to the desired location and output components. The TRNSYS components are referred to as component-specific Type numbers. The program also enables the ability to interface with other relevant simulation softwares [65]. TRNSYS is based on an open, modular structure, and both the component models and source code of the operating system are available for the end-users. A standard library of Types is included in TRNSYS. When a more complex system is being studied, it is possible to implement Types developed by TESS inc. *(Thermal Energy System Specialists).* This component library is referred to as Tess component library and is commonly used in global research. Simulation start time, stop time, and step time can be determined in the control cards section in TRNSYS. Related building loads can be created by implementing building models integrated into the system using load files containing information about temperatures and mass flow rates [64].

The standard component models in the TRNSYS library are handling related mass flow rates, but the connected pressure drop is not being considered. In addition to this, both heat capacities and densities are assumed to be constant. Based on this information, TRNSYS is rather simplified simulation software. An essential benefit of the program is still the opportunities to implement and evaluate current control functions. This is accomplished by using components of equations, PID controllers, and ON-OFF controllers [66].

In addition to this, it is essential to point out that the TRNSYS program itself does not consider if the system energy balances are correct. This further leads to situations where energy easily can be "invented" or "disappear" because of mistakes in the system setup. Therefore, the user must evaluate the system's energy balances and temperatures by doing parametric studies. This can be accomplished by using output-producing components [66].

4.3 Presentation of case building and trigeneration system

This section will contain the presentation of the case building and trigeneration system. All information regarding the case building and trigeneration system provided by the Chinese ChiNoZEN project partners will be presented. Not all necessary data has been assigned, and some assumptions have therefore been made. The specific assumptions will be specified and explained.

4.3.1 Case building description

The case building is a low-carbon neighbourhood, located in Jiuquan (China). The number of households is 10, with an area of 120m^2 per household. The total number of users is 40, and the case building is hypothetical.

Table 5 summarizes all information regarding user parameters for the neighbourhood, in addition to the reference. As seen from the table, annual peak loads have been assigned from the Chinese ChiNoZEN project partners. Annual load profiles will be established based on the annual energy demand for a similar building. This is explained and illustrated in section 4.4.

Table 5: User parameters, low-carbon neighbourhood [67].

User parameter	Value	Reference	Comments
Maximum electricity-specific appliances load [kW]	1.31	ChiNoZEN [67].	Provided by project partners
Maximum heating load [kW]	51.22	ChiNoZEN [67].	Provided by project partners
Maximum cooling load [kW]	22.30	Research performed in [68].	See chapter 4.4.1
Maximum DHW load [kW]	7.33	SN-NSPEK 3031:2020, Table A.2 [69].	Annual load profile established based on daily energy consumption
Total number of users [-]	40	ChiNoZEN [67].	Provided by project partners
Household heating area [m^2]	120	ChiNoZEN [67].	Provided by project partners
Number of households [-]	10	ChiNoZEN [67].	Provided by project partners

4.3.2 Trigeneration system configuration and equipment capacities

System configuration – ChiNoZEN CCHP system

Figure 9 illustrates the schematic system diagram and energy transfers for the CCHP system provided by Chinese ChiNoZEN project partners. The figure illustrates the renewable energy input, the CCHP system, and the building energy demand. The building energy demand is including space heating and space cooling, DHW, and electricity-specific appliances. The figure also illustrates the system boundary, not considering how the energy is delivered in the specific buildings. *Table 7* and *Table 8* summarize the different energy flows, shown in *Figure 9.*

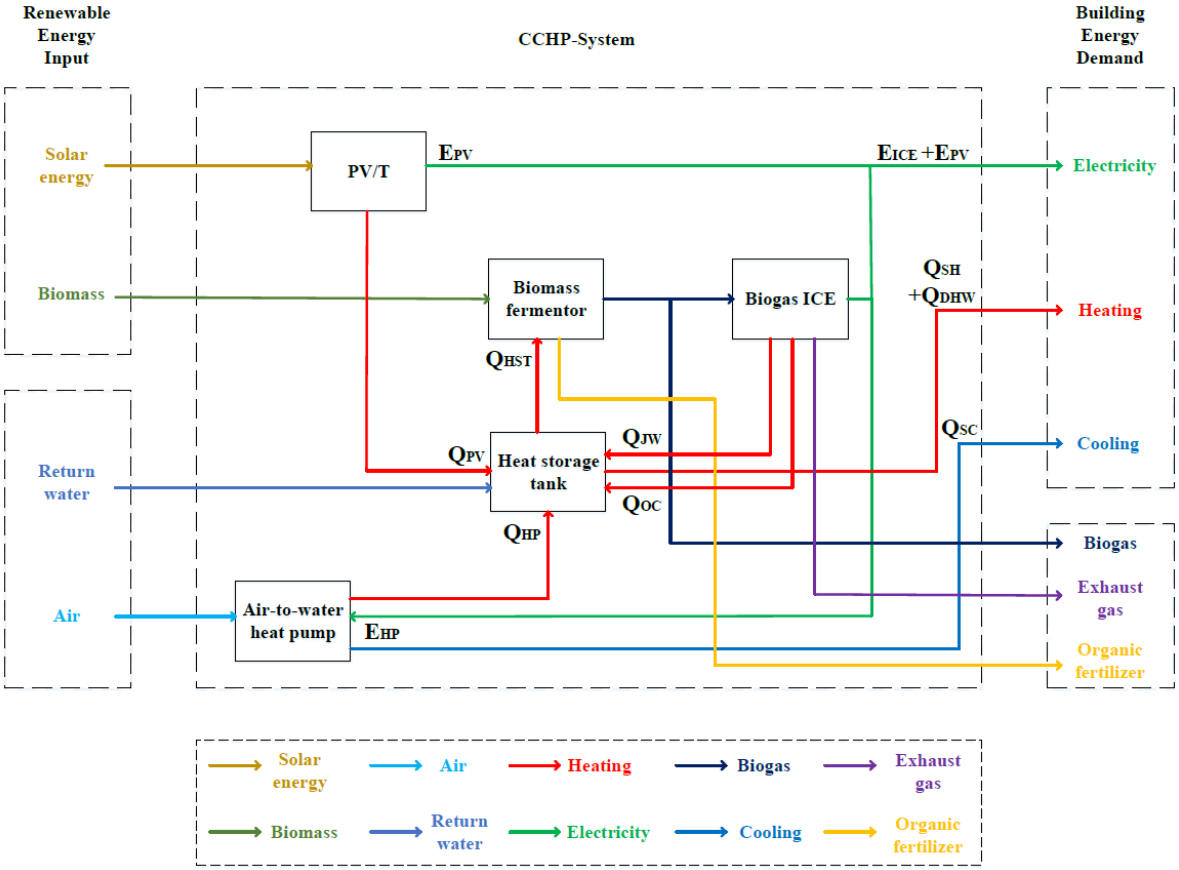

Figure 9: Schematic system diagram and energy transfers of the CCHP system provided by Chinese ChiNoZEN project partners [67].

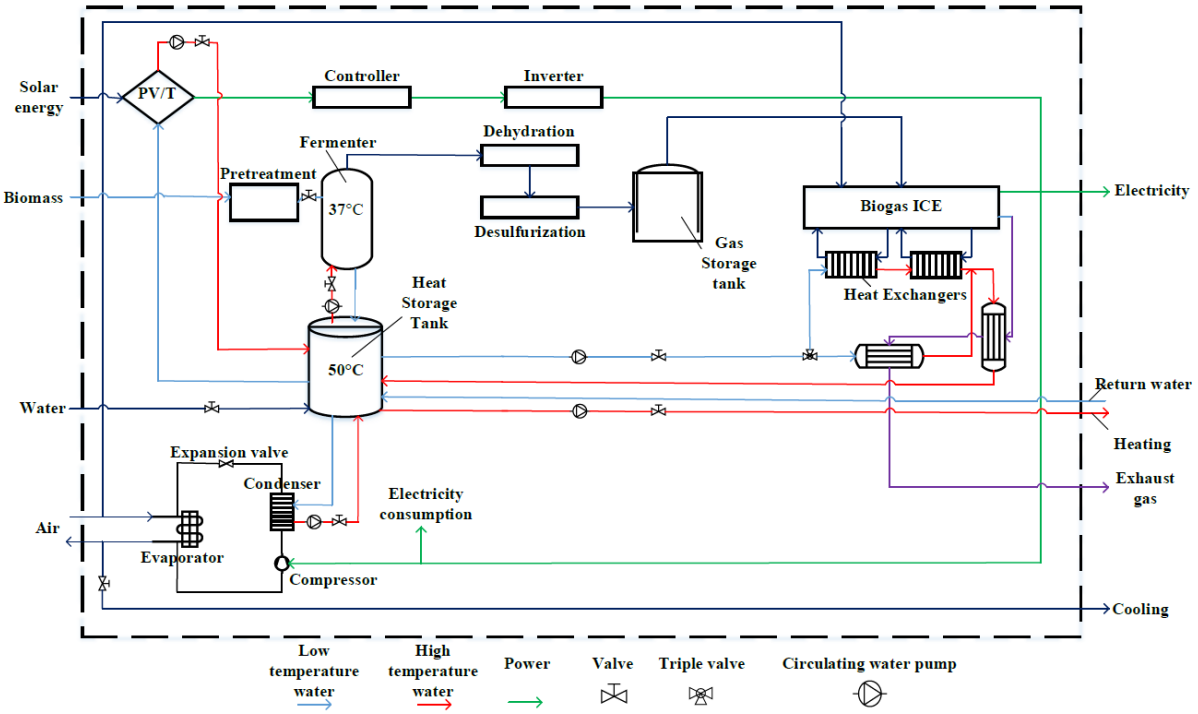

Figure 10: System configuration of the CCHP system provided by Chinese ChiNoZEN project partners [67].

System configuration – CCHP system

Some simplification and adaptions have been made on the system configuration of the CCHP system provided by Chinese ChiNoZEN project partners. This is mainly for adapting the system to a level of complexity and detail, suitable for achieving reliable and desired results in TRNSYS. It is further desirable to consider the integration of wind turbines in the system configuration to increase electricity production based on renewable energy. As pointed out in section 3.2.3, the literature review regarding wind power in CCHP systems indicates promising results. This is both in terms of economy, energy efficiency, and from an environmental perspective. The specific system configuration implemented in the TRNSYS environment will be described in section 5.1.

Table 6 summarizes simplifications and changes for the system configuration of the CCHP system used in the dynamic performance analysis, compared to the CCHP system provided by the Chinese ChiNoZEN project partners.

Table 6: Summary of simplifications and changes in CCHP system implemented in TRNSYS environment for the dynamic performance analysis.

System component	Implemented	Not implemented	Based on
Heat exchangers		X	Adapted to a suitable level of complexity in the TRNSYS environment
Controller (PV/T)		X	Not existing component in TRNSYS. Assessed as irrelevant concerning the purpose of analysis
Inverter (PV/T)		X	Not existing component in TRNSYS. Assessed as irrelevant concerning the purpose of analysis
Fermenter		X	Evaluated by static calculation, based on a mathematical model provided by Chinese ChiNoZEN project partners.

Pre-treatment (fermenter)		X	Not existing component in TRNSYS. Assessed as irrelevant concerning the purpose of analysis
Dehydration (fermenter)		X	Not existing component in TRNSYS. Assessed as irrelevant concerning the purpose of analysis
Gas storage tank		X	Evaluated by static calculation, based on a mathematical model provided by Chinese ChiNoZEN project partners.
Wind turbine	X		Improvement suggestion
Solution for air-cooling supply	X		Not fully developed/functioning in ChiNoZEN configuration
Solution for DHW supply	X		Not implemented in ChiNoZEN configuration
Valves		X	Not existing component in TRNSYS. Adapted to a suitable level of complexity in the TRNSYS environment

Figure 11 is illustrating the schematic system diagram and energy transfers for the CCHP system evaluated in the dynamic performance analysis. As shown, the electricity production from wind turbines is implemented. *Figure 12* is illustrating the schematic system diagram of the CCHP system.

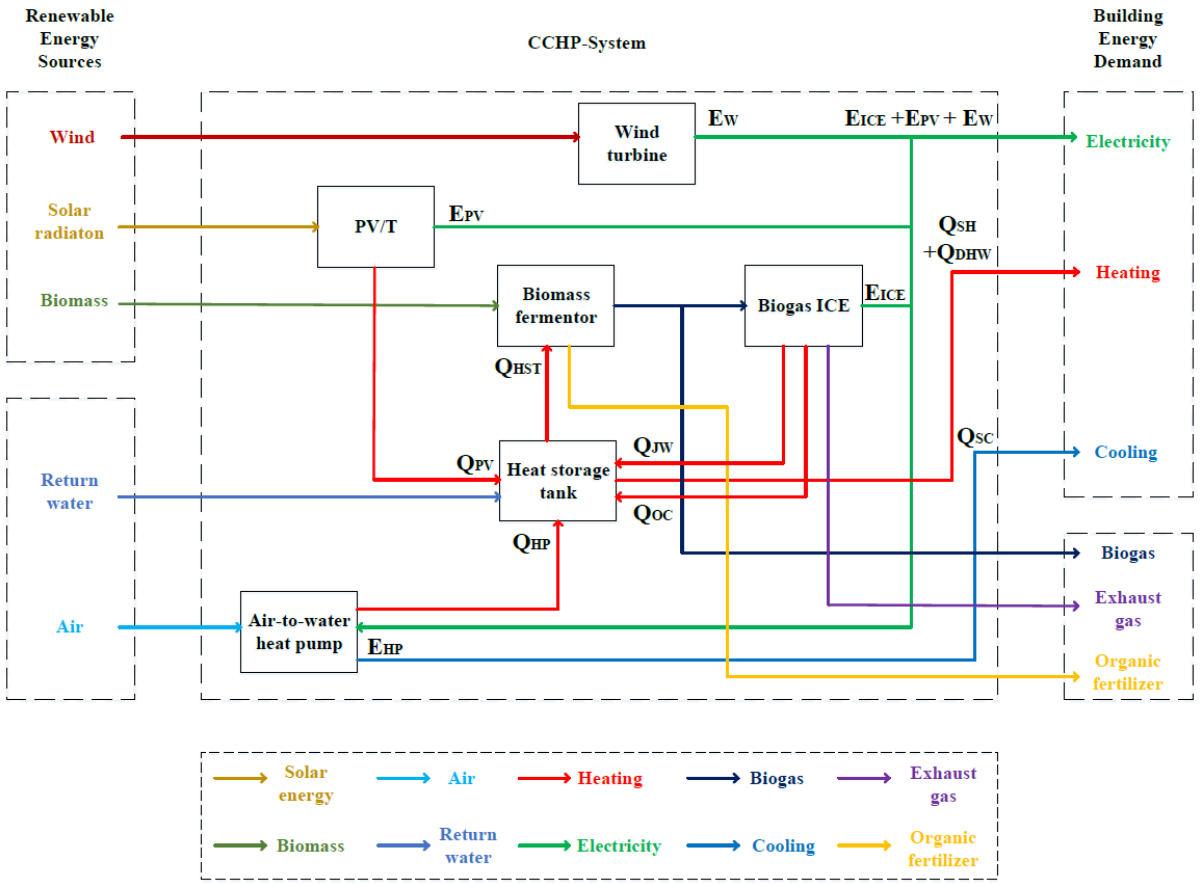

Figure 11: Schematic system diagram and energy transfers for the CCHP system evaluated in the dynamic performance analysis.

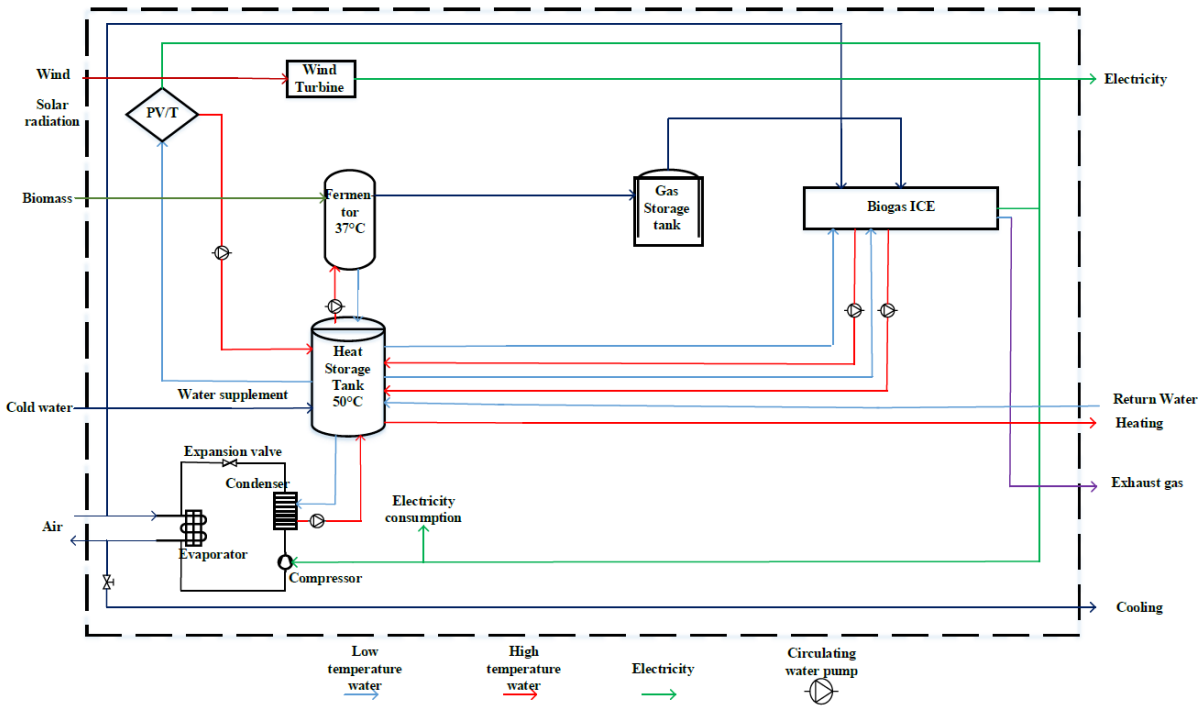

Figure 12: System configuration for the CCHP system evaluated in the dynamic performance analysis.

Table 7 is summarizing the system electricity mix by technology. This applies to both electricity demand and electricity production. The system heating mix by technology is further outlined in *Table 8.*

Table 7: System electricity mix by technology.

Electric components	Variable
Electricity demand	
Heat pump (air-to-water)	E_{HP}
Electricity specific-appliances	E_{SA}
Electricity production	
PV/T electric	$E_{PV/T}$
Wind turbine	E_{W}
Biogas ICE	E_{ICE}

Table 8: System heating mix by technology.

Heat transfers	Variable
Heat demand	
DHW	Q_{DHW}
Space heating	Q_{SH}
Space cooling	Q_{SC}
Heat production	
PV/T thermal	$Q_{PV/T}$
Heat pump (air-to-water)	Q_{HP}
Jacket water ICE (heat recovery unit)	Q_{JW}
Oil cooler ICE (heat recovery unit)	Q_{OC}

System equipment capacities and temperatures nodes

Table 9 is summarizing all system equipment capacities and temperature nodes for the CCHP system. As pointed out in *Table 9*, all data is provided by the Chinese ChiNoZEN project partners.

Table 9: System equipment capacities and temperature nodes for the CCHP system, required by Chinese ChiNoZEN project partners.

System parameter	Value	Reference	Comments
System equipment capacities			
Maximum capacity biogas ICE [kW]	1.3	ChiNoZEN [67].	From project partners
Maximum capacity heat pump [kW]	12	ChiNoZEN [67].	From project partners
COP of heat pump [-]	2	ChiNoZEN [67].	From project partners
Total PV/T net area [m^2]	120	ChiNoZEN [67].	From project partners
System temperature nodes			
Jacket water outlet temperature [°C]	90	ChiNoZEN [67].	From project partners
Jacket water inlet temperature [°C]	75	ChiNoZEN [67].	From project partners
Heat storage tank average water temperature [°C]	50	ChiNoZEN [67].	From project partners
Oil cooler outlet temperature [°C]	75	ChiNoZEN [67].	From project partners
Oil cooler inlet temperature [°C]	62	ChiNoZEN [67].	From project partners
Return temperature space heating [°C]	42	ChiNoZEN [67].	From project partners

4.3.3 System component technologies

This section will consist of a small technical introduction to the technology and fundamentals connected to the different system components which the CCHP system consists of.

Internal combustion engine (ICE)

As illustrated in *Figure 12*, an ICE based on biogas as fuel is implemented in the CCHP system. The ICE converts chemical energy into mechanical work by combustion of the fuel in the presence of atmospheric air. This combustion occurs at a very high temperature, and the released energy is converted into useful work via a working fluid [70]. The total efficiency of the generator is most often between 30 and 40% at full load, which further implies that there is a nontrivial amount of heat energy available. Therefore, it is common for this energy to be rejected to the engine jacket water, oil cooler, aftercooler, or to the exhaust stream when using a heat exchanger. *Figure 13* illustrates an example of a heat recovery system in the ICE and a CCHP system design for power generation. The jacket water, oil cooler, and aftercooler are often referred to as heat transfer units.

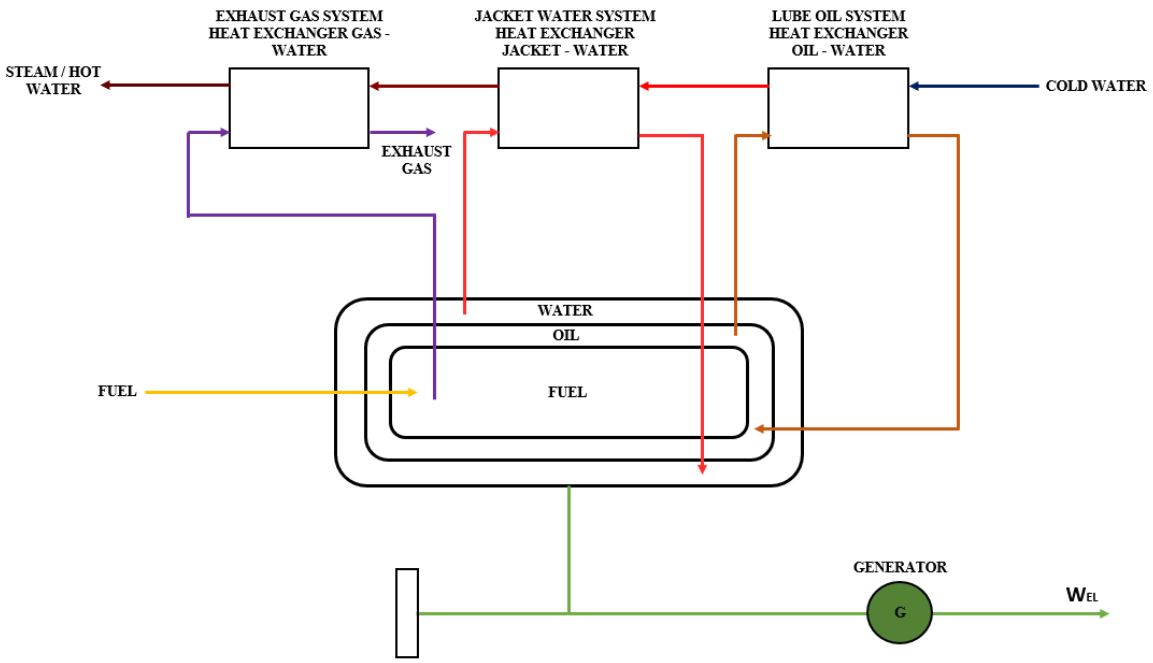

Figure 13: Example of heat recovery system in the ICE. Redrawn from [71].

The manufacturers of current engine generators will typically provide the engine's efficiency and the amount of waste heat that could be transferred to the mentioned cooling streams as a function of the engine's part load ratio. The part load ratio is defined as the ratio between the desired output power and the maximum output power (rated power output) of the engine.

Heat pump (air-to-water)

Heat pump systems are a viable solution for the greenhouse effect and have evolved to become a more utilized technology in the last decade. This can be explained by the heat pump being capable of recirculating environmental and waste heat back into a process of heat production [72]. The heat pump removes energy from the ambient air to heat the supply water to the required return water temperature. This is accomplished by conducting a refrigerant (referred to as the "working fluid"). Heat is transferred from the ambient air (heat source) to the evaporator because of the temperature difference between the ambient air and refrigerant. In the compressor, the refrigerant's enthalpy increases (increased temperature and pressure) because the compressor supplies mechanical energy to the refrigerant. In the condenser, the energy is transferred from the refrigerant to the water because of the temperature difference between the water and refrigerant. Finally, the pressure and temperature of the refrigerant decrease in the expansion valve, back to condenser temperature and pressure [73] [74].

The coefficient of performance (COP) are defined as the heating capacity to the effective power input of the heat pump unit and is further determined as [75]:

$$COP_{hp} = \frac{\phi_{hp}}{P_{el,hp}} \tag{1}$$

Where ϕ_{hp} are defined as the thermal heating capacity of the heat pump and $P_{el,hp}$ are defined as the electrical power of the heat pump. This is when the heat pump is operating in heating mode. *Figure 14* is illustrating an example of a simplified heat pump (air-to-water) system.

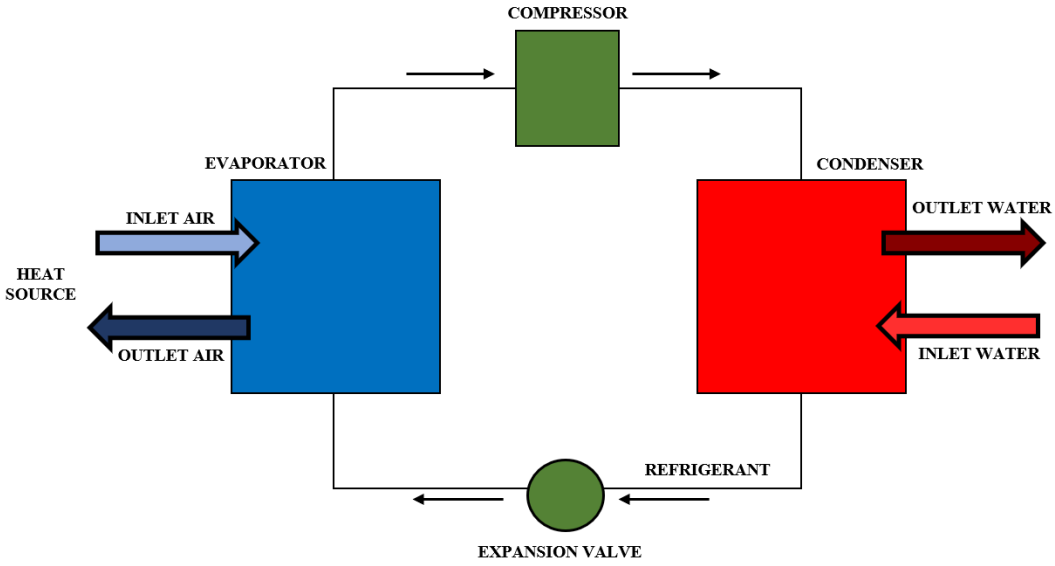

Figure 14: Simplified heat pump (air-to-water) system. Redrawn from [73].

Fermenter

Biomass fermentation is defined as a biological conversion process and is used to biologically convert biomass feedstock into biofuels, materials, chemicals, or combustible gasses. The feedstock of the process of producing biofuels is usually molasses and starch. In the process, the feedstock is further fermented into biofuels (such as biobutanol and bioethanol). Overall, the main operation variables that affect the fermentation efficiency, and the ethanol yield, are the osmotic pressure. In addition, the presence and removal of by-products of the hydrolysis reactions could affect the efficiency [76]. *Figure 15* is illustrating an example of a biological conversion process of biomass to biofuels. The pre-treatment process mainly increases the digestibility of maximum available sugar, and several methods are existing for this process today. In enzymatic hydrolysis, the macromolecules are being split from food by the enzymatic addition of water [77].

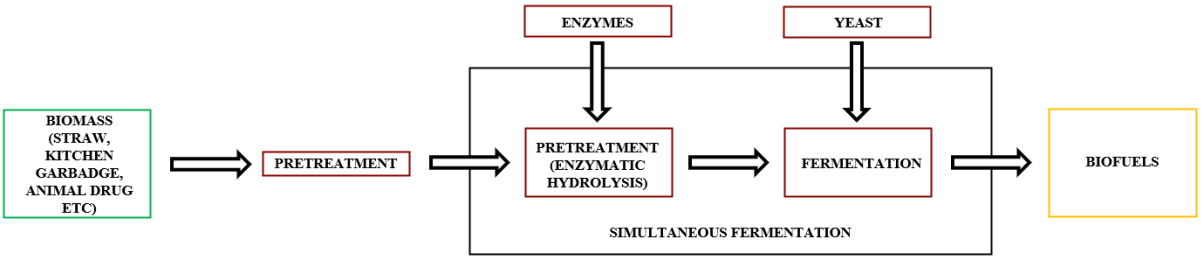

Figure 15: Example of the biological conversion process of biomass to biofuels. Redrawn from [77].

Heat storage tank

Concerning seasonal and long-duration thermal energy storage systems, heat storage tanks are often used. To minimize the overall heat loss, the water tanks are surrounded by thick insulation and reinforced concrete or stainless steel. Furthermore, the water tanks operate with stratified cold and hot layers because of density differences [78]. Thermal storage is further proven to be a successful method adapting the energy demand and supply in buildings and handling challenges related to the current mismatch between the electric and thermal demands [79].

According to NS-EN 12897:2016+A1 "*Water supply. Specifications for indirectly heated (closed) storage water heaters*", the temperature of the stored water in the water tank should not exceed 100°C, for safety

reasons [80]. The Norwegian building technical regulation (TEK 17) further specifies recommended water temperatures to prevent bacterial growth. This applies to indoor water regulations. The optimum growth temperature for the legionella bacterium is 37°C, but it could multiply between 20°C and 45°C. At temperatures above 60°C, the bacterium will die within a few minutes. Based on this information, both the water stored in the hot water tank and the water in circulating systems should keep temperatures above 60°C [81].

Furthermore, the stored water temperature and the load temperature are dependent on whether the tank is assumed to be well stratified or fully mixed. When the water tank is stratified, temperature difference between the top and the bottom of the tank will occur. When the water tank is fully mixed, the temperature levels are assumed to be constant. A benefit of using a stratified water tank is the possibility to supply water to the load at a higher temperature. At the same time, problems associated with bacterial growth can occur because the temperatures at lower levels are not high enough [82].

Photovoltaic thermal collector (PV/T)

In general, a typical PV/T collector consists of a PV module attached to an absorber plate. The absorber plate is also referred to as a heat exchanger device. The primary purpose of the absorption plate is both to collect the produced thermal energy and cool down and improve the electrical performance of the PV module. The collected thermal energy would have been lost to the environment without the absorber plate but can now instead be exploited for low-temperature applications [41].

The PV/T is classified based on whether water or air is used as the working fluid. The collector could be both concentrating and flat plate [41]. The PV/T collector used in the existing CCHP system described in 5.2.3 uses water as working fluid and consists of several flow tubes for the providing of heat to the fluid stream passing through the tubes. The flow tubes are further bonded to an absorber plate located beneath the PV cells, and the module also consists of insulation material [83]. *Figure 16* is illustrating a typical schematic PV/T collector module.

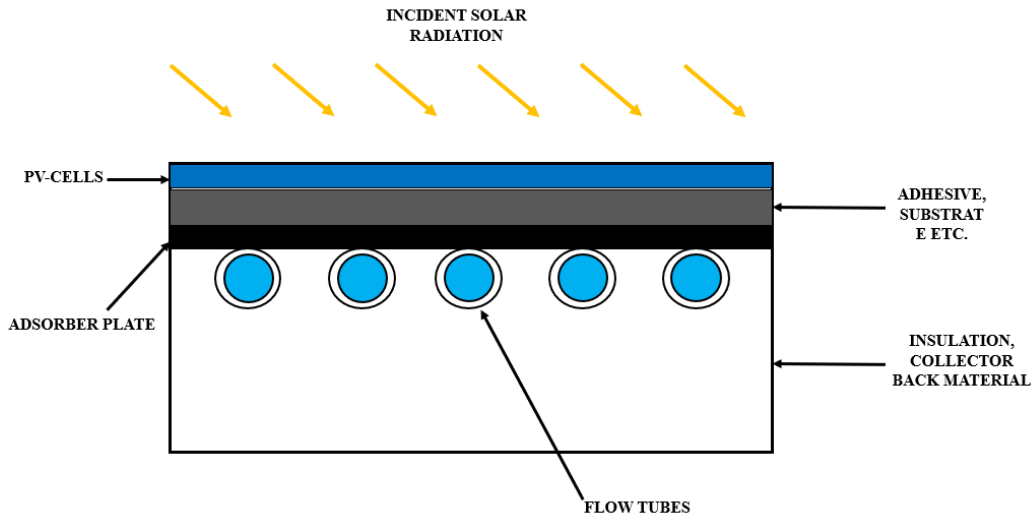

Figure 16: Schematic PV/T collector module. Redrawn from [83].

Wind turbine

A wind turbine is an energy-converting machine for converting kinetic wind energy into mechanical energy and eventually into electrical energy. Remarkable advances in the design of wind turbines have been achieved during recent years, in parallel with modern technological development. Based on this, several wind turbines concept has been developed to minimize the turbine cost, increase turbine efficiency, and maximize the wind

energy output. Most of the modern wind turbines existing today are consisting of three blades, with horizontal-axis turbines.

The first stage of converting wind energy into electrical energy is converting kinetic wind energy into mechanical energy. The wind blades must be appropriately designed for maximizing the capture of wind energy. In this stage of the converting process, the power coefficient (C_p) are defining the converting efficiency. The coefficient is defined as the ratio of captured mechanical power to the available power in wind energy. The following equation is used to calculate the power coefficient:

$$C_p = \frac{P_{me,out}}{P_w} = \frac{P_{me,out}}{\frac{1}{2} \cdot \rho \cdot A \cdot u^3} \tag{2}$$

Where (A) is defined as the blade swept area, (ρ) are defined as the density of air, and (u) is the wind velocity.

In the second stage, the mechanical energy is further converted into electrical energy. The gearbox efficiency determines the converting efficiency (n_{gear}), the generator efficiency (n_{gen}) and the electrical efficiency (n_{ele}). Based on this, the total power conversion efficiency, from the process from wind energy to electricity, are given:

$$n_t = C_p \cdot n_{gear} \cdot n_{gen} \cdot n_{ele} \tag{3}$$

4.4 Load profiles and meteorological data

This section will present annual load profiles for space heating, space cooling, electricity-specific appliances, and DHW. Furthermore, relevant meteorological data implemented in the dynamic performance analysis will be presented.

4.4.1 Load profiles

The Chinese ChiNoZEN project partners were not able to provide information regarding annual load profiles for the neighbourhood. Therefore, annual load profiles a developed based on research performed in [68], on energy pathways for future Norwegian building areas. In the study, a reference building, built-in 1980, was chosen. The building has a heated area of 122m^2 and a ceiling height of 2.5m. As shown in *Table 5*, the buildings in the low-carbon neighbourhood, used as case building in this master thesis, has a heating area of 120m^2. Annual energy demand was simulated dynamically in IDA-ICE for an old building, medium-aged, low energy, and a passive house. Because this is a low-carbon neighbourhood, it has been chosen to use results associated with the passive house.

The research has developed load profiles for space heating, space cooling, and electricity-specific appliances. Load profiles are created based on the ratio of peak load and the hourly load demand. The ratio is further multiplied with peak loads specified in *Table 5* for current energy demands.

For DHW, the annual load profile is established based on daily energy consumption for detached houses, collected from SN-NSPEK 3031:2020 *Energy performance of buildings. Calculation of energy needs and energy supply*, Table A.2 [69].

Figure 17 illustrates load profiles for electricity-specific appliances, and DHW, with a timescale of 72 h. The load profiles have the same characteristics throughout the year. The peak load specified in *Table 5* of both demands is further illustrated in the figure. *Figure 18* is presenting space heating and space cooling load profiles, with a timescale of 8760 h. As shown, the energy demand for space heating is increasing during wintertime and decreasing during summertime.

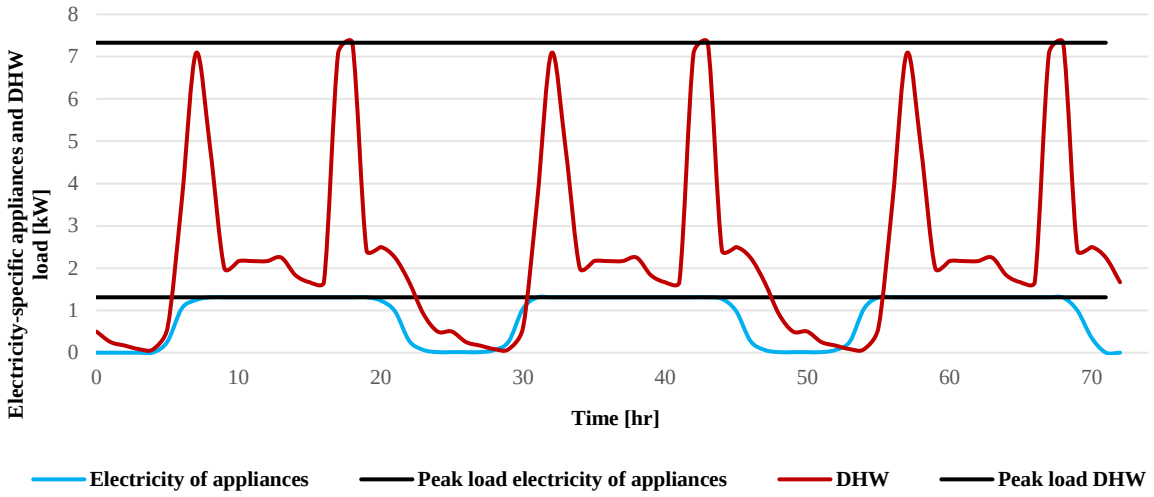

Figure 17: Load profile for electricity-specific appliances and DHW.

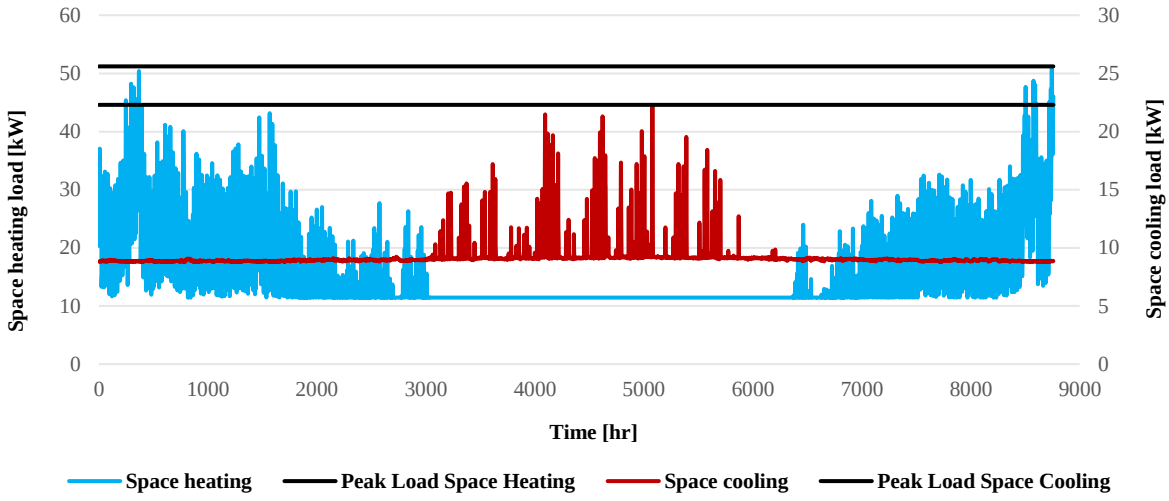

Figure 18: Annual load profile for space heating and space cooling.

4.4.2 Meteorological data

In the dynamic performance analysis, different meteorological data have been implemented. The low-carbon neighbourhood is located in Jiuquan, China. Based on this information, relevant weather data implemented in the simulation model will be presented.

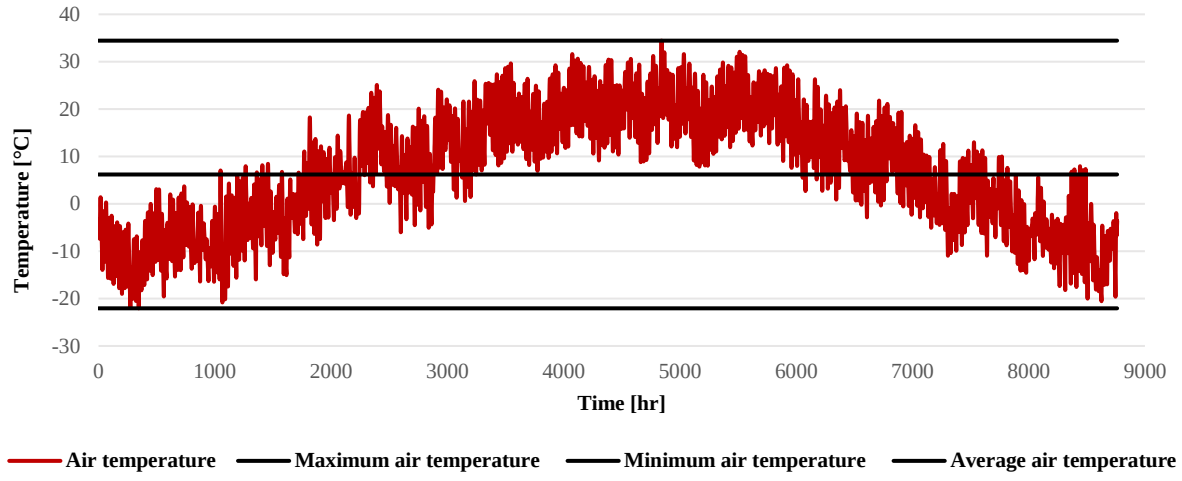

Figure 19: Annual variation air temperature, Jiuquan, China.

Figure 19 is illustrating the annual variation in air temperature for Jiuquan. The maximum air temperature is 34.45°C, and the minimum temperature is -22.05°C. The annual air temperature is equal to 6.2°C.

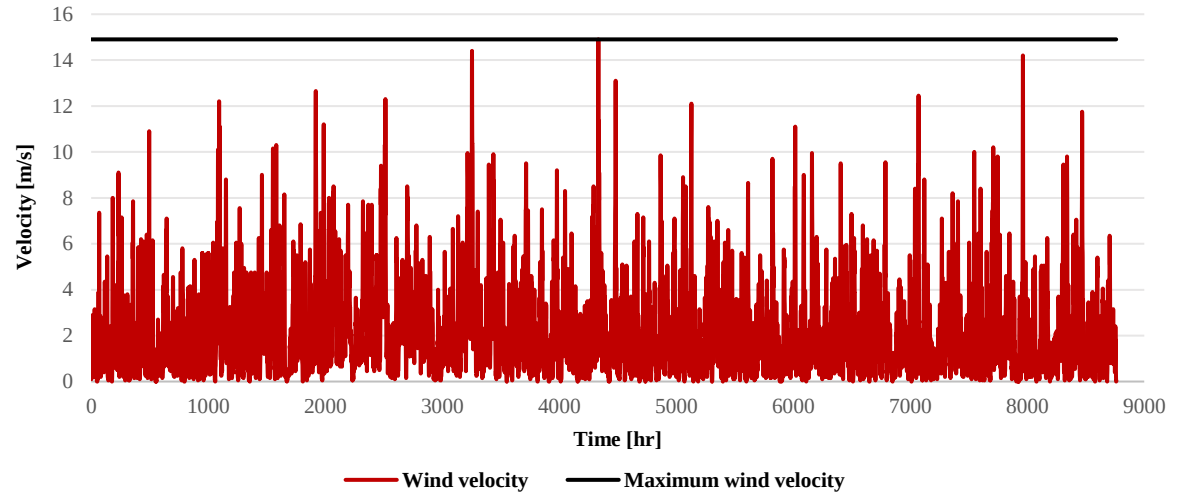

Figure 20: Annual variation wind velocity, Jiuquan, China.

Figure 20 is illustrating the annual variations in wind velocity for Jiuquan. As shown, the maximum wind velocity is equal to 14.9 m/s.

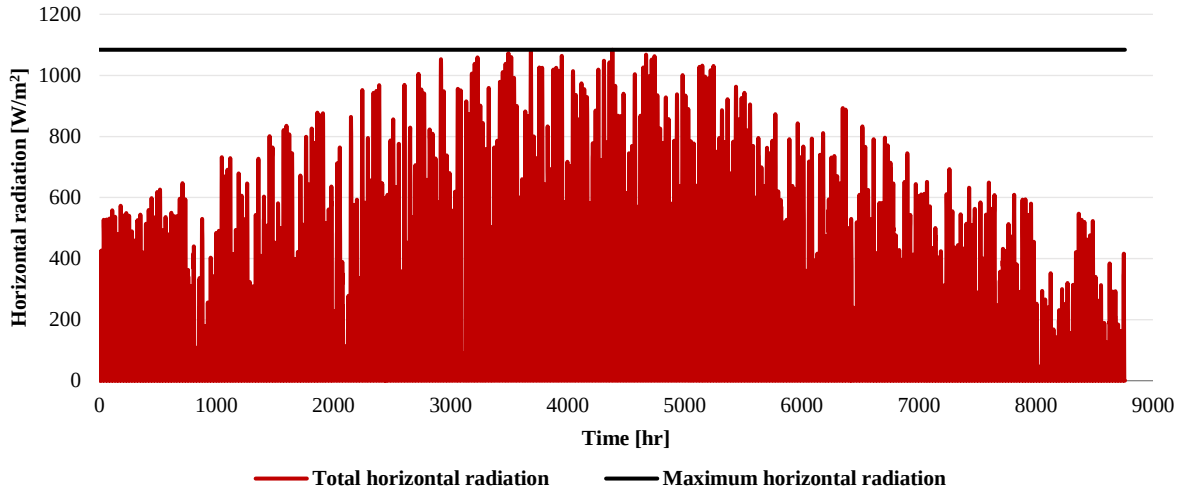

Figure 21: Annual variation horizontal radiation, Jiuquan, China.

Figure 21 is illustrating the annual variation in horizontal radiation for Jiuquan. As shown, the maximum radiation is equal to 1084 W/m^2.

5 Dynamic performance analysis

This chapter will present all relevant information about the transient dynamic simulation that is performed in the dynamic performance analysis. This involves a description of the overall system configuration that is implemented in the TRNSYS environment. System component models, which involve a description of all component parameters and input variables, will be described. In addition, the mathematical model of the fermenter, as well as the chosen control strategies, will be presented.

5.1 System configuration in TRNSYS environment

The main objective of the simulations is to assess whether the CCHP system can cover the energy demand regarding space heating and space cooling, DHW, and electricity-specific appliances based on a multi-renewable energy supply and under specified climatic conditions. In addition, implemented control strategies and operation strategies will be evaluated. The primary purpose is not to consider a fully developed practical solution. *Figure 22* is illustrating the overall system configuration implemented in the TRNSYS environment.

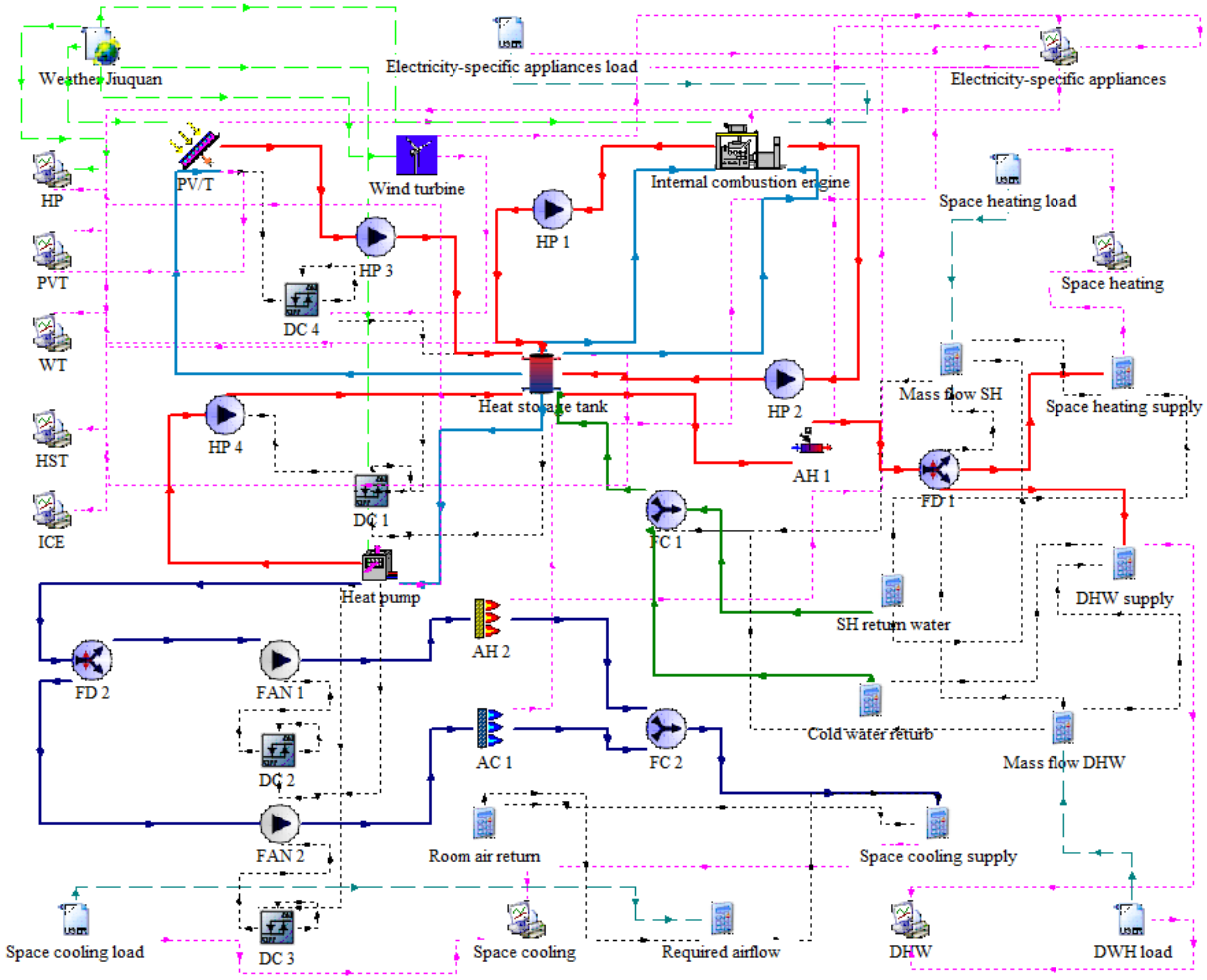

Figure 22: System configuration of the model in TRNSYS environment.

5.2 System component models

In this section, major system components that are implemented in the simulation are described. To access a full mathematical reference of the various components, the reader is referred to the specific library where the component is retrieved from in each section. Only those equations evaluated to be relevant to the reader are presented here with component parameters and input values. The types of minor importance are not included in the documentation. This applies to flow diverters, flow connecters, printers, file readers, and online plotters. Overall energy loss, or energy consumption by a component of minor importance, is not included in the evaluation of the system heating mix or electricity mix by components. *Table 10* gives a summary of the significant Types used in the simulation.

Table 10: Component types implemented in TRNSYS simulation.

Component	TRNSYS Type	Obtained from
Biogas ICE	Type 907	Cogeneration (CHP) Tess component library
Heat pump (air-to-water)	Type 941	HVAC TESS component library
PV/T collectors	Type 560	Electrical TESS component library
Heat storage tank	Type 534	Storage tank TESS component
Wind turbine	Type 90	Standard TRNSYS component library
Hydronic pumps (HP)	Type 3d	Standard TRNSYS component library
Fans (FAN)	Type 3c	Standard TRNSYS component library
Controllers (DC)	Type 2b	Standard TRNSYS component library
Data reader	Type 9	Standard TRNSYS component library
Auxilliary heater (AH 1)	Type 6	Standard TRNSYS component library
Auxilliary heater (AH 2)	Type 1246	HVAC TESS component library
Auxilliary cooler (AC 1)	Type 659	HVAC TESS component library

Component parameters and input data are based on both manufacturer data, data provided by Chinese ChiNoZEN project partners, mathematical calculations, default values in TRNSYS, and linked variables in TRNSYS.

5.2.1 Internal combustion engine (Type 907)

The mathematical model representing the biogas ICE is based on Type 907: *Internal Combustion Engine / Generator Set*, obtained from the TESS Component package in TRNSYS [84]. A complete mathematical reference can be found in [84]. The model is based on an external data file, which consists of air flow rate (fraction of rated flow rate), efficiency, and heat transfer data (fraction of total energy output). The heat transfer data is modelled as a function of the part load ratio (power over-rated power) and the intake temperature. A catalogue data lookup approach is used to predict the general performance of the engine/generator, and a data file consisting of relevant data obtained from a manufacturer must be created. All component parameters and input data are available in Appendix C, *Table 17.*

It has not been possible to find a suitable existing biogas ICE. Thus, an existing data file available in TRNSYS is used. This is normalized data based on an existing engine referred to as *Woodward Governor controlled engine.* The same method is used in the thermal energy storage performance analysis prepared in [85]. The data file contains all relevant values based on the engine's part load ratio (defined as the ratio between the desired output power and the maximum output power of the engine). For example, this applies to the mechanical efficiency, electrical efficiency, fraction of total waste heat to the various coolant streams, and heat transfer rates. *Table 16* found in Appendix C illustrates the mechanical efficiency and electrical

efficiency, in addition to heat fraction rates, as a function of the part load ratio (PLR), for the specific engine. Values are collected from the data file in TRNSYS.

Representative data for the generator's mass flow rates have not been provided from the Chinese ChiNoZEN project partners. Custom mass flow rates for the jacket water, oil cooler, and aftercooler are therefore calculated, based on values in *Table 16* and desired output temperatures for the jacket water and oil cooler, given in *Table 9*. The equations are based on the mathematical model representing Type 907, taken directly from TRNSYS. The mass flow rates are calculated when the engine power output is equal to the maximum power output (engine peak load), given in *Table 9*.

The desired part load ratio is defined as the ratio of desired electrical load ($\dot{P}_{des}$) and the rated power of the device ($\dot{P}_{rtd}$):

$$PLR_{des} = \frac{\dot{P}_{des}}{\dot{P}_{rtd}} \tag{4}$$

$$PLR_{des} = 1$$

This gives the following efficiencies, obtained from *Table 16*:

$$n_{mech} = 0.364 \tag{5}$$

$$n_{elec} = 0.939 \tag{6}$$

The total mechanical shaft power ($\dot{P}_{shaft}$) which is generated by the engine/generator, are then calculated by dividing the actually delivered power output ($\dot{P}_{des}$) on the mechanical efficiency (n_{mech}):

$$\dot{P}_{shaft} = \frac{\dot{P}_{des}}{n_{mech}} \tag{7}$$

$$\dot{P}_{shaft} = \frac{1.31kW}{0.939}$$

$$\dot{P}_{shaft} = 1.395kW$$

And then, the total energy input required by the engine/generator ($\dot{q}_{required}$), is given by dividing the actual total mechanical shaft power ($\dot{P}_{shaft}$) on the mechanical efficiency (n_{mech}):

$$\dot{q}_{required} = \frac{\dot{P}_{shaft}}{n_{mech}} \tag{8}$$

$$\dot{q}_{required} = \frac{1.395kW}{0.364}$$

$$\dot{q}_{required} = 3.83kW$$

Furthermore, the component is calculating the energy transferred to the jacket water steam ($\dot{q}_{JW}$), the energy transferred to the oil cooler steam ($\dot{q}_{OC}$) and the energy transferred to the aftercooler coolant steam ($\dot{q}_{AC}$), in the following way:

$$\dot{q}_{JW} = \frac{f_{jacketWater}}{f_{total}}\left(\dot{q}_{required} - \dot{P}_{shaft}\right) \tag{9}$$

$$\dot{q}_{JW} = \frac{0.307}{1} \cdot (3.83 - 1.38)kW$$

$$\dot{q}_{JW} = 0.752kW$$

$$\dot{q}_{OC} = \frac{f_{oilCooler}}{f_{total}}(\dot{q}_{required} - \dot{P}_{shaft} \tag{10}$$

$$\dot{q}_{OC} = \frac{0.068}{1} \cdot (3.83 - 1.38)kW$$

$$\dot{q}_{OC} = 0.166kW$$

$$\dot{q}_{AC} = \frac{f_{afterCooler}}{f_{total}}(\dot{q}_{required} - \dot{P}_{shaft} \tag{11}$$

$$\dot{q}_{AC} = \frac{0.065}{1} \cdot (3.83 - 1.38)kW$$

$$\dot{q}_{AC} = 0.159W$$

Heat fraction rates are based on values, summarized in *Table 16.* The temperature of the inlet jacket water ($T_{jacketWater,out}$), the oil cooler ($T_{oilCooler,out}$), and the aftercooler ($T_{afterCooler,out}$) are then calculating in the following way, based on the energy transferred to the current liquid streams:

$$\dot{q}_{jacketwater} = \dot{m}_{jacketWater} Cp_{jacketWater} \cdot (T_{jacketWater,out} - T_{jacketWater,in}) \tag{12}$$

$$\dot{q}_{oilCooler} = \dot{m}_{oilCooler} \cdot Cp_{oilCooler} \cdot (T_{oilCooler,out} - T_{oilCooler,in}) \tag{13}$$

$$\dot{q}_{afterCooler} = \dot{m}_{afterCooler} \cdot Cp_{afterCooler} \cdot (T_{afterCooler,out} - T_{afterCooler,in}) \tag{14}$$

Based on Equation 12, the required mass flow rate for the jacket water steam is calculated in the following way:

$$\dot{m}_{jacketWater} = \frac{\dot{q}_{JW}}{Cp_{jacketWater} \cdot (T_{jacketWater,out} - T_{jacketWater,in})} \tag{15}$$

$$\dot{m}_{jacketWater} = \frac{2707.2\,kJ/hr}{4.19\,kJ/kg \cdot K \cdot (90 - 75)K}$$

$$\dot{m}_{jacketWater} = 43kg/hr$$

Mass flow rates for the oil cooler and aftercooler are calculated similarly. The energy transferred to the jacket water stream and aftercooler coolant stream is approximately equivalent. Temperatures regarding the aftercooler streams have not been provided. Based on this information, corresponding mass flow rates are being used. The jacket water and oil cooler are further referred to as heat transfer units (ICE).

5.2.2 Heat pump (Type 941)

The heat pump model chosen for the system is Type 941: *Air to Water Heat Pump (Performance Map; Humidity Effects Neglected),* obtained from the TESS Component Package in TRNSYS [86]. The specific component type has been considered acceptable after the state-of-the-art review indicates that the type is preferred for studies related to energy systems conducting air to water heat pumps, evaluated in TRNSYS. A

complete mathematical reference can be found in [86]. *Table 19* in Appendix D summarizes all component parameters and input data implemented in the TRNSYS environment for the component model.

The model is based on a user-defined data file containing catalog data for heating capacity and required power input. This is as a function of the entering water temperature and air temperature to the heat pump, and different fractions connected to various temperature levels are specified. Based on this, variation in performance at different temperature levels is considered. The amount of data required to develop a specific user-define data file were not available from the manufacturer. Based on this, the normalized performance data developed by TRNSYS for Type 941 will be used. *Table 18*, in Appendix D, summarizes different fractions of rated heating capacity and power for the heat pump, collected from the implemented user-defined data file.

The heat pump utilized in this thesis is manufactured by Foshan Blueway Electric Appliances, located in China and Australia [87]. The type is an air-to-water high-temperature heat pump with scroll compressors. The unit can produce hot water with a maximum temperature up to 75 °C. The heat pump is adapted to an ambient temperature range between -10°C to 43°C.

The maximum air temperature in Jiuquan is 34.45°C, and the minimum temperature is -22.05°C. The annual average air temperature is equal to 6.2°C. Based on the few days the temperature is as low as -22.05°C, the current heat pump is considered qualified. R134a is being used as a refrigerant (HFC-fluid), which is well suited for producing high-temperature water [74]. The supplier provides different data associated with desired capacity and inlet air temperatures, and water temperatures.

5.2.3 Photovoltaic thermal collector (PV/T) (Type 560)

The PV/T collector chosen for the system is Type 560: *Combined PV/T Solar Collector*, obtained from the TESS Component Package in TRNSYS [83]. In general, the component will model an un-glazed solar collector to provide heat to a fluid stream. A complete mathematical reference can be found in [83]. *Table 20* in Appendix E summarizes all component parameters and input data implemented in the TRNSYS environment for Type 650.

The fluid stream is passing through tubes, which are further bonded to an absorber plate. The plate is located beneath the PV cells [83]. Important parameters are the electrical power output (Q_{el}), the thermal power output (Q_{th}) and the outlet fluid temperature (T_{fo}).

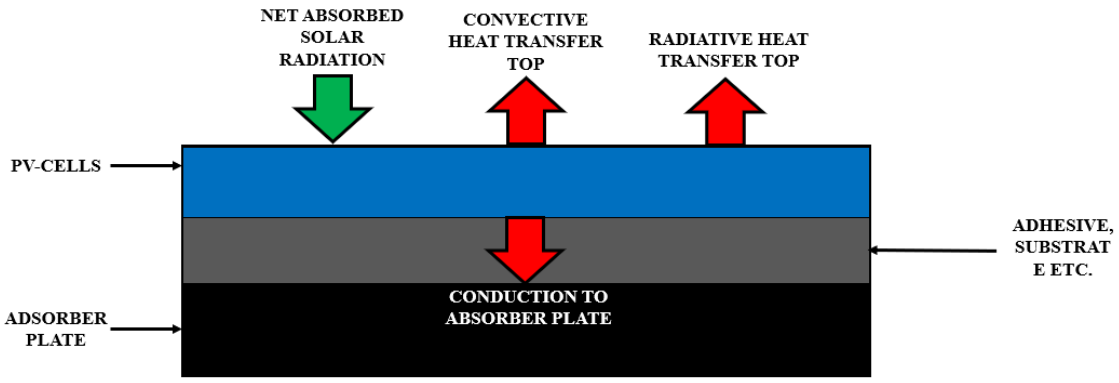

Figure 23: Energy balance PV surface. Inspired by [83].

The electrical power output (Q_{el}) is calculated in the following way:

$$Q_{el} = (\tau\alpha)_n \cdot IAM \cdot G_T \cdot Area \cdot \eta_{PV} \quad (16)$$

IAM is defined as the incident angle modifier, which considers changes in the sun's angle and thereby the output performance of the solar collector. The $(\tau\alpha)_n$ is defined as the transmittance-absorptance product and involves all radiation that is not reflected. G_T is defined as the total horizontal radiation upon the collector surface. The η_{PV} is the efficiency of the PV/T cells as a function of cell temperature and solar radiation.

The thermal power output (Q_{th}) is calculated with Equation 17:

$$Q_{th} = \dot{m} \cdot C_p \cdot (T_{fo} - T_{fi}) \tag{17}$$

Where $\dot{m}$ is the mass flow rate through the solar collector. T_{fo} and T_{fi} are the outlet temperature and inlet temperature of the fluid. The inlet water temperature is the outlet temperature from the hot water storage tank.

By performing relevant calculation processes, it is possible to express the fluid temperature moving through the collector in the y-direction:

$$T_{fo} = \left(T_{fi} + \frac{\varepsilon}{\kappa}\right) \exp\left(\frac{N_{tubes}}{\dot{m}C_p}\frac{\kappa}{\Theta}L\right) - \frac{\varepsilon}{\kappa} \tag{18}$$

The coefficients, ε, κ, and Θ, are based on the geometry of the fin-tube of the solar collector, in addition to material properties and the heat transfer coefficients [88].

A disadvantage of Type 560 is that it is best suited to simulate one single solar collector only. It is not possible to increase the number of solar cells. But according to the full model description, it is possible to assume that the top collector area is equal to the net required collector area [83]. This is not ideal but a result of limitations in existing PV/T models in TRNSYS. For the model to correspond to the required total PV/T collector area, as pointed out in *Table 9*, it is assumed that the total collector area is equal to 1200m^2.

For required parameters and input variables, values connected to tested prototypes from a research project regarding glazed PV/T collectors for DHW preparation on a multifamily building have been used [89]. In addition, the solar collector is modeled after the international manufacturer Vaillant Group, located in both Europe and China. The type is referred to as *auroTHERM exclusive VTK*, and is suitable for solar DHW generation and solar-supported systems [90]. Regarding mass flow rate, it is not given in the above. In [91], the authors have performed research on the efficiency improvement of a PV/T. Results show that high thermal efficiency is reached by using a mass flow rate equal to 0.05 kg/s for horizontal radiation in the range from 713.7 W/m^2 to 931.7 W/m^2. Maximum horizontal radiation for Jiuquan is illustrated in *Figure 21*, equivalent to 1084 W/m^2. For this reason, 0.05 kg/s are used as the mass flow rate for the component.

5.2.4 Heat storage tank (Type 534)

The heat storage tank chosen for the system is Type 534: *Vertical Cylindrical Storage Tank With Immersed Heat Exchanger*, obtained from the TESS Component Package in TRNSYS [92]. A complete mathematical reference can be found in [92]. *Table 21* in Appendix F summarizes all component parameters and input data implemented in the TRNSYS environment for Type 534.

A fluid-filled, constant volume storage tank with immersed heat exchangers is, in general, being modeled. The tank is divided into direct sections, referred to as nodes. The nodes could further be connected to the desired number of inlet ports and outlet ports, making the model suitable for the specific system. It allows the tank to be used for both DWH, space cooling, and space heating storage, and in connection with the solar collector and heat pump loop. Each tank node is considered isothermal, and the fluid is considered perfectly mixed in each node. Through conduction and fluid movements, heat transfer will occur between adjacent nodes. The uniform temperature of each node is passed as input to the next time step at each time step of the simulation. Immersed heat exchangers are not implemented for the storage tank used in this thesis. An

advantage of the component is that specified inlet flow rates will be equal to the outlet flow rate for the specific port. This is resulting in a naturally correct mass balance in the storage tank.

It is essential to point out that the maximum number of input and output ports for this component is equal to 5. Based on this, pure water supplemented for DHW is mixed with the water supplement for space heating. This is a simplification adapted to the simulation model and overall purpose with the simulation. A separate tank for DHW could have been implemented in practice, or a separate heat exchanger in the tank, specifically for DHW purposes.

Tank storage capacity, height, and maximum water temperature are modeled after the same manufacturer as the PV/T collector [90]. The tank could be used for both DWH, space cooling, and space heating storage connected with the solar collector and heat pump. The maximum water temperature is 95°C, which ensures that the temperature is not exceeded. The type is referred to as *multifunction storage allSTOR* [90]. Required loss coefficients are not specified in the associated datasheet. Because of this, default values from TRNSYS are used. *Figure 24* illustrates the number and place of tank nodes, in addition to input ports and output ports chosen for the model. The distribution has been carried out with a view to stratification, and that the water flow to building load should be carried from the tank top, where the temperature most likely is the highest.

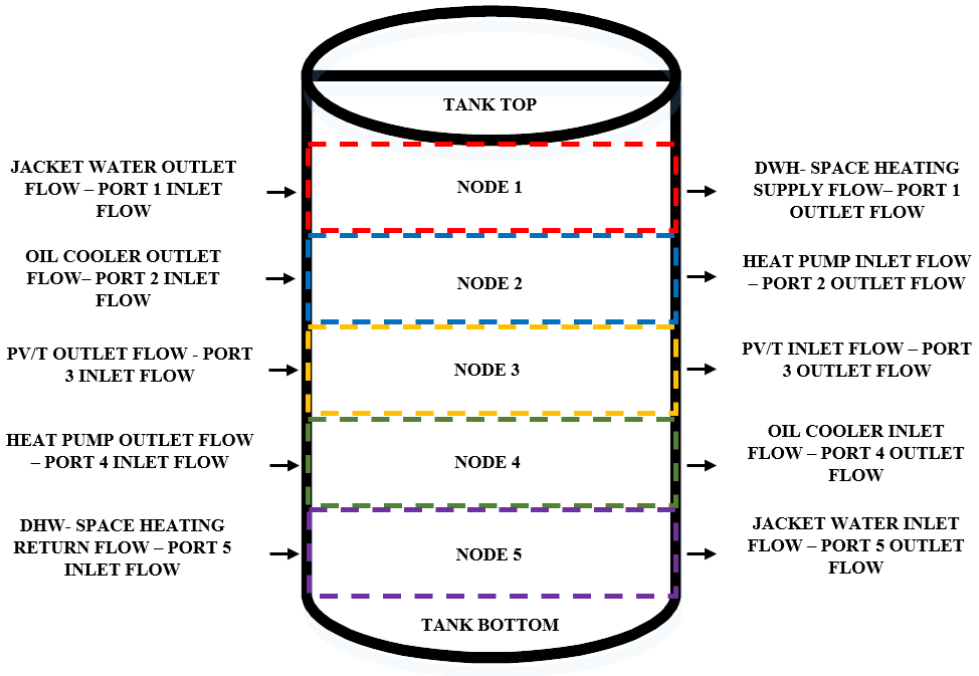

Figure 24: Number and place of tank nodes and input/output ports, heat storage tank.

5.2.5 Wind turbine (Type 90)

The wind turbine model chosen for the system is Type 90: *Wind Energy Conversion System*, obtained from the general component library in TRNSYS [93]. A complete mathematical reference can be found in [93]. Component parameters and input data for the wind turbine are available in Appendix G, *Table 22.*

The model transforms the kinetic energy of moving air into useful energy. Type 90 reads performance data for the wind turbine directly from an external data file. The existing data file in TRNSYS is based on a manufacturer called *Bonus Energy A/S*, mainly located in Denmark. The wind turbine model is referred to as *Vestas V39* and has a rated power of 500 kW. The rotor diameter is 39 m and is manufactured with 40.5 m and 53 m hub heights. The rated wind velocity for the wind turbine is 15 m/s. *Figure 20* are illustrating the annual variations in wind velocity for Jiuquan. As presented, the maximum wind velocity is equal to 14.9 m/s. Based on this, the wind turbine is well suited for the expected conditions in Jiuquan. The cut-in wind

speed is 4 m/s, and the cut-out wind speed is 25 m/s. In practice, this means when the turbine starts and stops operating [94].

The performance data are well suited for the system requirements, and the wind turbine model implemented in TRNSYS is based on this type. Required parameters and input data are retrieved from the manufacturer's datasheet [94]. *Figure 25* illustrates the power generation as a function of wind speed. The figure shows the mentioned cut-in- and out wind speeds, and that maximum power generation is reached at a wind speed of 15 m/s.

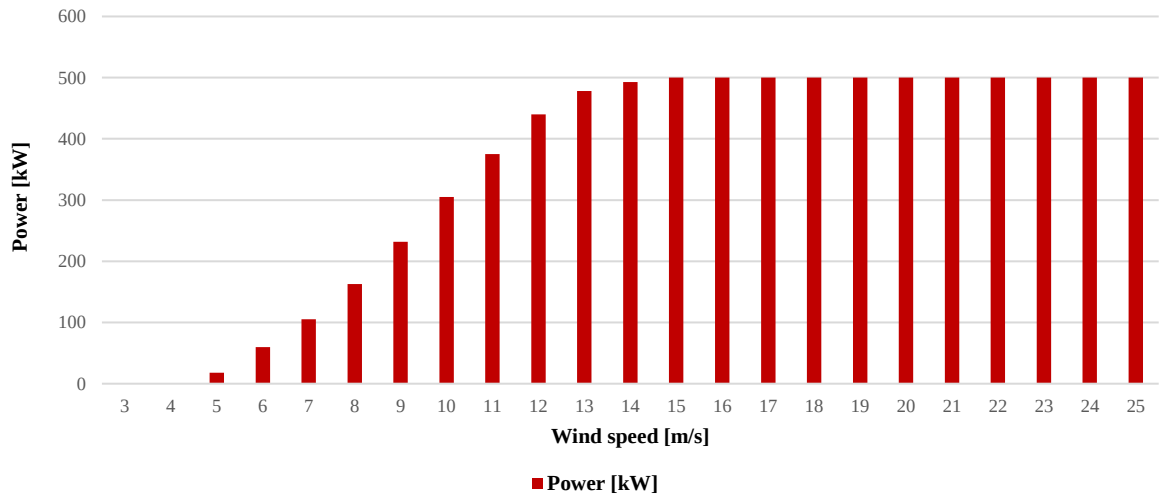

Figure 25: Wind power generation as a function of wind speed [94].

5.3 Fermenter

The biogas fermenter chosen for the system is based on a mathematical model mainly developed by the Chinese ChiNoZEN project partners. The fermenter is cylindrical, with an internal diameter of 11 m. The height of the fermenter is 13 m. The fermenter walls-top and bottom are built of a rigid polyurethane insulation layer and stainless steel. *Table 23*, in Appendix H, summarize all implemented model parameters and associated mathematical symbols for the fermenter model. In addition, data reference is given.

It is assumed that the produced biogas will be stored in a gas storage tank for later use, as illustrated *Figure 12*. The production is based on specified variables provided by the Chinese ChiNoZEN project partners, summarized in *Table 23*.

The overall energy balance in the fermenter is established based on the following equation:

$$m_{f,d} C_{p,d} \frac{dT_{f,d}}{dt} = Q_w - Q_{m,in} - Q_{f,g} - Q_{f,loss} \tag{19}$$

Where $m_{f,d}$ is the mass flow of fermentation liquid, and $C_{p,d}$ is the specific heat capacity of the fermentation liquid. $dT_{f,d}$ is the temperature of the fermentation liquid. Q_w is the heat supplied by the hot water from the heat storage tank, $Q_{m,in}$ is heat supplied by fresh biomass feeding. $Q_{f,g}$ is the heat extracted by biogas (methane), and $Q_{f,loss}$ is the heat loss to the environment.

Energy balance of biogas fermenter:

It is assumed that the internal energy change is equal to zero, and thereby static conditions for the fermenter occurs during calculations. Based on this, the following energy balance is assumed:

$$Q_w - Q_{m,in} - Q_{f,g} - Q_{f,loss} = 0 \quad (20)$$

Figure 26 are illustrating the energy balance and associated temperatures of the fermenter.

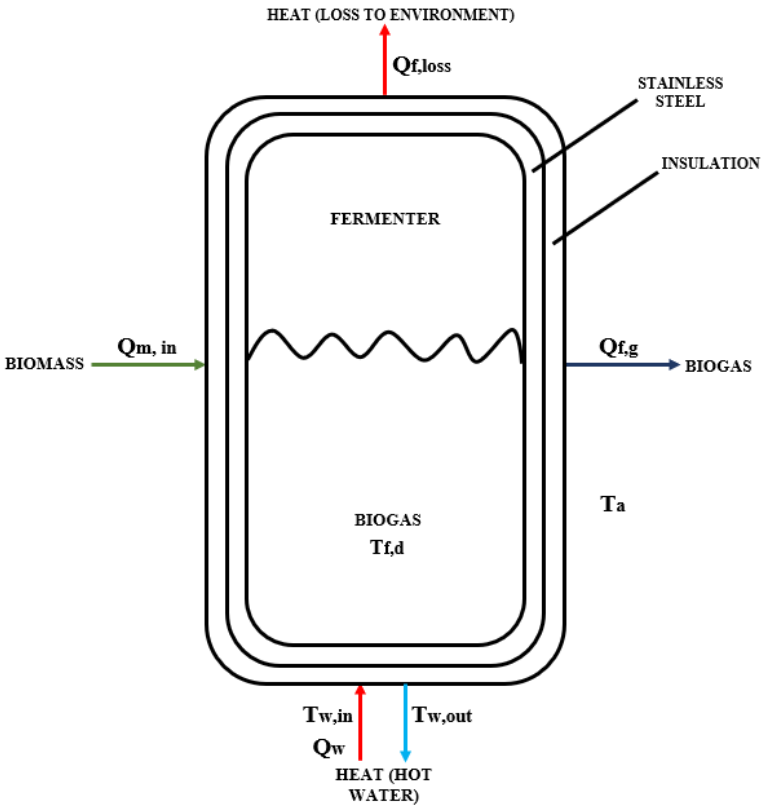

Figure 26: Energy balance and associated temperatures fermenter.

Q_w, $Q_{m,in}$, and $Q_{f,g}$ are further given:

$$Q_w = \dot{m}_{m,w} C_{p,w} (T_{w,in} - T_{w,out}) \quad (21)$$

$$Q_{m,in} = \dot{m}_{m,in} C_{p,d} (T_{f,o} - T_{f,d}) \quad (22)$$

$$Q_{f,g} = \dot{m}_{m,g} C_{p,g} (T_{f,d} - T_a) \quad (23)$$

Where $\dot{m}_{m,w}$, $\dot{m}_{m,in}$, $\dot{m}_{m,in}$ are the fluid flowrates of hot water, fresh biomass feeding and biogas (methane). $C_{p,w}$, $C_{p,d}$ and $C_{p,g}$ are associated fluid specific heat capacities. $T_{w,in}$ is the inlet water temperature of the heat storage tank, and $T_{w,out}$ is the outlet water temperature from the fermenter. $T_{f,o}$ is the initial temperature of the fermenter liquid, approximate to the cold-water temperature, and $T_{f,d}$ is the fermenter liquid temperature.

The heat capacity of biogas ($C_{p,g}$) is calculated in the following way, based on mass fractions and specific heat capacities of CH_4 (methane) and CO_2 (carbon dioxide), listed in *Table 11*.

$$C_{p,g} = 2.254\frac{kJ}{kgK} \cdot 0.355 + 0.842\frac{kJ}{kgK} \cdot 0.647 = 1.341\frac{kJ}{kgK} \quad (24)$$

Table 11: Mass fraction and specific heat capacities, CH_4 and CO_2.

	CH_4	**CO_2**
Mass fraction [%]	35.5	64.7
Specific heat capacity [$\frac{kJ}{kgK}$]	2.254	0.842

The heat loss from the fermenter tank to the environment is calculated based on the following formula:

$$Q_{f,loss} = (Q_{f,r} + Q_{f,f} + Q_{f,w}) \quad (25)$$

$Q_{f,r}$ is the heat loss through the top of the fermenter, $Q_{f,f}$ is the heat loss through the bottom, and $Q_{f,w}$ is the heat loss through the side walls of the fermenter.

Both the heat loss through the top of fermenter ($Q_{f,r}$) and the heat loss through the bottom ($Q_{f,f}$) is calculated based on the following formula:

$$Q_{f,r} = A \cdot K(T_{f,d} - T_a) \quad (26)$$

A is defined as the top fermenter area and bottom fermenter area, and is further calculated:

$$A = \pi r^2 \quad (27)$$

K is the average heat transfer coefficient of the top and bottom of the fermenter. It is calculated based on the following equation:

$$K_r = \frac{1}{\frac{1}{h_1} + \frac{\delta_1}{\lambda_1} + \frac{1}{h_2} + \frac{\delta_2}{\lambda_2}}: \quad (28)$$

$$K_f = \frac{1}{\frac{1}{h_{1'}} + \frac{\delta_1}{\lambda_1} + \frac{1}{h_{2'}} + \frac{\delta_2}{\lambda_2}} \quad (29)$$

h_1 is the heat transfer coefficient of the gas at the top of the fermenter to the fermenter wall. h_2 is the heat transfer coefficient between the outer surface of the insulation layer, and the environment, for the heat loss through the top of the fermenter. λ_1 is the thermal conductivity of stainless steel, and λ_2 is the thermal conductivity of the rigid polyurethane insulation layer. δ_1 is the thickness of stainless steel on the fermenter top, and δ_2 is the thickness of the polyurethane insulation layer. When it comes to the side walls of the fermenter, the following equations is used to calculate the heat transfer:

$$Q_{f,w} = A_{ws}K_{ws}(T_{f,d} - T_a) + A_{wb}K_{wb}(T_{f,d} - T_a) \quad (30)$$

$$A = 2\pi rH \quad (31)$$

$$K_{ws} = \frac{1}{\frac{1}{h_s} + \frac{r_1}{\lambda_1}\ln\left(\frac{r_2}{r_1}\right) + \frac{r_1}{\lambda_1}\ln\left(\frac{r_3}{r_2}\right) + \frac{1}{h_2" r_3}} \quad (32)$$

$$K_{wb} = \frac{1}{\frac{1}{h_b} + \frac{r_1}{\lambda_1}\ln\left(\frac{r_2}{r_1}\right) + \frac{r_1}{\lambda_1}\ln\left(\frac{r_3}{r_2}\right) + \frac{1}{h_2'' r_3}} \quad (33)$$

$$r_2 = r_1 + \delta_1 \quad (34)$$

$$r_3 = r_2 + \delta_2 \quad (35)$$

A is the area of the current side wall of the fermenter (applies to the wall in contact with the wall, and in contact with the biogas). K_{ws} and K_{wb} are the heat transfer coefficients between the inner liquid of the fermenter inside and biogas inside, to the external environment of the side wall. H_s and H_b are the height of the inside fermenter liquid, and the biogas inside the fermenter. h_s and h_b are the convective heat transfer coefficients between the inner liquid of fermenter, and the biogas, with the sidewalls of the fermenter. h_2'' is heat transfer coefficient between the outside of the fermenter wall, and the environment. δ_1' is the thickness of 304 stainless steel.

Calculation of biogas production in fermenter:

Maximum biogas production [kg/s] from the specific fermenter is calculated in the following way:

Methane production rate of organic waste [m^3/kgVS]:

$$B = B_0\left(1 - \frac{K}{HRT \cdot \mathrm{u}_m + K - 1}\right) \quad (36)$$

$$B = 0.33\frac{m^3}{kgVS} \cdot \left(1 - \frac{0.8156}{4d \cdot 0.352/d + (0.8156 - 1)}\right)$$

$$B = 0.11\frac{m^3}{\mathrm{kg} \cdot \mathrm{VS}}$$

B_0 is the limiting methane production rate of the organic waste in [m^3/kgVS]. K is a dimensionless dynamic parameter, calculated using Equation 39.

Gas production rate [m^3/m^3d]:

$$y_v = \frac{BS_0}{HRT} \quad (37)$$

$$y_v = \frac{\frac{0.11m^3}{kg\mathrm{VS}} \cdot \frac{60kgVS}{m^3}}{4d}$$

$$y_v = 1.65\frac{m^3}{m^3 d}$$

S_0 is the concentration of influent volatile solids (VS) in the production process in [kg/m^3], and HRT is the hydraulic retention time.

Biogas production [kg/s]:

$$\dot{m}_{m,g} = \frac{V \cdot y_v \cdot \rho_{CH_4}}{\frac{86400s}{d} \cdot x_{CH_4}} \tag{38}$$

$$\dot{m}_{m,g} = \frac{1032m^3 \cdot \frac{1.65m^3}{m^3 d} \cdot \frac{0.657kg}{m^3}}{\frac{86400s}{d} \cdot 0.45}$$

$$\dot{m}_{m,g} = 0.029 \frac{kg}{s}$$

$\dot{m}_{m,g}$ is the produced biogas, from the specific fermenter, in [kg/s]. V is the volume of fermented liquid, and y_v is the gas production rate based on fermenter capacity. ρ_{CH_4} is the density of methane, and x_{CH_4} is the mass fraction of methane in biogas.

K is a dimensionless dynamic parameter, calculated using the following equation:

$$K = 0.8 + 0.0016 \exp(0.06 \cdot S_0) = 0.8156 \tag{39}$$

u_m is the maximum growth rate of microorganisms per day, and is given by the following equation:

$$u_m = 0.013 \cdot T_{f,d} - 0.129 = 0.352 \tag{40}$$

Energy content in the biogas mass flow rate is calculated based on the lower heating value (LHV) for biogas and the plant availability factor for the fermenter.

Based on Equation 38, it is calculated in the following way:

$$Annual\ biogas\ production = \dot{m}_{m,g} \cdot LHV_{biogas} \cdot PLant\ availability\ factor \cdot hr \tag{41}$$

$$Annual\ biogas\ production = 0.029 \frac{kg}{s} \cdot 11.316 \frac{MJ}{kg} \cdot 0.97 \cdot 8760hr$$

$$Annual\ biogas\ production = 2788.5MWh$$

5.4 Implementation of control strategies

A suitable control strategy is required to match energy production and demand of the low carbon neighbourhood at each hour of the year. Control strategies are implemented in the simulation to assess whether the system can cover the existing load demands.

The electricity production from both PV/T collectors and wind turbine is dependent on season and time of day. The advantage is that they are entirely unlimited. A general system operation strategy has been developed to optimize the utilization of renewable energy sources.

5.4.1 Space heating and domestic hot water (DHW) load

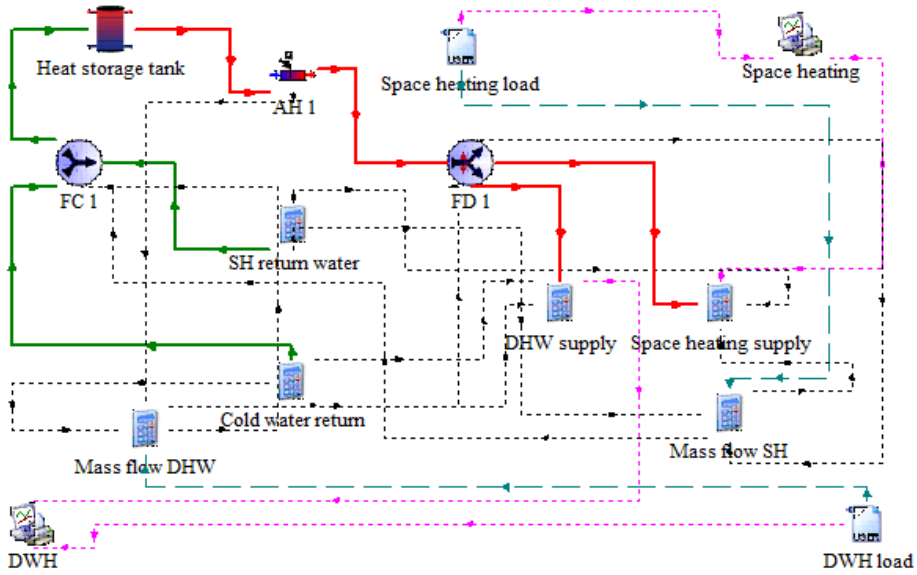

Figure 27: Control strategy of space heating load demand and DHW load demand.

A water flow control strategy for space heating and DHW is implemented in the TRNSYS simulation environment. *Figure 27* illustrates the water flow control strategy for space heating and DHW. It is important to specify the system boundary, which does not consider how the energy is delivered to the various buildings. Space heating load and DHW load profiles are implemented in the simulation model using Type 9: *Data reader (Generic Data Files)*, obtained from the general component library in TRNSYS [93]. The component serves the purpose of reading data at regular time intervals. The development of annual space heating and DHW load is described in section 4.4.1 and illustrated in *Figure 17* and *Figure 18*. Calculated values are implemented in Type 9.

As already pointed out in section 5.2.4, a substantial simplification in the simulation model is mixing water for space heating and DHW. This is not recommended in practice because the DHW must be completely clean, without any bacteria. This is implemented in the simulation model because the component model for the heat storage tank has a limit of 5 possible flow inputs. In addition, the simulation model is adapted to the required system configuration provided by Chinese ChiNoZEN project partners.

The TRNSYS equation type is offering the possibility of implementing its own equations and variables. The component calculates the required mass flow rate for space heating and DHW supplied to building users. The mass flow rates are calculated based on the following equations:

$$Q_{SH} = \dot{m}_{SH} \cdot C_{p,water} \cdot (T_{set-point,AH\,1} - T_{return,SH}) \tag{42}$$

$$Q_{DHW} = \dot{m}_{DHW} \cdot C_{p,water} \cdot (T_{set-point,AH\,1} - T_{Cold,water}) \tag{43}$$

The calculated $\dot{m}_{SH}$ and $\dot{m}_{DHW}$ is mixed and specified as port 5 inlet flow for the heat storage tank, as illustrated in *Figure 24*. This will be equivalent to the outlet flow for port 5. Specified mass flow rates are given as input for flow diverter 1 (FD 1), and correct mass flow rates, and thereby heat load and DHW load will be supplied to the building users.

T_{supply} is equal to port 1 outlet flow in *Figure 24*, and will variate throughout the year, as illustrated in *Figure 29.* An auxiliary heater (AH 1 in Figure 28) is implemented to achieve a more constant supply temperature. The heater will be turned OFF, if T_{supply} is higher than $T_{set-point,AH\,1}$. The set-point temperature, $T_{set-point,EH\,1}$, is basically set to 50°C. $T_{return,SH}$ is set to 42°C, based on system temperature nodes, specified in *Table 9*. $T_{Cold,water}$ is set to 6.2°C, which is equal to the average annual air temperature, as illustrated in *Figure 19.*

As pointed out in *Table 9* regarding system equipment capacities and temperature nodes, the desired heat storage tank average water temperature is 50°C. *Figure 28* is illustrating the average tank temperature, when $T_{return,SH}$ is set to 42 °C and $T_{set-point,AH\,1}$ is set to 50°C. The maximum water temperature is equal to 58.4°C and the minimum water temperature is equal to 41,3°C. *Figure 29* is illustrating the average tank temperature, when increasing $T_{return,SH}$ to 52°C and $T_{set-point,AH\,1}$ to 60°C. The maximum water temperature is equal to 64.9 °C and the minimum water temperature are equal to 49.9°C.

For the temperature in the storage tank to be above the required heat storage temperature, given in *Table 9*. It has been decided to use $T_{return,SH}$ equal to 52°C and $T_{set-point,AH\,1}$ equal to 60 °C. It is important to point out that the optimum growth temperature for the legionella bacterium is 37°C. Still, it could multiply between 20°C and 45°C, as already elaborated in section 4.3.3 both the water stored in the hot water tank and the water in circulating systems should keep at temperatures above 60°C.

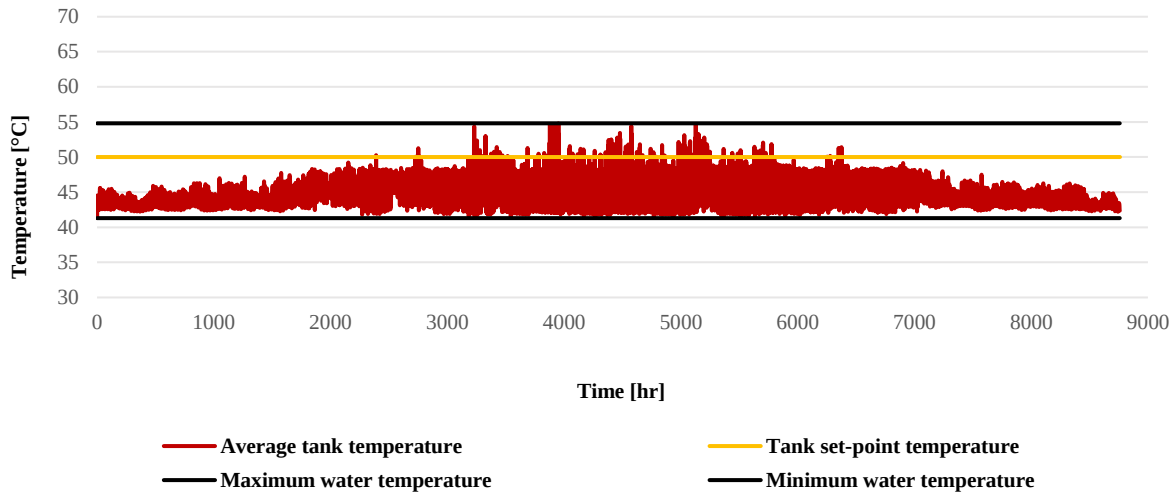

Figure 28: Average hourly heat storage tank temperature, low-temperature requirements.

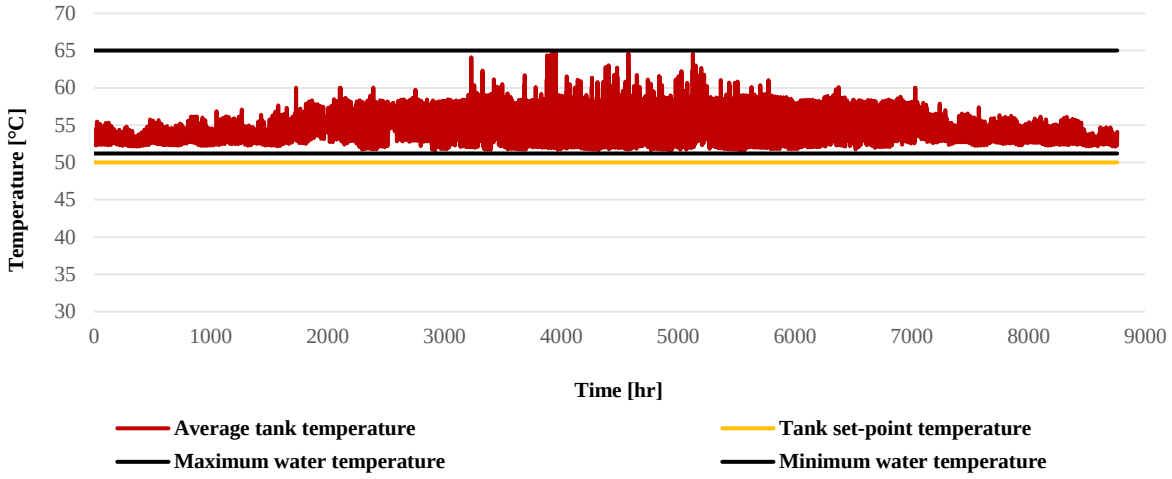

Figure 29: Average hourly heat storage tank temperature, high-temperature requirements.

5.4.2 Space cooling load

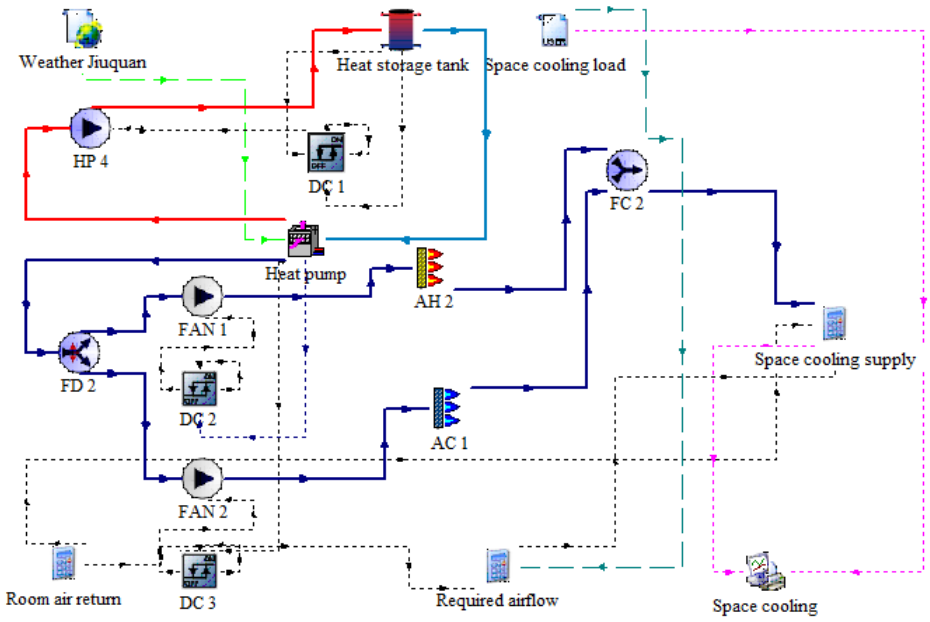

Figure 30: Control strategy of space cooling load demand.

Figure 30 is illustrating the proposed control strategy for space cooling. As pointed out in section 4.1, the system is in its early development stage, and a possible solution for the supplement of air cooling to the buildings is investigated. The solution has only been evaluated theoretically in TRNSYS. The primary purpose is not to consider a fully developed practical solution. There are practical challenges with the solution, including how pipes and the ventilation system itself should be implemented. In addition, the relative humidity or the air has not been considered, and the challenges associated with this.

The solution should satisfy annual space cooling load demands, illustrated in *Figure 18.* For calculating the required energy needed to be removed from the building space to maintain the desired indoor temperature, the following equation is being used:

$$Q_{SC} = \dot{m}_{air} \cdot C_{p,air} \cdot (T_{rom,air} - T_{cooling,supply}) \quad (44)$$

$T_{rom,air}$ is assumed, based on recommendations specified in NS-EN 15251:20+7, Table NA.4 [95]. For buildings within Category II (Normal level of expectations. Should be used for new and rehabilitated buildings), the indoor air temperature shall be between 20-24°C during the heating season and 23-26°C outside the heating season. Based on this, an average indoor air temperature equal to 23 °C (average of mean value) is assumed. $T_{cooling,supply}$ is set to 16°C.

Figure 14 are illustrating a simplified heat pump system. As shown in *Figure 10* the outlet air should be supplied as air-cooling to the building users, required by Chinese ChiNoZEN project partners. Annual cooling load profiles are implemented in the simulation model using Type 9: *Data reader (Generic Data Files).* Type 2: *Differential Controller* has been used for regulating the outlet air flow from the heat pump. A flow diverter (FD 2) has been implemented, in addition to two fans (FAN 1 and FAN 2). FAN 1 and FAN 2 are controlled by Type 2. Controlled by Type 2, FAN 1 will operate if the air temperature is lower than $T_{cooling\ set-point}$, and the auxiliary heater (AH 2) will heat the air to the required set point temperature. FAN 2 will operate if the temperature is higher than $T_{cooling\ set-point}$, and the auxiliary cooler (AC 1) will cool the air to the required set point temperature. Because of the control strategy, the supplied air-cooling temperature will maintain a constant temperature of 16°C. $\dot{m}_{air}$ are the outlet air flow from the heat pump, divided by two, based on the air flow either being passed through FAN 1 or FAN 2.

Required airflow rates in residential buildings could be calculated according to recommendations given in NS-EN 15251: 2007 + NA: 2014, and requirements in TEK17, paragraph 13-2 *Ventilation in residential buildings.* It is assumed that the buildings are defined as low-emitting, and based on this, the fresh air supply should be 26 m^3 per hour per person when the contamination arises from personal use. When the contaminants occur from either products, materials, or installations, the fresh air supply should be a minimum of 1.2 m^3 per hour per m^2 of floor area. The calculation of required $\dot{m}_{air}$ will be assessed against the recommendation.

For each building to satisfy the recommendation, the following formula for the calculation of the required air flow rate is being used:

$$q_{tot} = nq_p + Aq_B \quad (45)$$

Where n equals the number of planed residents in the specified area, and A is equal to floor area.

5.4.3 System electricity demand and electricity-specific appliances load

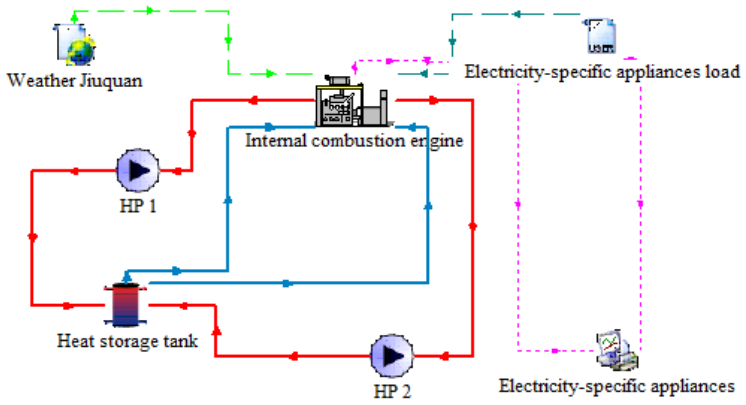

Figure 31: Control strategy for biogas ICE, required by Chinese ChiNoZEN project partners.

Figure 31 is illustrating the primary control strategy for the operation of the biogas ICE. The required control strategy for the biogas ICE from the Chinese ChiNoZEN project partners is to follow the annual load profile for electricity-specific appliances, as pointed out in *Table 9.* Based on this, the desired output power for the engine is controlled to cover the exact load profile demand for electricity-specific appliances. An annual load profile for electricity-specific appliances is implemented in the simulation model using Type 9: *Data reader (Generic Data Files).* The optimal control strategy for the biogas ICE, based on the produced electricity from wind energy and solar energy, will be evaluated in section 6.2.

The system is also supposed to cover the electricity demand for electrical system components, summarized in *Table 7.* As pointed out, wind power and solar energy are unlimited renewable energy sources, while biomass is a limited resource. Therefore, it is desirable to maximize the production of electrical power from wind turbines and PV/T collectors. An overall control algorithm has been developed and evaluated to optimize the system's energy performance. The proposed controlled algorithm is illustrated in *Figure 32.*

The operation strategy is mainly based on the total electricity production and demand. Based on the system electricity mix by technology, summarized in *Table 7,* two parameters $\triangle E1$ and $\triangle E2$ are introduced:

- $\triangle E1 =$ PV/T electricity production + Wind turbine electricity production – Heat pump electricity demand – Auxiliary heaters/cooler electricity demand – Load demand electricity-specific appliances

- $\triangle E2 =$ PV/T electricity production + Wind turbine electricity production + Biogas ICE electricity production – Heat pump electricity demand – Auxiliary heaters/cooler electricity demand – Load demand electricity-specific appliances

The first step of the operation strategy is to evaluate if the PV/T collectors and wind turbines can cover the required system electrical power input. If $\triangle E1 > 0$, the biogas ICE will be OFF. If $\triangle E1 < 0$ biogas ICE will be turned ON.

A prerequisite for the operation strategy in the thesis is that the specific fermenter can produce the required annual biogas demand for the engine. If $\triangle E2 < 0$, meaning that the maximum biogas production in the fermenter is not sufficient to cover the annual biogas demand for the biogas ICE, electricity-saving measures should be implemented.

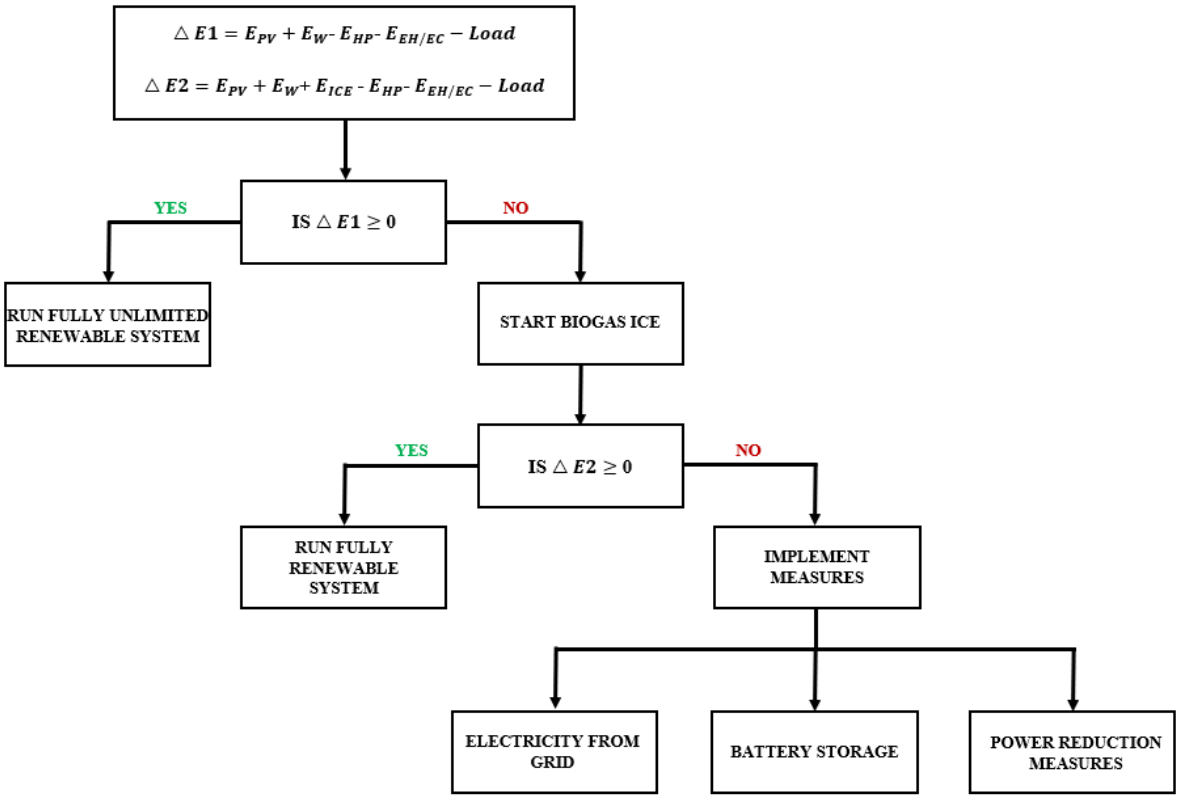

Figure 32: Proposed control strategy block diagram.

5.4.4 System components

Heat pump

Figure 33 illustrates the control strategy for the heat pump in the TRNSYS environment. The heat pump operation is being controlled by Type 2: *Differential Controller* (DC 1). Type 2 is connected to hydronic pump 4 (HP 4), which will be turned OFF if the average water temperature of the heat storage tank is above 60°C.

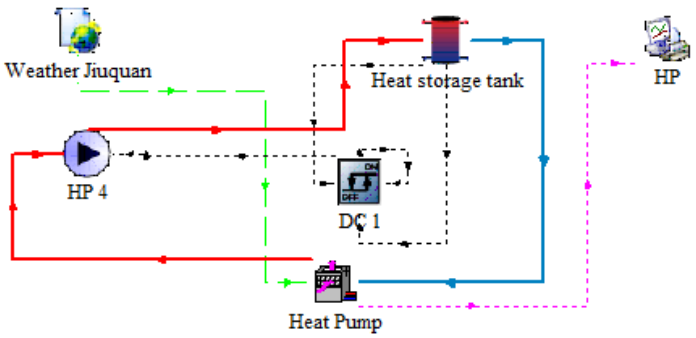

Figure 33: Control strategy for the heat pump.

Heat storage tank

The average storage tank water temperature is mainly controlled only by the water temperature of the 5 port inlet flows, as illustrated in *Figure 24.* It is not possible to specify a set-point temperature for this component in TRNSYS.

Photovoltaic thermal collector (PV/T)

Figure 34 illustrates the control strategy for the PV/T collector in the TRNSYS environment. The component will generate unlimited electricity, but the heat flow to the heat storage tank is controlled by Type 2: *Differential Controller* (DC 4). Type 2 is connected to hydronic pump 3 (HP 3), which will be turned OFF if the average water temperature of the heat storage tank is higher than the outlet water temperature of the collector. HP 3 will be turned ON when the average water temperature of the heat storage tank is lower than the outlet water temperature of the collector.

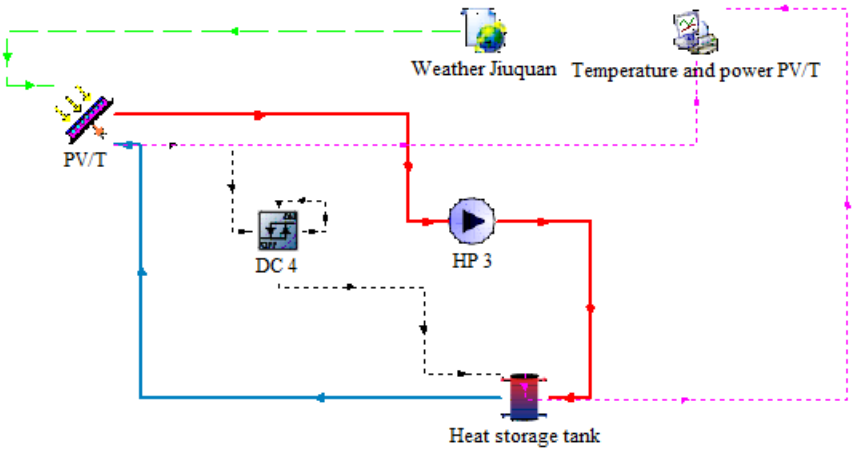

Figure 34: Control strategy for PV/T collector.

Wind turbines:

As pointed out, it is desirable to maximize the production of electrical power from the PV/T and wind turbines. Based on this, the wind turbines are operating unlimitedly through the whole year. This is within specifications elaborated in section 5.2.5, summarized in *Table 22*.

5.5 Model validation

As pointed out in [66], the TRNSYS program does not consider if the system energy balances are correct. This further leads to situations where energy easily can be "invented" or "disappear" because of mistakes in the system setup. All implemented component models are carefully examined according to the mathematical reference to the model, and an evaluation of the system heat balance has been carried out. Results presented in section 6.4, and specifically illustrated in *Figure 39*, are confirming that the overall system heat production is corresponding to the demand.

Also pointed out in [66], the user must evaluate mass balances and temperatures of the system by using output producing components like printers and online plotters. This has been performed for all relevant components and parameters connections for the system.

In addition, it has been investigated whether the results correspond to the associated data files for the components. This is performed and shown in Appendix A, *Figure 51*, and *Figure 52* for the heat pump (type 941) and in *Figure 53* for the internal combustion engine (Type 907). Appendix B, *Figure 54*, illustrates the corresponding for the wind turbine (Type 90), and *Figure 55* for the PV/T collector model.

As pointed out in section 4.3.1, the low-carbon neighbourhood and trigeneration system are fictive. It has not been possible to access experimental data for validation and comparison framework. In addition, the Chinese ChiNoZEN project partners have not been able to provide any current data for this purpose. In chapter 7, relevant results and component models are verified by comparison with prior similar studies.

6 Results

The primary purpose of the analysis was to investigate whether the CCHP system could cover the case building load demand for space heating, space cooling, DHW, and electricity-specific appliances. This is based on a multi-renewable energy supply. This chapter will therefore present the results regarding seasonal electricity and heating mix by technology. The validation of control strategies and operation strategies, in addition to the calculation of required biogas input, will further be reviewed. Finally, a simplified evaluation of environmental system impacts has been carried out. The results will be elaborated and discussed in chapter 7.

6.1 Electricity production mix by technology

This section will present the electricity production mix by technology and an evaluation of annual produced renewable energy in relation to the demand.

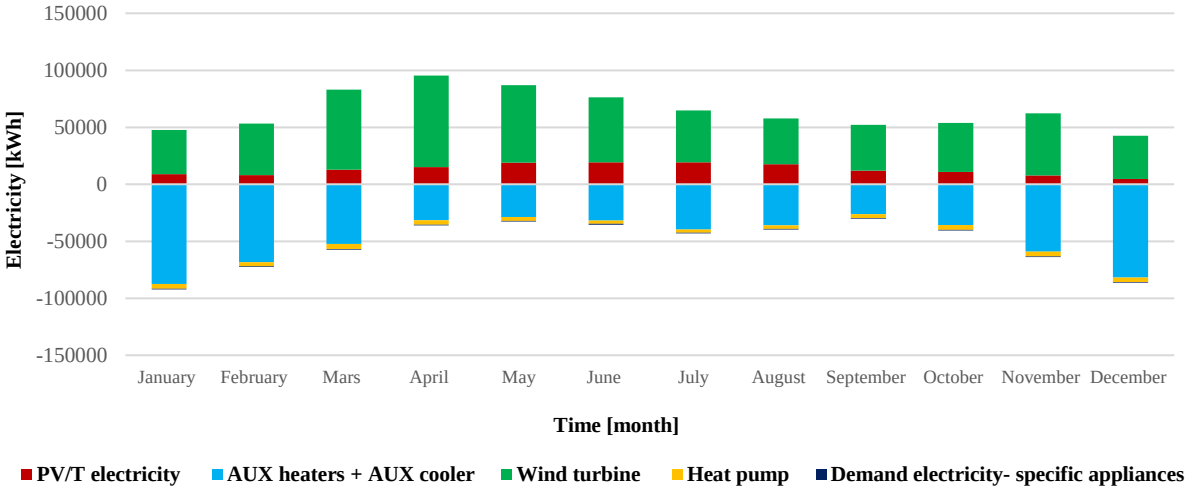

Figure 35: Seasonal electricity mix by production technology and demand. Negative values indicate demand/consumption, while positive values indicate production.

Figure 35 illustrates the seasonal electricity mix by technology. The negative values are indicating demand/consumption, while positive values are indicating production. A summary of electric system components is given in *Table 7.* In addition, the extra implemented auxiliary cooler and heaters are included (AH 1, AH 2, and AC 1 in *Figure 22)* in the figure. The implementation process regarding the auxiliary units is elaborated in section 5.4.

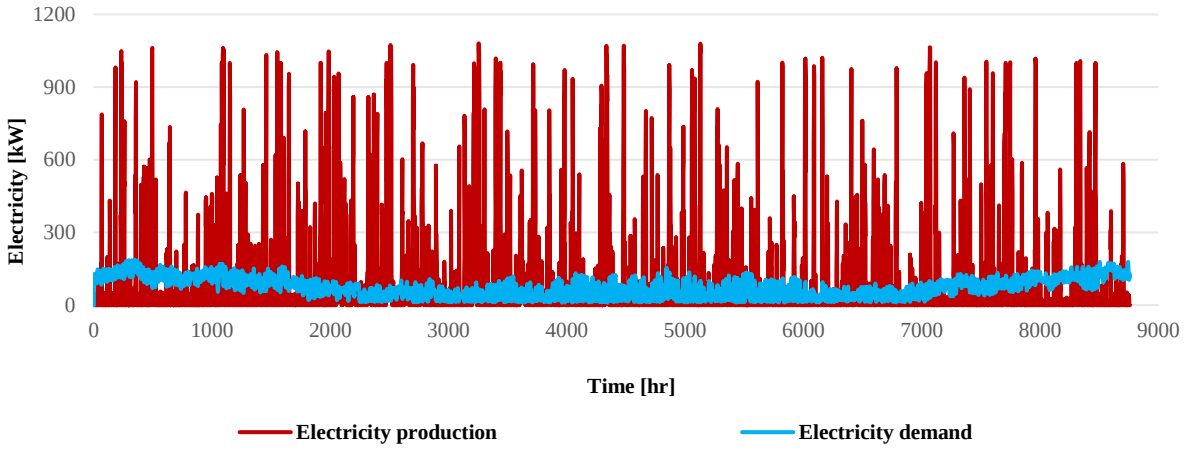

Figure 36: Hourly annual wind and solar electricity production (PV/T electricity + wind turbine) versus hourly annual electricity demand.

Figure 36 is illustrating annual electricity production and the annual electricity demand. The annual electricity production is 775.7MWh. The total annual demand is 630.5MWh. The energy production is thereby 18.7% higher than the demand. Because of daily fluctuations in both energy demand and energy production, wind energy and solar energy are still only able to cover 37.5% of the total electricity demand. 62.5% is then required to be covered by biomass energy. *Table 12* is summarizing total energy consumption and renewable energy share in total energy consumption. *Figure 37* illustrates the share in total energy consumption for the renewable energy sources.

Table 12: Summary of total energy consumption and renewable energy share.

	Energy [MWh]	**Percentage [%]**
Total energy consumption	630.5	100
Solar energy share	47.3	7.5
Wind energy share	189.1	30.0
Biomass energy share	394.1	62.5

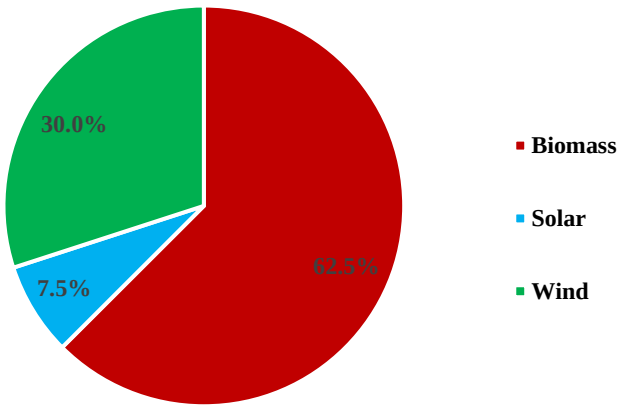

Figure 37: Renewable energy share in total energy consumption.

6.2 Evaluation of system operation strategy

This subchapter will present an evaluation of the system operation strategy based on results presented in section 6.1.

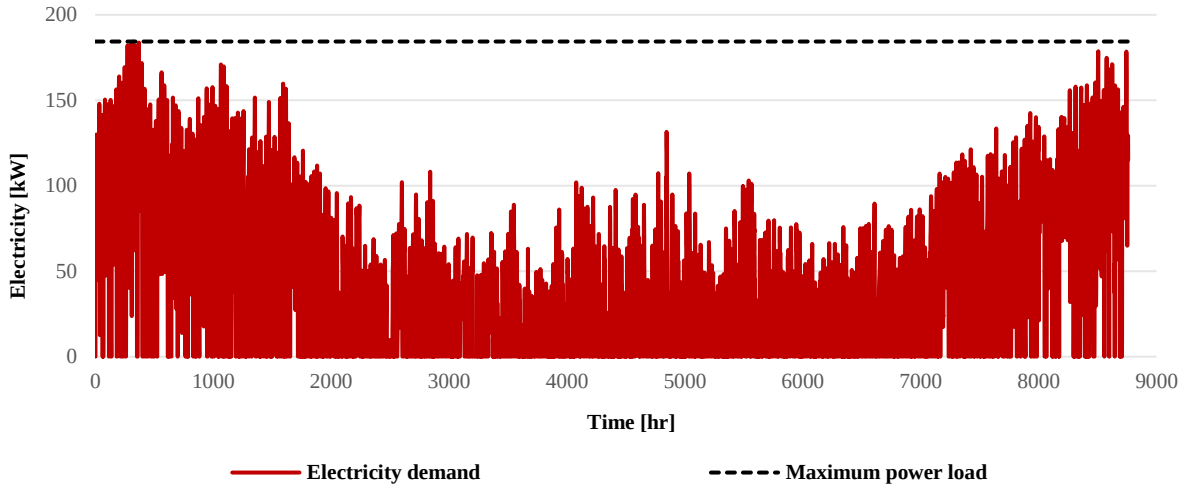

Figure 38: Required electricity production by the internal combustion engine.

Figure 38 shows the annual electricity demand required to be covered by the biogas ICE when implementing the system operation strategy introduced in section 5.4.3. This is further based on the result presented in section 6.1. The block diagram of the operation strategy is illustrated in *Figure 32*. The maximum power demand/peak load is 184 kW. Based on *Table 12*, the required annual electricity production by the biogas ICE is found to be 394.1 kWh.

Table 13 is illustrating annual peak hour demand covered by wind energy and solar energy. The biogas ICE is then required to be operating 62.5% of the annual hours.

Table 13: Summary of annual peak hours demand covered by the renewable energy sources.

	Annual hours [hr]	**Percentage [%]**
Total annual hours	8760	100
Annual peak hour demand covered by wind energy and solar energy	2748	31.4
Annual peak hour demand covered by biomass	6012	68.6

6.3 Evaluation of biogas production and consumption

As illustrated in *Figure 12* and elaborated in section 5.3, a fermenter will supply the required biogas to the biogas ICE. This section will present the results regarding the calculation of biogas production in the fermenter. All equations and parameters, with associated input data, are reviewed in section 5.3 and specified in *Table 23*.

To fully provide the required annual electricity demand, the rated capacity of the biogas ICE must be increased to 184 kW. As shown in *Table 9*, the required rated capacity of the engine from Chinese ChiNoZEN

project partners was only 1.31 kW. A simplified dynamic simulation in TRNSYS of the biogas ICE with increased capacity has been performed. This is only for establishing the required biogas consumption, and the model is not implemented in the general system configuration illustrated in *Figure 22*. Annual load profile, equal to annual electricity demand illustrated in *Figure 38*, is implemented in the simulation model using Type 9: *Data reader (Generic Data Files)*. Mass flow rates are established using the same method as in section 5.2.1 *Table 14* summarizes the annual biogas production in the fermenter and annual biogas consumption for the biogas ICE, with rated capacity.

Table 14: Annual biogas production in the fermenter and annual biogas consumption biogas ICE.

	Energy [MWh]	Based on
Annual biogas production fermenter	2788.5	Equation 41, section 5.3
Annual biogas consumption biogas ICE	1153	Isolated dynamic simulation in TRNSYS

Maximum annual biogas production is 58.7% higher than the annual biogas consumption. It is assumed that the produced biogas will be stored in a gas storage tank for later use.

If the fermenter is located on-site, as required from Chinese ChiNoZEN project partners, illustrated in *Figure 12*, a hot water mass flow rate equal to 0.10 kg/s is required from the hot water tank, equivalent to 5.5 kW heat supply. Calculations are based on Equation 22, Equation 23, and Equation 25, elaborated in section 5.3. The calculation is available in Appendix I.

6.4 Heating production mix by technology

This subchapter will present the heating mix by all system components. *Table 8* are summarizing all system heating components. In addition, the annual heat production by technology will be presented.

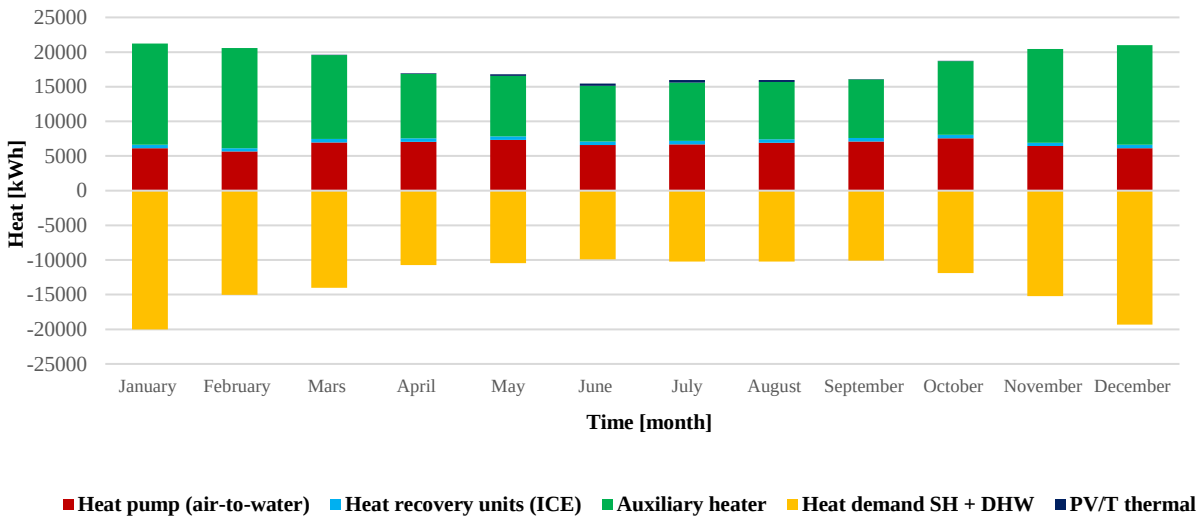

Figure 39: Seasonal system heating mix by technology and DHW + Space heating. Negative values indicate demand/consumption, while positive values indicate production.

Figure 39 illustrates the seasonal system heating mix by technology and heat demand for DHW and space heating. This is when including the auxiliary heater named AH 1 in *Figure 22.* As shown, the heat production to the system is approximately corresponding to the demand. In the analysis of heating production mix by technology, the jacket water, and oil cooler are referred to as heat transfer units (ICE).

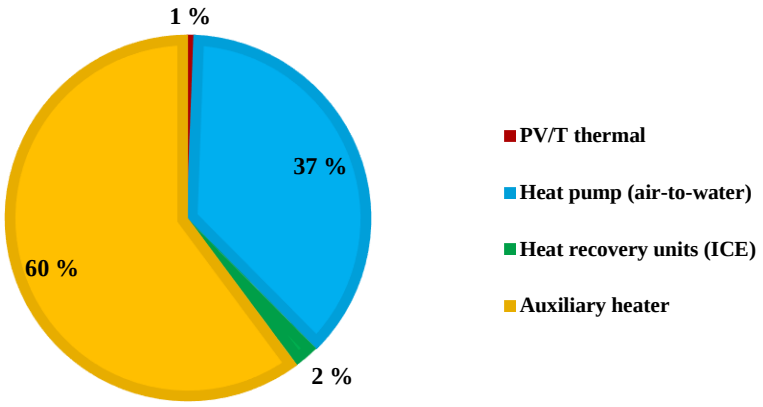

Figure 40: Heat energy share in total heat production by technology.

Figure 40 is illustrating the annual heat distribution by technology for providing DHW and Space heating demand. Heat supplied from the PV/T collector, heat recovery units (ICE), and heat pump is 40%, compared to 60% for the auxiliary heater.

6.5 Validation of control strategies

This subchapter will present the validation of implemented control system strategies. The validation confirms that the CCHP system covers the case building load demand for space heating, space cooling, DHW, and electricity-specific appliances.

6.5.1 Space heating load

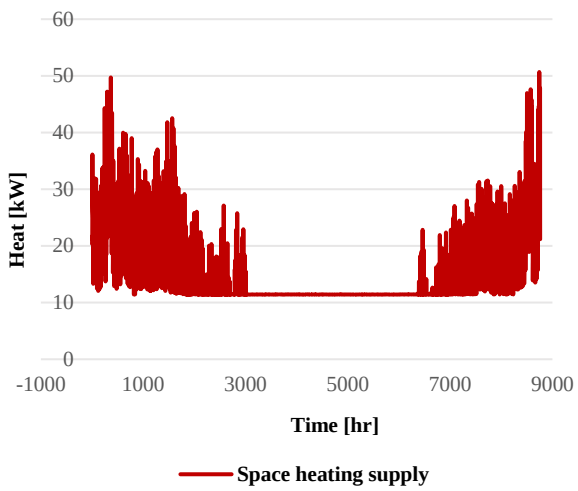

Figure 41: Space heating supply.

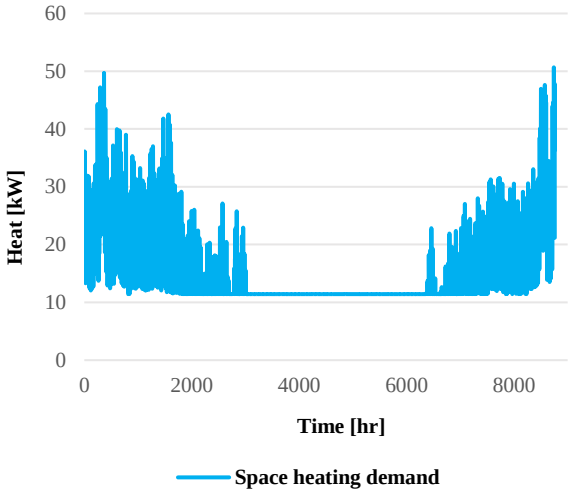

Figure 42: Space heating demand.

Figure 41 and *Figure 42* illustrate the space heating supply and space heating demand. The load profiles are equivalent, and the system is covering the specified case building load demand.

6.5.2 Space cooling load

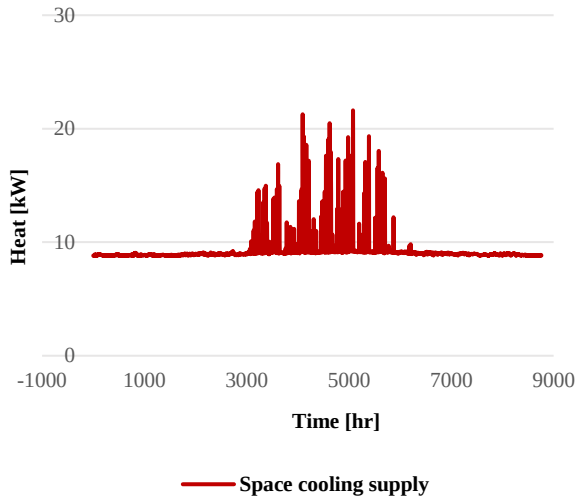

Figure 43: Space cooling supply.

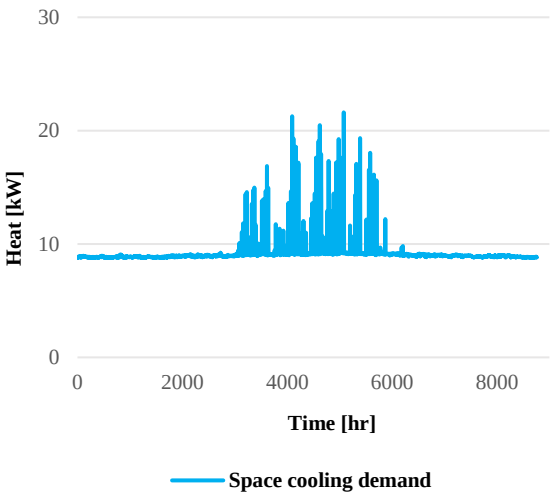

Figure 44: Space cooling demand.

Figure 43 and *Figure 44* illustrate the space cooling supply and space cooling demand. The load profiles are equivalent, and the system is covering the specified case building load demand.

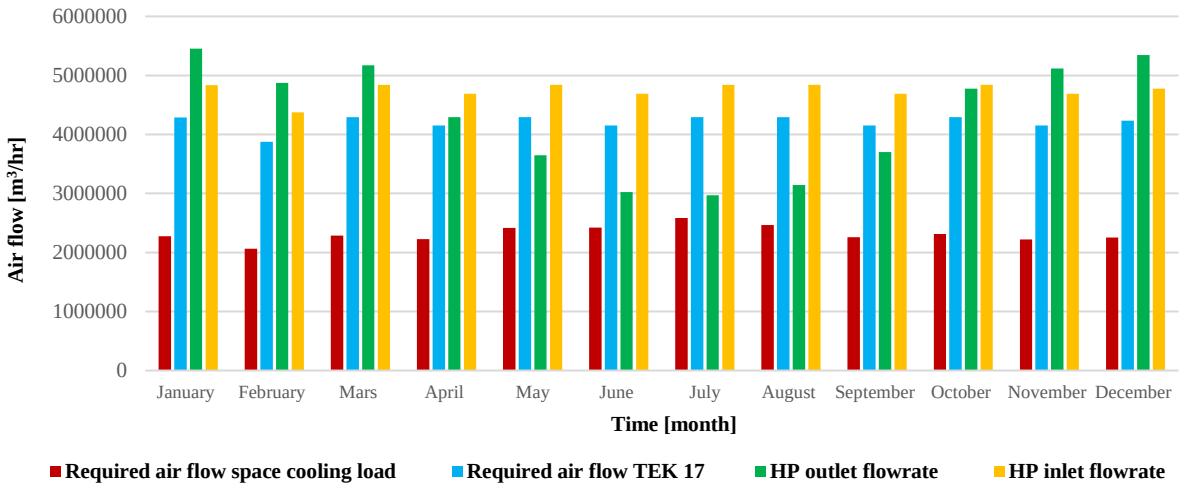

Figure 45: Airflow rates connected to control strategy for space cooling load demand.

Figure 45 illustrates the monthly required airflow rate for covering the specified case building load demand, calculated based on Equation 41. In addition, calculated required airflow based on TEK17 recommendations is illustrated. The airflow is calculated using Equation 42. Furthermore, both the outlet- and inlet airflow rates for the heat pump are illustrated.

6.5.3 Domestic hot water (DHW) load

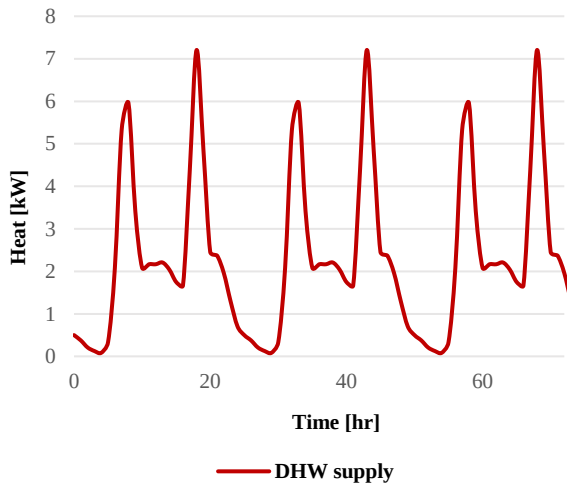

Figure 46: DHW supply.

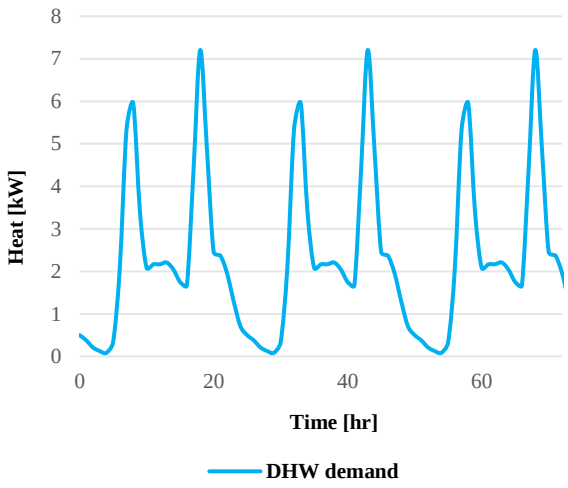

Figure 47: DHW demand.

Figure 46 and *Figure 47* are illustrating the DHW supply and DHW demand. The load profiles are equivalent, and the system is covering the specified case building load demand.

6.5.4 Electricity-specific appliances load

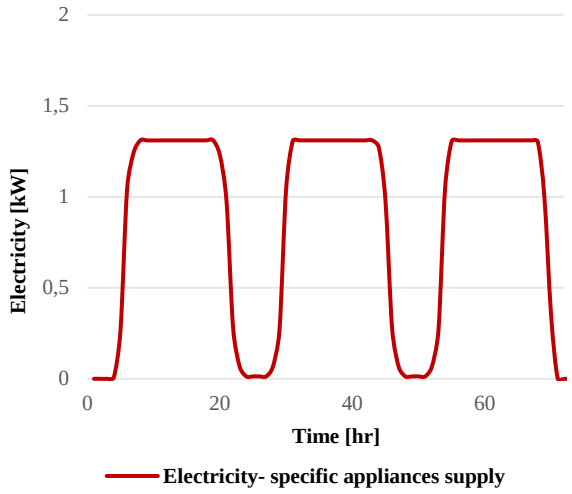

Figure 48: Electricity-specific appliances supply.

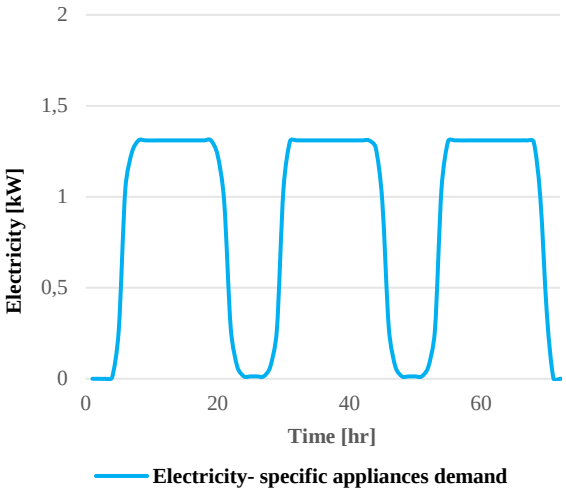

Figure 49: Electricity-specific appliances demand.

Figure 48 and *Figure 49* are illustrating the electricity-specific appliances supply and electricity-specific appliances demand. The load profiles are equivalent, and the system is covering the specified case building load demand.

6.6 Evaluation of environmental performance

The evaluation of environmental performance is based on considerations from the ZEB research center, thereby the specific CO_2 factors given in *Table 4.* For comparison, the annual CO_2 emissions are calculated for the CCHP system and for a reference system based on electricity from the grid only. The annual energy consumption for the two system scenarios is based on results presented in section 6.1 in *Table 12.*

Thereby, the following two system scenarios have been evaluated:

$$CCHP_{system,scenario} = Biogas\ ICE + Wind\ turbine + PV/T$$

$$Ref_{system,scenario} = Electricity\ from\ grid$$

Table 15: Annual energy consumption and annual CO_2 emissions for the system scenarios.

	Annual energy consumption [MWh]	**CO_2 emission factor [gCO_2/kWh]**	**Annual CO_2 emissions [$kgCO_2$/year]**
CCHP system scenario	394.1	25	9853
Reference system scenario	630.5	130	81965

The CO_2 emission is reduced by 88.0% for the CCHP system, compared to a conventional system based on electricity from the grid only.

7 Discussion

This chapter presents a discussion of obtained results and a comparison with prior similar studies. The discussion also highlights the results concerning the main research questions (RQ) introduced in section 1.2.

RQ1. *How can the CCHP system provide the space heating, space cooling, domestic hot water (DHW), and electricity-specific appliances demands, based on a multi-renewable energy supply, for the low-carbon neighbourhood?*

The system control strategy is based on the assumption that the biogas ICE is only operating when production from wind energy and solar energy are not sufficient to cover the total hourly electricity demand (system electricity demand and electricity-specific appliances demand). Wind energy and solar energy are unlimited renewable energy sources, while biomass energy is a limited resource. It is therefore desirable to maximize the production of electricity from wind turbines and PV/T collectors. In [26], the correct sizing of the power generation unit is stated as a key design variable of the CCHP system. This is based on the device determining the capacity of other parts of the system and the total supplement of electricity. The proposed system control strategy is elaborated in section 5.4.3, and the block diagram is illustrated in *Figure 38.*

The control strategy is in line with the assumption presented in [28], focusing on maximizing energy extraction from wind energy and solar energy. This research emphasized the importance of a proper control strategy to increase the share of renewable sources in total energy consumption and decrease engine operating time. In addition, this research shows promising results regarding the implementation of battery storage in wind-based systems and solar-based systems. This is outside the main scope of this thesis, but it is further elaborated in chapter 9.

Results presented in section 6.1 are showing that the annual electricity production from wind energy and solar energy is 18.7% higher than the total annual electricity demand. Nevertheless, there is a daily fluctuation in energy demand and energy production. Because of this, wind energy and solar energy are only able to cover 37.5% of the total demand. The remaining 62.5% are then required to be covered by biomass energy. For covering the required annual electricity demand, the biogas ICE is required to operate 68.6% of the annual hours. As illustrated in *Figure 37*, the renewable energy share in total energy consumption for wind energy, solar energy, and biomass energy are 30.0%, 7.5%, and 62.5%, respectively. The maximum power demand/peak load for the engine is 184kW, illustrated in *Figure 38.*

The authors in [96] have evaluated the optimal design of a hybrid system based on solar energy, wind energy, and biomass energy. The study is conducted for a village in west China. The renewable energy share in total energy consumption for wind energy, solar energy, and biomass energy is 14.2%, 51.3%, and 35.5%, respectively. In [28], the transient simulation of a hybrid system (solar energy and wind energy) showed that the share in total energy consumption of solar energy and wind energy is 63% and 80%, respectively. Based on [96] and [28], it should be considered if it is possible and appropriate to increase the share of solar energy and decrease the share of wind energy and biomass energy for the CCHP system evaluated in the thesis.

Nevertheless, in [58], the share in total energy consumption of biomass energy and solar energy for the CCHP system is 76.6% and 23.4%, respectively. This specific share shows promising results regarding the potential of reducing the emission of GHG. It is further specified that agricultural waste-based biogas could positively reduce methane emissions which otherwise would be released to the environment.

A prerequisite for the control strategy is that the specific fermenter is able to produce the required annual biogas consumption of the biogas ICE. The Chinese ChiNoZEN project partners have provided a mathematical model for the calculation of annual biogas production. It is similar to what has been proposed in [60]. The calculation performed in section 6.3 showed that the maximum annual produced biogas is 58.7% higher than the annual biogas demand, confirming that the fermenter can cover the required biogas demand for the biogas ICE. It is assumed that the produced biogas is stored in a gas storage tank, as illustrated in

Figure 12. The storage system will compensate for fluctuations in the production and consumption of the biogas.

Calculations are showing that the required heat in the fermenter is equal to 5.5 kW. This is based on the assumption that the fermenter is co-located with the CCHP system, as required by Chinese ChiNoZEN project partners, illustrated in *Figure 10.* Due to limitations elaborated in section 1.4, dynamic simulations regarding the fermenter and biogas ICE with increased maximum power demand/peak load are not implemented in this thesis. During this research, the Chinese ChiNoZEN project partners specified that the maximum rated power for the engine should be equal to 1.31 kW, as pointed out in *Table 9.*

TRNSYS has extensively been used for CCHP system simulation in [63], [53], [28] and [62]. The authors has further studied TRNSYS as simulation software in [66]. The theory from this report is elaborated in section 4.2. As pointed out in [66], the TRNSYS program itself does not consider if the system energy balances are correct. Results presented in section 6.4, specifically illustrated in *Figure 39*, confirms that the seasonal heat production mix by technology is in balance with the corresponding monthly demand/consumption. But results regarding annual distribution by technology, illustrated in *Figure 40* show that the heat contribution from the PV/T collector, heat recovery units (ICE), and heat pump is 40%, compared to 60% for the auxiliary heater. This is for providing the annual DHW and space heating demand. The seasonal electricity mix by technology, illustrated in *Figure 35*, confirms that the auxiliary heater and auxiliary cooler provide the greatest electricity demand. The results correspond to the annual space heating load and space cooling load, illustrated in *Figure 18.* The results are also affected by the temperature in the heat storage tank.

CCHP systems are often combined with an auxiliary heater. In [97], a control algorithm for a combined PV and heat pump system is investigated. An electric auxiliary heater is activated for the system when the thermal power provided by the heat pump is not sufficient to cover the required demand. The annual electricity consumption for the heat pump and the auxiliary heater is 57.4% and 12.2%, respectively. In [25], it is further pointed out that the auxiliary heater should only purchase additional fuel for increased thermal energy generation if the primary heating units are not sufficient to cover the required demand.

Several factors influence the rather high heat contribution from the auxiliary heater in the CCHP system of this thesis. The maximum capacity of the heat pump is assumed to be 12 kW, and the COP-factor is assumed to be 2 by the Chinese ChiNoZEN project partners, shown in *Table 9.* For an increased heat contribution from the heat pump, it should be considered to increase the rated heating capacity. As pointed out in Appendix A and illustrated in *Figure 51* and *Figure 52,* the heating capacity is calculated based on the inlet and outlet air and water temperatures as a fraction of the rated heating capacity for Type 941 in TRNSYS. As pointed out in section 5.2.2, the amount of data required to develop a specific user-defined data file was not available from the manufacturer. Based on this, the normalized performance data generated by TRNSYS for Type 941 is used. Based on fraction and temperature levels summarized in *Table 18,* the heat contribution increases during summer because of the increased outdoor air temperature. The opposite effect occurs during the winter period. Annual maximum capacity and minimum capacity are calculated for illustration in Appendix A, in relation to *Figure 51.*

The chosen control strategy for DHW and space heating is based on mass flow regulations implemented in TRNSYS, with some limitations. The supply temperature for DHW and space heating (referred to as port 1 outlet flow in *Figure 24)* will vary throughout the year, as illustrated in *Figure 29.* When connecting this directly to a custom equation component, the calculation of required mass flow rates does not work adequately. The auxiliary heater was implemented to ensure a constant supply temperature. It was also considered as a necessary measure to increase the set-point temperature of the auxiliary heater to 60°C, to satisfy the average water temperature for the heat storage tank, specified in *Table 9.* This is resulting in higher electricity consumption and heat contribution for the auxiliary heater.

The system configuration is further adapted to the CCHP system, shown in *Figure 12.* As pointed out in section 5.2.4, this requires that pure water supplemented for DHW is mixed with water supplement for space heating. In addition, the maximum number of input/output ports for the heat storage tank component (Type 534) is equal to 5. This is a simplification adapted to the simulation model and overall purpose with the

simulation. In addition, the cold-water temperature is 6.2°C and will reduce the average water temperature in the storage tank. A separate tank for DHW, or a separate heat exchanger in the tank, could have been implemented in practice specifically for DHW purposes.

Based on this, it is confirmed that the results are highly sensitive to the required component capacities, assumed temperature nodes, necessary measures implemented in the simulation model regarding chosen control strategy, and the configuration of the system needed. This is in line with research performed in [31], where it is pointed out that the system configuration scheme affects both the energy utilization rate and operation effect. It is further pointed out that optimizing the system configuration and equipment capacities is an essential part of the overall CCHP system research.

The result presented in section 6.4 is showing that the annual heat production for the PV/T collectors, illustrated in *Figure 50,* is increasing during the summer months as expected. During the winter months, the heat production is equal to zero because of the lack of solar radiation. Based on relevant research, it appears that the annual heat production potentially could have been higher. In [98], the PV/T collector heat output is higher than the PV/T collector electrical output. Furthermore, the results presented in [99] are more equivalent to the results shown in *Figure 50* and *Figure 55.* The authors have performed an analysis on the effects of PV/T models in CHP systems. The percentage difference between maximum electricity production and heat production for the PV/T model in [99] is 45.8%, compared to 83.8% for the PV/T model implemented in *Figure 22.* As explained in section 5.2.3, discovered limitations regarding Type 560 may explain the current result. Type 560 is best suited to simulate a single solar collector only, with input data partially adapted to this. In addition, the mass flow rate had to be assumed based on research performed in [91].

The daily heat recovery for the heat recovery units (ICE) illustrated in *Figure 53* corresponds to the daily load demand for electricity-specific appliances. It is essential to specify that this applies to the basic control strategy, elaborated in section 5.4.3, with rated engine capacity established by the Chinese ChiNoZEN project partners, shown in *Table 9.* Furthermore, the daily heat recovery corresponds to the calculated heat transfer, elaborated in section 5.2.1, shown in Equation 10 and Equation 11 for the heat recovery units (jacket water and oil cooler).

From the performed analysis, it is concluded that the CCHP system has the basic prerequisites to provide the space heating, space cooling, DHW, and electricity-specific appliances demands, based on a multi-renewable energy supply. Nevertheless, for a robust and dynamic system, some of the system components capacities and the proposed operation strategy should be further improved and optimized.

RQ2. *How are the implemented control strategies and operation strategies for the CCHP system able to meet the annual energy consumption load profiles of space heating, space cooling, domestic hot water (DHW), and electricity-specific appliances demands, for the low-carbon neighbourhood?*

Both electric and thermal demands in buildings have a high variation based on differences in climate and level of activity. It is pointed out by authors in [27] that it is challenging to match the existing requirements with the energy produced. Based on results presented in section 6.5, the implemented control strategies for space heating, DHW, and electricity-specific appliances ensure that the supplied energy is equivalent to the specific case building load demands. It is essential to point out that the Chinese ChiNoZEN project partners could not provide information regarding annual load profiles for the neighbourhood. Therefore, annual load profiles are developed based on the results from a study of an approximately equivalent reference building in [68]. It is to be expected that the annual load profiles of this study would have been equal to the case building based on building type. There is, however, uncertainty associated with the fact that this applies to one single building, not a neighbourhood. Furthermore, the building is located in Norway and not in Jiuquan, China.

Regarding the control strategy of space cooling load demand, elaborated in section 5.4.2, the outlet flow rate is sufficient to cover specified requirements during the winter months. During summer, the outlet flow rate

is insufficient because of the implemented heat pump control strategy (elaborated in section 5.4.4). Based on this, direct outdoor air (HP inlet flowrate) could be used on days when the heat pump is OFF. In the summer period (highest space cooling load demand), the outdoor air temperature is most likely to be higher than the indoor air temperature. As illustrated in *Figure 43* and *Figure 44*, by implementing current measures, the control strategy ensures that supplied energy is equivalent to space cooling load demand.

RQ3. How is the environmental performance of the CCHP system?

The evaluation of environmental impacts in section 6.6 is based on ZEB research center considerations, elaborated in section 2.8 and CO_2-factors given in *Table 4*. The calculations showed that it is possible to reduce the annual emission of CO_2 by 88.0% when the system is based on the renewable energy share in total energy consumption specified in *Figure 37*, compared with electricity from the grid only. Results presented in this section are assuming that the ICE is covering the annual demand shown in *Figure 38.* In addition, it is concluded in [57] that the gas fermentation thermochemical conversion route has lower emission of CO_2 compared to other thermochemical conversion routes, illustrated in *Figure 8.* The result is further in line with the research performed in [58]. The results obtained from the energy and environmental analysis showed that the current CCHP system is highly preferable concerning reducing GHG emissions.

8 Conclusion

In the light of the concern towards global warming and climate change, several studies have investigated alternative energy solutions. Cutting-edge renewable energy technologies, improving energy efficiency, and providing sustainable energy production and utilization, are needed to reduce greenhouse gas emissions. The combined cooling, heating, and power (CCHP) system has proven to be one of the most effective alternative energy solutions, and it could potentially contribute to the energy transition in neighbourhood level energy systems.

In light of the aforementioned challenges, the main objective of this thesis was to evaluate how a CCHP system could provide household energy demands based on a multi-renewable energy supply. The specific CCHP system configuration and its associated user parameters and equipment capacities are mainly provided by the Chinese ChiNoZEN project partners.

The system control strategy is based on the assumption that the biogas internal combustion engine (ICE) is only operating when production from wind energy and solar energy are not sufficient to cover the total hourly electricity demand. Its role is mainly to integrate wind energy and solar energy into the CCHP system and achieve a multi-renewable energy supply. Wind energy and solar energy are unlimited renewable energy sources, while biomass energy is a limited resource. Therefore, it is desirable to maximize the production of electricity from wind energy and solar energy.

The results showed that the annual electricity production from wind energy and solar energy above the required annual electricity demand is 18.7%. Nevertheless, due to hourly fluctuations in both energy demand and energy production, wind energy and solar energy are still only able to cover 37.5% of the total demand. The remaining 62.5% is then required to be covered by biomass energy, and the biogas internal combustion engine (ICE) is required to be operating 68.6% of the annual hours. The renewable energy share in total energy consumption for wind energy, solar energy, and biomass energy are 30.0%, 7.5%, and 62.5%, respectively

Evaluations of the system control strategy confirmed that the fermenter is able to cover the required biogas consumption by the biogas internal combustion engine (ICE). Maximum fermenter biogas production is 58.7% higher than the annual biogas consumption. A biogas storage tank is assumed to be incorporated in the CCHP system to balance the biogas production and consumption in the system.

The seasonal heating mix analysis showed that the monthly heat production and consumption are in match. The analysis further showed that the combined heat production of the PV/T collectors, heat transfer units (ICE), and heat pump is 40% of the total heat demand (DHW and space heating) while the remaining 60% is covered by the auxiliary heater. The results confirmed that the assumed maximum capacities of the biogas ICE and heat pump are insufficient to cover the required peak heating demand.

Several factors influence the heating contribution of the auxiliary heater. A water flow control strategy for space heating and DHW load is implemented in TRNSYS, with discovered limitations. The supply temperature for DHW and space heating varies throughout the year. When connecting this directly to a custom equation component, the calculation of required mass flow rates does not work adequately. The auxiliary heater was implemented to ensure a constant supply temperature. It is further essential to point out that the results are susceptible to component capacities, adaptions to the required system configuration, and temperature nodes set by the Chinese ChiNoZEN project partners.

It is concluded that the proposed CCHP system is able to provide the space heating, space cooling, DHW, and electricity-specific appliance demands, based on a multi-renewable energy supply. However, specific limitations are associated with the proposed ChiNoZEN CCHP system that needs to be further improved, such as system component capacities and the assumed operation strategy.

The implemented control strategies regarding space heating, DHW, and electricity-specific appliances are also validated. It was found that the total energy production and consumption are equal for the specific

building load demands. Evaluations of the proposed solution for the supplement of air cooling showed that the outlet heat pump (air-to-water) flow rate is sufficient to cover specified requirements during winter months. In summer, direct outdoor air must be used during hours when the heat pump (air-to-water) is OFF.

Evaluation of environmental impacts showed that it is possible to reduce the annual CO_2 emissions by 88.0% for the proposed CCHP system, compared with a system based on electricity from the grid only.

9 Future work

In this thesis, the impact of increasing the rated capacity of each model component on the overall system has not been investigated and needs to be studied in future work. It is desirable to limit the contribution of the auxiliary heater only to peak load hours whereby the role of the heat pump is increased to supply the bulk load

The system operation strategy and the fermenter itself were not evaluated dynamically in TRNSYS. Future work should establish the dynamic performance of the CCHP system with increased rated capacity for the biogas ICE. In addition, the fermenter should be included in the dynamic simulation. Concerning the general simplifications of the simulation model that applied in this thesis, in future work, it should be considered to implement a separate storage tank- or a heat exchanger for the DHW supply component.

The implemented control strategies are only evaluated theoretically in TRNSYS and should be evaluated with a more practical approach. There have not been any assessments performed regarding heat gains and heat losses in the specific buildings. For a realistic simulation and better results, the building itself should be part of the CCHP system model. In this regard, component models like Type 56: *Multi-Zone Building and TRNBuild* could potentially be implemented in the TRNSYS simulation model. The component models the thermal behaviour of a building divided into different thermal zones.

It is worth considering further sensitivity analysis on the various assumed solar PV/T parameters and explore its contribution for increased use of solar energy in the proposed CCHP system.

In addition, for a holistic and comprehensive assessment, it should further be considered to implement relevant key performance assessments and indicators (such as primary energy saving, overall energy efficiency, and cost) to improve the CCHP system further.

Finally, it might interest the ChiNoZEN project to further integrate battery storage into the proposed CCHP system for a more efficient integration of variable renewable energy sources (for instant wind energy and solar energy).

Bibliography

[1] The environmental status editorial office in collaboration with the Norwegian Environment Agency, “The UN's climate panel's fifth main report Climate in change - Major challenges, a diversity of solutions,” Trondheim , 2014.

[2] M. Puig-Arnavat, J. Bruno D and A. Coronas, “Modeling of trigeneration configurations based on biomass gasification and comparison of performance,” *Applied Energy*, pp. 846-856, 9 October 2013.

[3] X. Gong, F. Li, B. Sun and D. Liu, “Collabrative Optimization of Multi-Energy Complementary Combined Cooling, Heating, and Power Systems Considering Schedulable Loads,” *Energies* , 18 February 2020.

[4] International Energy Agency (IEA), “2018 Global Status Report: Towards a zero-emission, efficient and resilient buildings and construction sector,” Global Alliance for buildings and Construction (Global ABC), 2018.

[5] T. Abergel and C. Delmastro, “Tracking Buildings 2020,” 2020 .

[6] M. Höök and X. Tang, “Depletion of fossil fuels and anthropogenic climate change. A review,” *Energy Policy*, pp. 797-809, 8 November 2012.

[7] Internatonal Energy Agency (IEA), “Data and Statistics: CO2 emission statistics, CO2 emission by sector, Europe 1990-2018,” 8 September 2020. [Online]. Available: https://www.iea.org/data-and-statistics?country=WEOEUR&fuel=CO2%20emissions&indicator=CO2%20emissions%20by%20sector. [Accessed 9 September 2020].

[8] T. Kerr, “IEA Information Paper. Combined Heat & Power and Emission Trading: Options for Policy Makers,” International Energy Agency, IEA, Paris, 2008.

[9] V. Palomba, M. Prestipino and A. Galvagno, “Tri-generation for industrial applications: Development of a simulation model for a gasification-SOFC based system,” *International Journal of Hydrogen Energy* , pp. 27866-27883, 18 July 2017.

[10] Y. Huang, Y. D. Wang, S. Rezvani, D. R. McIlveen-Wright, M. Anderson and J. N. Hewitt, “Biomass fuelled trigeneration system in selected buildings,” *Energy Conversion and Management*, pp. 2448-2454, 21 February 2011.

[11] B. Su, W. Han and H. Jin, “Proposal and assessment of a novel integrated CCHP system with biogas steam reforming using solar energy,” *Applied Energy* , pp. 1-11, 2017 August 2017.

[12] B. Su, W. Han, Y. Chen, Wang, Z, W. Qu and H. Jin, “Performance optimization of a solar assisted CCHP based on biogas reforming,” *Energy Conversion and Management* , pp. 604-617, 14 June 2018.

[13] W. D. Wu and Z. R. Wang, “Combined cooling, heating and power: A review,” *Progress in Energy and Combustion Science*, pp. 459-495, 21 August 2006.

[14] J. Xu, J. Sui, B. Li and M. Yang, “Research, development and the prospect of combined cooling, heating, and power systems,” *Energy,* pp. 4361-4367, 21 June 2009.

[15] M. Liu, Y. Shi and F. Fang, “Combined cooling, heating and power systems: A survey,” *Renewable and Sustainable Energy Reviews ,* pp. 1-22, 12 April 2014.

[16] F. A. Al-Sulaiman, F. Hamdullahpur and I. Dincer, “Tringeneration: A comprehensive review based on prime movers,” *International Journal Of Energy Research,* pp. 234-258, 30 March 2010.

[17] D. Maraver, A. Sin, J. Royo and F. Sebastian, “Assessment of CCHP systems based on biomass combustion for small-scale applications through a review of the technology and analysis of energy efficiency parameters,” *Applied Energy ,* pp. 1303-1313, 4 August 2012.

[18] D. Maraver, A. Sin, F. Sebastian and J. Royo, “Environmental assessment of CCHP (combined cooling heating and power) systems based on biomass combustion in comparison to conventional generation,” *Energy ,* pp. 17-23, 9 March 2013.

[19] I. Obernberger, H. Carlsen and F. Biedermann, “State-of-the-art and future developments regarding small-scale biomass CHP systems with a special focus on ORC and Stirling Engine Technologies,” in *International Nordic Bioenergy 2003 conference,* 2003.

[20] Ø. Skreiberg and K. Lien, “Evaluations og biomass CHP technologies in a Norwegian context,” SINTEF Energiforskning AS, Trondheim, 2009.

[21] K. Darrow, R. Tidball, J. Wang and A. Hampson, “Catalog of CHP Technologies,” U.S Environmental Protection Agency Combined Heat and Power Partnership and U.S Department of Energy , 2007 .

[22] J. Deng, R. Z. Wang and G. Y. Han, “A review of thermally activated cooling technologies for combined cooling, heating and power systems,” *Progress in Energy and Combustion Science,* pp. 172-203, 1 July 2010.

[23] P. Srikhirin, S. Aphornratana and S. Chungpaibulpatana, “A review of absorption refrigeration technologies,” *Renewable and Sustainable Energy Reviews ,* pp. 343-372, 11 January 2001.

[24] K. Wang and E. Vineyard A, “New Opportunities for Solar Adsorption Refrigeration,” *The article was published in ASHRAE Journal ,* pp. 14-24, September 2011.

[25] Y. Shi, M. Liu, Fang and F, State-of-the-Art of Combined Cooling, Heating, and Power (CCHP) Systems. First Edition (Chapter 1)., John Wiley & Sons Ltd, 2017.

[26] X. Teng, X. Wang, Y. Chen and W. Shi, “A simple method to determine the optimal gas turbine capacity andoperating strategy in building cooling, heating and power system,” *Energy and Buildings ,* pp. 623-630, 9 May 2014.

[27] C. Y. Zheng, J. Y. Wu, X. Q. Zhai and R. Z. Wang, “A novel thermal storage strategy for CCHP system based on energy demands and state og storage tank,” *Electrical Power and Energy Systems ,* pp. 117-129, 1 September 2016.

[28] S. G. Sigarchian, M. Malmquist and T. Fransson, “Modeling and control strategy for a hybrid PV/Wind/Engine/Battery system to provide electricity and drinkable water for remote applications,” *2013 ISES Solar World Congress* , pp. 1401-1410, 2014.

[29] M. Li, H. Mu, N. Li and B. Ma, “Optimal design and operation strategy for integrated evaluation of CCHP (combined cooling heating and power) system.,” *Energy* , pp. 202-220, 14 February 2016.

[30] P. J. Mago and L. M. Chamra, “Analysis and optimization of CCHP systems based on energy, economical, and environmental considerations,” *Energy and Buildings* , pp. 1099-1106, 29 May 2009.

[31] A. Lu, Y. Li and H. Xia, “Study on the configuration and operation optimization of CCHP coupling multiple energy system,” *Energy Conversion and Management* , pp. 773-791, 12 October 2018.

[32] J. L. Hensen and R. Lamberts, Building performance simulation for design and operation, Abingdon, England : Spon Press, 2011.

[33] H. E. Garcia, A. Mohanty, W. Lin and R. S. Cherry, “Dynamic analysis of hybrid energy systems under flexible operation and variable renewable generation - Part 1: Dynamic performance analysis,” *Energy*, pp. 1-16, 19 March 2013.

[34] T. Hong, S. K. Chou and T. Y. Bong, “Building simulation: An overview of developments and information sources,” *Building and Environment* , pp. 347-361, 29 March 2000.

[35] P. Thornley, P. Upham, Y. Huang, S. Rezvani, J. Brammer and J. Rogers, “Integrated assessment of bioelectricity technology options,” *Energy Policy*, pp. 890-903, 6 December 2008.

[36] U. K. Mirza, N. Ahmad and T. Majeed, “An overview of biomass energy utilization in Pakistan,” *Renewable and Sustainable Energy Reviews* , pp. 1988-1996, 11 April 2007.

[37] J. Herbert and U. A. Krishnan, “Quantifying environmental performance of biomass energy,” *Renewable and Sustainable Energy Reviews*, pp. 292-308, 21 January 2016.

[38] D. Zhang, M. Bui, M. Fajardy, P. Patrizio, F. Kraxner and N. M. Dowell, “Unlocking the potential of BECCS with indigenous sources of biomass at a national stage,” *Sustainable Energy and Fuels* , 19 September 2019.

[39] M. Patel, X. Zhang and A. Kumar, “Techno-economic and life cycle assessment on lignocellulosic biomass thermochemical conversion technologies: A review,” *Renewable and Sustainable Energy Reviews* , pp. 1486-1499, 10 November 2015.

[40] H. Guan, R. Sun, W. Zhang, X. Fan, J. Jiang and B. Zhao, “Study on the application of combined cooling, heating and power system with biomass energy in China,” *AIP Conference Proceedings* , 3 August 2017.

[41] P. G. Charalambous, G. G. Maidment, S. A. Kalogirou and K. Yiakoumetti, “Photovoltaic thermal (PV/T) collectors: A review,” *Applied Thermal Engineering 27,* pp. 275-286, 11 June 2006.

[42] X. Zhu, X. Zhan, H. Liang, X. Zheng, Y. Qui, J. Lin, J. Chen, C. Meng and Y. Zhao, “The optimal design and operation strategy of renewable energy-CCHP coupled system applied in five building objects,” *Renewable Energy* , pp. 2700-2715, 2 July 2019.

[43] W. Tong, WInd Power Generation and Wind Turbine Design (Chapter 1: Fundamentals of wind energy), USA: WIT Press, 2010.

[44] G. Li, R. Zhang, T. Jiang, H. Chen, L. Bai, H. Cui and X. Li, "Optimal dispatch strategy for integrated energy systems with CCHP and wind power," *Applied Energy,* pp. 408-419, 2 September 2016.

[45] Ø. Skreiberg, "Small-scale biomass biomass CHP recommendations for Norway," KRAV project consortium (SINTEF Energy Research) , Trondheim , 2011.

[46] S. Backe and A. K. (. a. S. Kvellheim, "ZERO EMISSION NEIGHBOURHOODS. Drivers and barriers towards future development (ZEN REPORT No, 22-2020)," Norwegian University of Science and Technology (NTNU) and SINTEF Community, Trondheim , 2020.

[47] K. M. Lien, "CO2 emissions from Biofuels and District Heating in Zero Emission Buildings (ZEB)," ZEB (Research Centre On Zero Emission Buildings), Trondheim, 2013.

[48] T. H. Dokka, "Proposal for CO2-factor for electricity and outline of a full ZEB-definition," ZEB (The Research Centre On Zero Emission Buildings), Trondheim, 2011.

[49] I. Graabak and N. Feilberg, "CO2 emissions in a different scenarios of electricity generation in Europe (TR A7058)," SINTEF, Trondheim, 2011.

[50] Y. Huang, Y. D. Wang, S. Rezvani, D. R. McIlveen-Wright, M. Anderson, J. Mondol, A. Zacharopolus and N. J. Hewitt, "A techno-economic assessment of biomass fuelled trigeneration system integrated with organic Rankine cycle," *Applied Thermal Engineering,* pp. 325-331, 5 April 2012.

[51] I. Obenberger and G. Thek, "Cobustion and gasification of solid biomass for heat and power production in Europe-state-of-the-art and relevant future developments.," in *8th European conference on industrial furnaces and boilers* , Vilamoura, Portugal, 2008.

[52] M. Baratieri, P. Baggio, B. Bosio, M. Grigiante and G. Longo A, "The use of biomass syngas in IC engines and CCGT plants: A comparative analysis," *Applied Thermal Engineering* , pp. 3309-3318, 10 May 2009.

[53] M. Wegener, A. Malmquist, A. Isalgue, A. Martin, P. Arranz, O. Camara and E. Velo, "A techno-economic optimization model of a biomass-based CCHP/heat pump system under evolving climate conditions," *Energy Conversion and Management* , pp. 1-16, 2020.

[54] D. Maraver, S. Quoilin and J. Royo, "Optimization of Biomass-Fuelled Combined Cooling, Heating and Power (CCHP) Systems Integrated with Subcritical or Transcritical Organic Rankine Cycles (ORCs)," *Entropy,* pp. 2434-2453, 30 April 2014.

[55] C. C. Cornado, J. T. Yoshioka and J. L. Silveira, "Electricity, hot water and cold water production from biomass. Energetic and economical analysis of the compact system of cogeneration run with woodgas from a small downdraft gasifier," *Renewable Energy,* pp. 1861-1868, 3 January 2011.

[56] Y. Huang, D. R. Wright-McIlveen, S. H. M. J. Rezvani, Y. D. Wang, A. P. Roskilly and N. J. Hewitt, "Comparative techno-economic analysis of biomass fuelled combined heat and power for commercial buildings," *Applied Energy,* pp. 518-525, 15 April 2013.

[57] D. Griffin and M. Schultz, “Fuel and Chemical Products from Biomass Syngas: A Comparison of Gas Fermentation to Chemical Conversion Routes,” *Wiley Online Library* , pp. 219-224, 23 March 2012.

[58] W. Gazda and W. Stanek, “Energy and environmental assessment of integrated biogas trigeneration and photovoltaic plant as more sustainable industrial system,” *Applied Energy* , pp. 139-149, 17 February 2016.

[59] A. D. Ondeck, T. F. Edgar and M. Baldea, “Optimal operation of a residential district-level combined photovoltaic/natural gas power and cooling system,” *Applied Energy* , pp. 593-606, 30 July 2015.

[60] A. Mohammadi, M. H. Ahmadi, M. Bidi, F. Joda, A. Valero and S. Uson, “Exergy analysis of a Combined Cooling, Heating and Power system integrated with wind turbine and compressed air energy storage system,” *Energy Conversion and Management,* pp. 69-78, 5 November 2016.

[61] L. Ju, Z. Tan, H. Li, Q. Tan, X. Yu and X. Song, “Multi-objective operation optimization and evaluation model for CCHP and renewable energy based hybrid energy system driven by distributed energy resources in China,” *Energy,* pp. 322-340, 9 June 2016.

[62] F. Calise, G. di Vastogirardi, M. d`Accadia and M. Vicidomini, “Simulation of polygeneration systems,” *Energy,* pp. 290-337, 16 August 2018.

[63] K. J. Chua, W. M. Yang, S. S. Er and C. A. Ho, “Sustainable energy systems for a remote island community,” *Applied Energy* , pp. 1752-1763, 11 October 2013.

[64] TRNSYS Contributors: S. A. Klein et al. , *TRNSYS17 - a TRaNsient SYstem Simulation program: Manual,* Madison, United States: Thermal Energy system Specialist and University of Wisconsin-Solar Energy Laboratory et al., 2012.

[65] M. J. Duffy, M. Hiller, D. E. Bradley, W. Keilholz and J. W. Thornton, “TRNSYS - Features and functionalitity. For building simulation 2009 conference,” in *Eleventh International IBPSA Conference* , Scotland , 2009.

[66] T. Persson, O. Stavset, R. K. Ramstad, M. J. Alonso and K. Lorenz, “Software for modelling and simulation of ground source heating and cooling systems (REPORT NO: A7570),” SINTEF Energi AS and , Trondheim , 2016.

[67] J. Jinping, W. Baolong, W. Li and V. Novakovic, *Combined Cooling, Heating, Power and Biogas System with Multi-renewable Energy for Town or Agricultural Park (WP4 Key CCHP Technologies of Low Carbon Neighbouthood and Buildings with Multiple Energy Sources).,* 2020.

[68] N. Nord, Y. Ding, O. Skrautvol and S. F. Eliassen, “Energy Pathways for Future Norwegian Residential Building Areas,” *Energies* , pp. 1-19, 21 February 2021.

[69] *Norsk standard SN-NSPEK 3031:2020: Bygningers energiytelse. Beregning av energibehov og energiforsyning.,* 2020.

[70] H. N. Gupta, “Chapter 1: Introduction to Internal Combustion Engines,” in *Fundamentals of Internal Combustion Engines (Second Edition),* Sonepat, Haryana, Asoke K. Ghosh, PHI Learning Private Limited , 2013, pp. 1-50.

[71] M. Stojkov, E. Hnatko, M. Kljajin, M. Zivic and K. Hornung, "CHP and CCHP Systems Today," *Development of Power Engineering in Croatia,* 21 October 2011.

[72] K. J. Chua, C. S. K and W. M. Yang, "Advances in heat pump systems: A review," *Applied Energy ,* pp. 3611-3624, 11 June 2010.

[73] A. Hepbasli and Y. Kalinci, "A review of heat pump water heating systems," *Renewable and Sustainable Energy Reviews ,* p. 1211, 20 August 2008.

[74] J. Stene, *Lecture TEP4260: Basic thermodynamics for the heat pump process,* Trondheim, Norway : NTNU: Norwegian University of Science and Technology, 2020.

[75] *Norsk standard NS-EN 15450:2007: Varmesystemer i bygninger. Utforming av varmesystemer med varmepumpe,* 2007.

[76] R. Wei, H. Li, Y. Chen, Y. Hu, H. Long, J. Li and C. C. Wu, "Environmental Issues Related to Bioenergy," *Earth Systems and Environmental Sciences ,* 2020.

[77] D. P. Maurya and A. Singla, "An overview of key pretreatment processes for biological conversion of lignocellulosic biomass to bioethanol," *Biotech ,* pp. 597-609, 31 January 2015.

[78] G. Alva, Y. Lin and G. Fang, "An overview of thermal energy storage systems," *Energy,* pp. 341-378, 9 December 2017.

[79] R. Z. Wang, X. Yu, T. S. Ge and T. X. Li, "The present and future of residential refrigeration, power generation and energy storage," *Applied Thermal Engineering ,* pp. 256-270, 28 February 2012.

[80] *Norsk Standard NS-EN 12897:2016+A1: Water supply. Specifications for indirectly heated unvented (closed) storage water heaters.,* 2016.

[81] *Building technical regulations (TEK17) with guidance. Chapter 15: Installations and facilities (§ 15-5. Internal water installations),* 2017.

[82] F. Aguilar, D. Crespi and P. Quiles, "Experimental and numerical study of the domestic hot water production with PV panels and a heat pump," in *E3S Web of Conferences 111, 01066 (CLIMA 2019),* 2019.

[83] TESS - Thermal Energy System Specialists, LCC, "TESSLibs 17 (Component Libraries for the TRNSYS Simulation Environment): Electrical LIbrary Mathematical Reference (Volume 03)," Madison, USA, 2017.

[84] TESS - Thermal Energy Systems Specialist, LCC. , "TESSLibs 17 (Component Libraries for the TRNSYS Simulation Environment): Combined Heat and Power (CHP)/CoGeneration Library Mathematical Reference (Volume 13).," Madison, USA, 2017.

[85] J. Yuan, C. Cui, Z. Xiao, C. Zhang and W. Gang, "Performance analysis of thermal energy storage in distributed energy system under different load profiles," *Energy Conversion and Management ,* 20 February 2020.

[86] TESS - Thermal Energy Systems Specialists, LCC, “TESSLibs 17 (Component Libraries for the TRNSYS Simulation Environment): HVAC Library Mathematical Reference (Volume 06),” Madison, USA, 2017.

[87] Heat pump manufacturer supplier in China-Blueway, “Air-to-Water High Temperature Heat Pump,” 2020. [Online]. Available: https://www.blueway.hk/high-temperature-heat-pump/. [Accessed 20 April 2021].

[88] M. Pressani, N. Sommerfeld and H. Madani, “Investigation of PV/Thermal collector models for use with ground source heat pumps in transient simulations.,” in *EuroSun* , Palma de Mallorca (Spain), 2016.

[89] N. Pokorny and T. Matuska, “Glazed Photovoltaic-thermal (PVT) Collectors for Domestic HotWater Preparation in Multifamily Building.,” *Sustainability* , 28 July 2020.

[90] V. G. I. GmbH, “Solar thermal systems for warm water generation and central heating suppor,” *System Brochure Solar Systemt* , pp. 1-16, 2014.

[91] J. Lee, G. Whang and G. Lee, *Energies* , pp. 1-16, 6 August 2019.

[92] L. TESS - Thermal Energy Systems Specialist, “TESSLibs 17 (Compoent Libraries for the TRNSYS Simulation Environment): Storage Tank Library,” Madison, USA, 2017.

[93] L. TESS - Thermal Energy System Specialists, *Mathematical Reference (Volume 4). TRNSYS 17,* Madison, USA, 2017.

[94] V. W. S. A. (. f. Denmark), “Manufcaturer data type Vestas V39 500kW,” 1 January 2013. [Online]. Available: https://en.wind-turbine-models.com/turbines/383-vestas-v39. [Accessed 4 April 2021].

[95] *Norsk standard NS-EN 15251:2007+NA:2014: Inneklimaparametere for dimensjonering og vurdering av bygningers energiytelse inkludert innluftkvalitet, termisk miljø, belysning og akustikk.,* 2014.

[96] J. Li, P. Liu and Z. Li, “Optimal design and techno-economic analysis of a solar-wind-biomass off-grid hybrid power system for remote rural electrification: A case study of west China,” *Energy* , 17 July 2020.

[97] E. Psimopoulos, L. Leppin, R. Luthander and C. Bales, “Control algorithms for PV and Heat Pump system using thermal and electrical storage,” in *EuroSun 2016,* Spain , 2016.

[98] A. Abdelrazik, F. Al-Sulaiman, R. Saidur and R. Ben-Mansour, “A review on recent development for the design and packaging of hybrid photovoltaic/thermal (PV/T) solar systems,” *Contents lists available atScienceDirectRenewable and Sustainable Energy Reviews,* pp. 110-129, 8 July 2018.

[99] M. Nambat and M. Nazari, “The effects of PV/T utilization on short-term scheduling of integrated distributed CHP system,” in *Electrical power distribution conference* , 2019.

[100] A. Hashimoto and R. Hruska, “Methane from Cattle Waste: Effects of Temperature, Hydraulic Retention Time, and Influent Substrate Concentration on Kinetic Parameter (K)*,” pp. 2039-2052, 1992.

[101] Engineering ToolBox, “Fuel Gases Heating Values,” 2005. [Online]. Available: https://www.engineeringtoolbox.com/heating-values-fuel-gases-d_823.html. [Accessed 18 May 2021].

[102] K. H. Yang, Basic Finite Element Method as Applied to Injury Biomechanics. Chapter 8: Model and Transient Dynamic Analysis, Academic Press in an imprint of Elsevier , 2018.

Appendix

Appendix A – Annual heating by technology

Appendix B – Annual electricity production by technology

Appendix C – Component parameters and input data Type 907

Appendix D – Component parameters and input data Type 941

Appendix E – Component parameters and input data Type 560

Appendix F – Component parameters and input data Type 534

Appendix G – Component parameters and input data Type 90

Appendix H – Fermenter model

Appendix I – Calculation of required hot water to fermenter

Appendix A – Annual heating by technology

Photovoltaic thermal collector (PV/T):

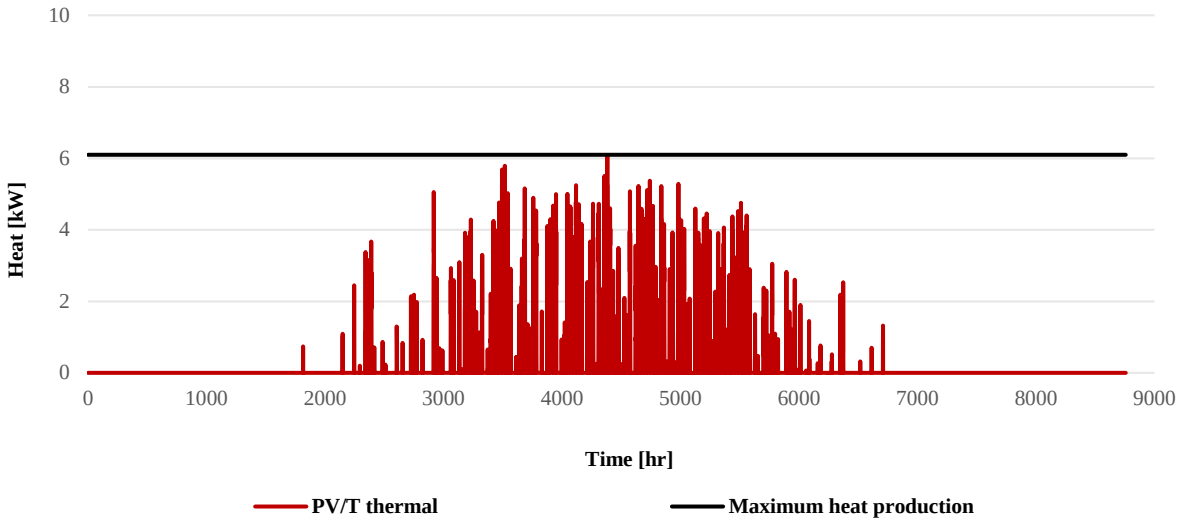

Figure 50: Annual heat production PV/T thermal.

Figure 50 are illustrating the annual heat production for the PV/T collector.

Condenser air-to-water heat pump:

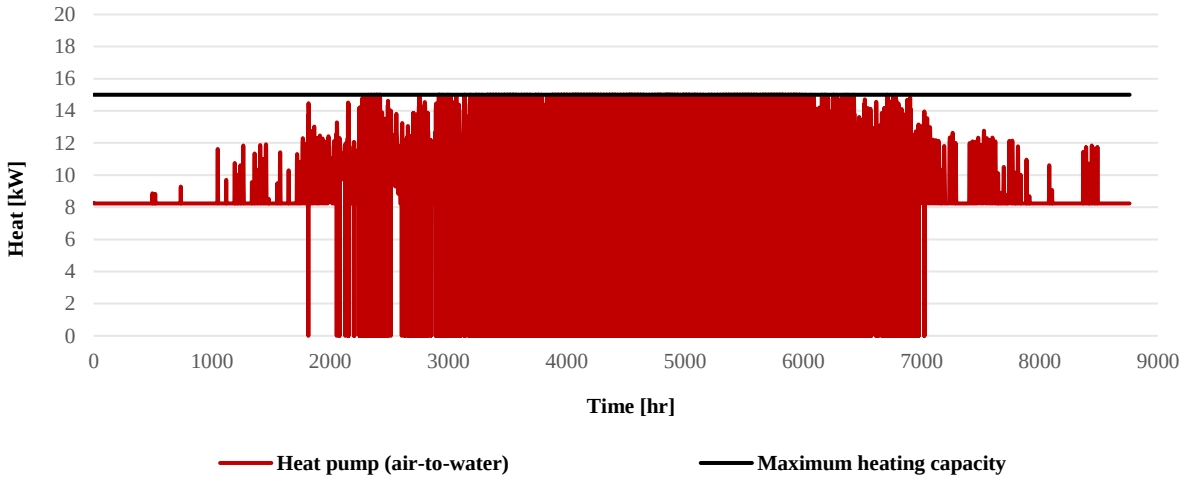

Figure 51: Annual heat production heat pump.

Figure 51 are illustrating the annual heat production for the air-to-water heat pump condenser. In addition, the maximum- and minimum heating capacity are illustrated. As pointed out in chapter 5.2.2, the heating capacity are calculated based on the inlet- water and air temperature, as a fraction of the rated heating capacity for Type 941 in TRNSYS. The maximum- and minimum heating capacity are calculated in the following

way, based on fraction and temperature levels summarized in *Table 18*, and rated heating capacity, pointed out in *Table 19*.

$$Maximum\ heating\ capacity = 1.180 \cdot 12.71kW = 15.0kW$$

$$Minimum\ heating\ capacity = 0.648 \cdot 12.71kW = 8.2kW$$

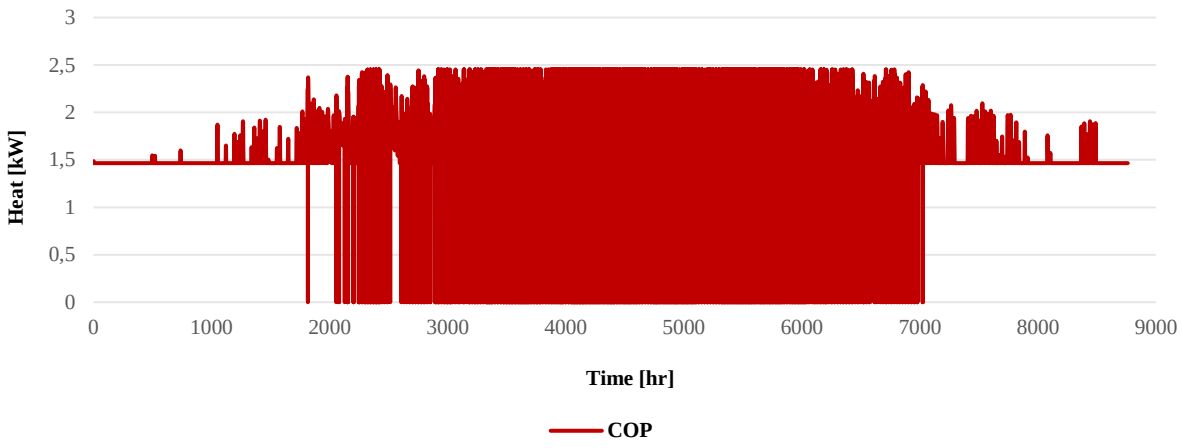

Figure 52: Annual variation of COP heat pump.

As illustrating in *Figure 52* the calculation of rated heating capacity are as expected, affecting the COP of the heat pump. Annual COP is variating between 1.47 and 2.45. Required COP from Chinese ChiNoZEN project partners is 2, as specified in *Table 9*.

Internal combustion engine:

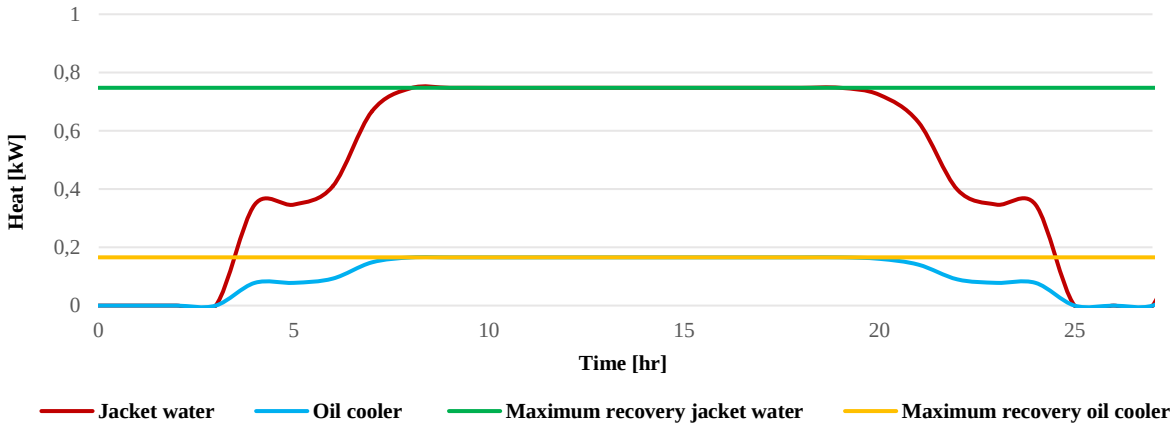

Figure 53: Daily heat recovery, jacket water, and oil cooler.

Figure 53 are illustrating the daily heat recovery for the oil cooler- and jacket water of the internal combustion engine. The heat recovery profile is equivalent for the whole year.

Appendix B – Annual electricity production by technology

Wind turbine:

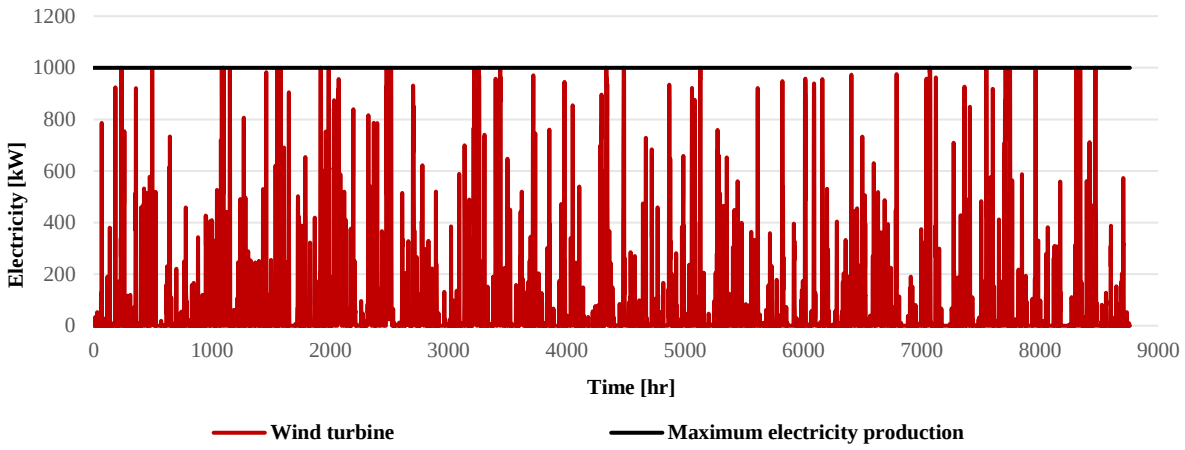

Figure 54: Annual electricity production wind turbine.

Figure 54 are illustrating annual electricity production, for the wind turbine. In addition, the maximum electricity generation are illustrated, equal to the rated power of 2000 kW for the wind turbine.

Photovoltaic thermal collector (PV/T):

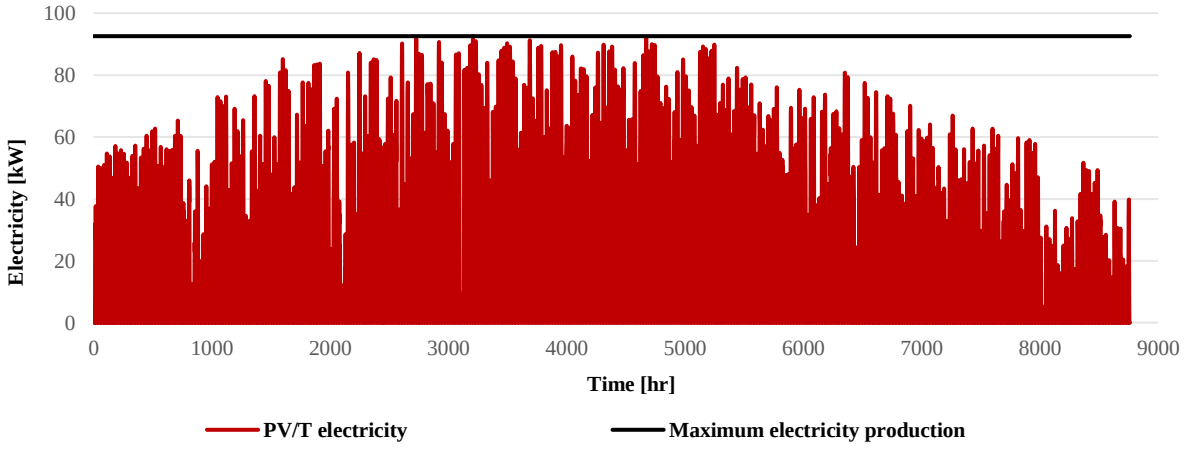

Figure 55: Annual electricity production PV/T collector.

Figure 55 are illustrating the annual electricity production for the PV/T collector. In addition, the maximum electricity production is illustrated, equal to 92.6 kW.

Appendix C – Component parameters and input data Type 907

Table 16: Mechanical- and electrical efficiencies, in addition to heat fraction rates, as a function of the part load ratio (PLR).

Part load ratio (PLR) [%]	Mechanical efficiency [%]	Electrical efficiency [%]	Heat fraction exhaust gas [%]	Heat fraction jacket water [%]	Heat fraction oil cooler [%]
100	36	94	51.4	30.7	6.8
90	37	94	51.2	31	6.9
80	37	94	51.3	31.3	7.0
70	37	94	51.7	31.4	7.0
60	36	94	52.1	31.4	7.1
50	35	93	52.6	31.4	7.1
40	34	92	53.2	31.1	7.0

Table 17: Component parameters and input data, internal combustion engine (Type 907).

Variable	Value	Based on	Comments
Parameters			
Maximum power output Blower power [kW]	1.31	User parameters, case building. See *Table 5*	Data provided by Chinese ChiNoZEN project partners [67].
Specific heat of jacket water fluid [kJ/kg·K]	4.190	Default value TRNSYS.	Water specific heat.
Specific heat of oil cooler fluid [kJ/kg·K]	4.190	Default value TRNSYS.	Water specific heat.
Specific heat of exhaust gas [kJ/kg·K]	1.007	Default value TRNSYS.	Air specific heat.
Specific heat of aftercooler fluid [kJ/kg·K]	1.007	Default value TRNSYS.	Air specific heat.
Rated exhaust air flowrate [kg/hr]	-	Default value TRNSYS	-
Input data			
Intake air temperature [°C]	-	Dry bulb temperature Jiuquan (China). See *Figure 19*	Variables linked in TRNSYS.
Desired output power [°C]	-	Equal to annual load profile, electricity-specific appliances. See *Figure 17*	Variables linked in TRNSYS.
Jacket fluid inlet temperature [°C]	75	System temperature nodes. See *Table 9*	Data provided by Chinese ChiNoZEN project partners [67].
Jacket fluid flowrate [kg/hr]	43	Mathematical reference [84]. See section 5.2.4	Calculated value, based on data provided by Chinese ChiNoZEN project partners [67].
Oil cooler fluid inlet temperature [°C]	62	System temperature nodes. See *Table 9*	Data provided by Chinese ChiNoZEN project partners [67].
Oil cooler fluid flowrate [kg/hr]	9.5	Mathematical reference in [84]. See section 5.2.4	Calculated value, based on data provided by Chinese ChiNoZEN project partners [67].

Aftercooler fluid temperature [°C]	20	Default value TRNSYS	Corresponding to average indoor air temperature.
Aftercooler fluid flowrate [kg/hr]	9.5	Mathematical reference in [84]. See section 5.2.4	Calculated value, based on data provided by Chinese ChiNoZEN project partners [67].

Appendix D – Component parameters and input data Type 941

Table 18: Fraction of rated heating and power capacity, based on different temperature levels [86].

Inlet water temperature [°C]	Inlet air temperature [°C]	Fraction of rated heating capacity [%]	Fraction of rated heating power [%]
2.2	25	0.759	0.787
7.2	25	1.080	0.868
12.2	25	1.137	0.843
15.0	25	1.233	0.843
20.0	25	1.403	0.844
2.2	30	0.737	0.860
7.2	30	1.048	0.938
12.2	30	1.106	0.923
15.0	30	1.199	0.924
20.0	30	1.359	0.924
2.2	35	0.714	0.944
7.2	35	1.017	1.044
12.2	35	1.075	1.016
15.0	35	1.165	1.017
20.0	35	1.314	1.018
2.2	40	0.692	1.027
7.20	40	0.986	1.136
12.2	40	1.043	1.108
15.0	40	1.131	1.109
20.0	40	1.269	1.112
2.2	45	0.670	1.132
7.2	45	0.955	1.255
12.2	45	1.012	1.224
15.0	45	1.097	1.226
20.0	45	1.224	1.229
2.2	50	0.648	1.249
7.2	50	0.923	1.385
12.2	50	0.981	1.352
15.0	50	1.062	1.355
20.0	50	1.180	1.359

Table 19: Component parameters and input data, air-to-water heat pump (Type 941).

Parameters / Input - Variables	Value	Based on	Comments
		Parameters	
Specific heat of liquid stream [kJ/kg·K]	4.190	Default value TRNSYS	Water specific heat
Blower power [kW]	0.85	Manufacturer data [87]	Table for heat pump specifications in [87]
Total air flowrate [m^3/hr]	6500	Manufacturer data [87]	Table for heat pump specifications in [87]

Rated heating capacity [kW]	12.71	Desired heating capacity, See *Table 9* and Manufacturer data [87]	Desired heating capacity is adapted table for heat pump specifications in [87]
Rated heating power [kW]	4.50	Desired COP factor, *Table 9* and Manufacturer data [87]	Desired COP factor is adapted table for heat pump specifications in [87]
Capacity of auxiliary [kW]	0	-	Desired heating capacity of auxiliary heater is zero
		Input data	
Inlet liquid temperature [°C]	-	Temperature at outlet-4 heat storage tank	Variables linked in TRNSYS
Inlet liquid flowrate [°C]	2253	Manufacturer data [87]	-
Inlet air temperature [°C]	-	Dry bulb temperature Jiuquan (China). See *Figure 19.*	Variables linked in TRNSYS
Inlet humidity ratio [-]	-	Humidity ratio Jiuquan (China)	Variables linked in TRNSYS
Inlet air relative humidity [%]	-	Percent relative humidity Jiuquan (China)	Variables linked in TRNSYS
Inlet air pressure [atm]	-	Atmospheric pressure Jiuquan (China)	Variables linked in TRNSYS
Inlet air pressure rise across heat pump [atm]	0	Default value TRNSYS	Not considered
Cooling control signal [-]	0	-	Cooling mode is off
Heating control signal [-]	1	-	Heating mode is on
Auxiliary signal [-]	0	-	Auxiliary heater is off
Inlet DHW temperature [°C]	20	Default value TRNSYS	-
DHW flowrate [kg/hr]	0	-	DHW flowrate is equal to zero
Desuperheater temperature – cooling mode [°C]	20	Default value TRNSYS	-
Desuperheater temperature – heating mode [°C]	20	Default value TRNSYS	-
Desuperheater UA – cooling mode [-]	0	-	Desuperheater is off
Desuperheater UA – heating mode [-]	0	-	Desuperheater is off
Compressor loss fraction [-]	0.1	Default value TRNSYS	Fraction of compressor energy lost to environment

Appendix E – Component parameters and input data Type 560

Table 20: Component parameters and input data, PV/T collector (Type 560).

Parameter / Input	Value	Based on	Comments
	Parameters		
Net collectors' length [m]	30	Desired PV/T area. See *Table 9*	Data provided by Chinese ChiNoZEN project partners [67].
Net collectors' width [m]	40	Desired PV/T area. See *Table 9*	Data provided by Chinese ChiNoZEN project partners [67].
Absorber plate thickness [m]	0.0002	Data from research project [89]	Table 1 in [89].
Thermal conductivity of absorber [kJ/m·K]	0.35	Data from research project [89]	Table 1 in [89].
Total number of tubes [-]	1000	Manufacturer data, and total collector area (ratio) [90].	Reasonable assumption. Not possible to access.
Tube diameter [m]	0.00072	Data from research project [89]	Table 1 in [89].
Bond width [m]	0.01	Default value TRNSYS	Not available data
Bond thickness [m]	0.001	Default value TRNSYS	Not available data
Bond thermal conductivity [kJ/m·K]	1386	Default value TRNSYS	Not available data
Resistance of substrate material [h·m^2·K/kJ]	0.1	Default value TRNSYS	Not available data
Resistance of back material [h·m^2·K/kJ]	3.0	Default value TRNSYS	Not available data
Fluid specific heat [kJ/kg·K]	4.19	Default value TRNSYS	Water specific heat
Reflectance [%]	0.07	Manufacturer data [90], and total collector area.	Page 13, data for *auroTHERM exclusive VTK* in [90]
Emissivity [%]	0.85	Data from research project [89]	Table 1 in [89].
1st order IAM coefficient [-]	0.1	Default value TRNSYS	Not available data
PV cell reference temperature [°C]	20	Default value TRNSYS	Not available data
PV cell reference radiation [kJ/hr·m^2]	3600	Default value TRNSYS	Not available data
PV efficiency at reference condition [%]	0.12	Default value TRNSYS	Not available data
Efficiency modifier – temperature [1/°C]	-0.005	Default value TRNSYS	Not available data
Efficiency modifier – radiation [h·m^2/kJ]	0.000025	Default value TRNSYS	Not available data

Input data			
Inlet temperature [°C]	-	Temperature at outlet-3 heat storage tank	Variables linked in TRNSYS
Inlet flowrate [°C]	-	Flowrate at outlet-3 heat storage tank	Variables linked in TRNSYS
Ambient temperature [°C]	-	Dry bulb temperature Jiuquan (China). See *Figure 19.*	Variables linked in TRNSYS
Sky temperature [°C]	-	Sky temperature Jiuquan (China)	Variables linked in TRNSYS
Back-surface environment temperature [°C]	20	Default value TRNSYS	Corresponding to average indoor air temperature.
Incident solar radiation [kJ/hr·m^2]	-	Incident solar radiation Jiuquan (China)	Variables linked in TRNSYS
Total horizontal radiation [kJ/hr·m^2]	-	Total horizontal radiation Jiuquan (China)	Variables linked in TRNSYS
Horizontal diffuse radiation [kJ/hr·m^2]	-	Horizontal diffuse radiation Jiuquan (China)	Variables linked in TRNSYS
Ground reflectance [%]	-	Ground reflectance Jiuquan (China)	Variables linked in TRNSYS
Incident angle [°]	-	Incident angle	Variables linked in TRNSYS
Collector slope [°]	-	Latitude of Jiuquan (China)	Variables linked in TRNSYS
Top loss convection coefficient [kJ/hr·m^2·K]	20	Default value TRNSYS	Not available data
Back heat loss coefficient [kJ/hr·m^2·K]	15	Default value TRNSYS	Not available data
Fluid heat transfer coefficient [-]	2000	Default value TRNSYS	Not available data

Appendix F – Component parameters and input data Type 534

Table 21: Component parameters and input data, heat storage tank (Type 534).

Parameter / Input	Value	Based on	Comments
	Parameters		
Number of tank nodes [-]	5	Required input / output ports	Based on system configuration
Number of tank ports [-]	5	Required input / output water flows	Based on system configuration
Number of immersed heat exchangers [-]	0	-	Not implemented
Number of miscellaneous heat flows [-]	0	-	Not implemented
Tank volume [l]	491	Manufacturer data [90]	Page 14. Data for type *multifunction storage allSTORE* in [90]
Tank height [m]	0.833	Manufacturer data [90]	Page 14. Data for type *multifunction storage allSTORE* in [90].
Tank fluid [-]	0	Default value TRNSYS	User provided properties
Fluid specific heat [kJ/kg·K]	4.19	Default value TRNSYS	Water specific heat
Fluid density [kg/m^3]	1000	Default value TRNSYS	Water density
Fluid thermal conductivity [W/m·K]	0.6	Default value TRNSYS	Water thermal conductivity
Fluid viscosity [kg/m·hr]	3.21	Default value TRNSYS	Viscosity of water
Fluid thermal expansion coefficient [1/K]	0.00026	Default value TRNSYS	Water thermal expansion coefficient
Top loss coefficient [kJ/hr·m^2·K]	5	Default value TRNSYS	Not available data
Edge loss coefficient for node-1 [kJ/hr·m^2·K]	5	Default value TRNSYS	Not available data
Edge loss coefficient for node-2 [kJ/hr·m^2·K]	5	Default value TRNSYS	Not available data
Edge loss coefficient for node-3 [kJ/hr·m^2·K]	5	Default value TRNSYS	Not available data
Edge loss coefficient for node-4 [kJ/hr·m^2·K]	5	Default value TRNSYS	Not available data
Edge loss coefficient for node-5 [kJ/hr·m^2·K]	5	Default value TRNSYS	Not available data
Bottom loss coefficient [kJ/hr·m^2·K]	5	Default value TRNSYS	Not available data
Additional thermal conductivity [kJ/hr·m·K]	0	Default value TRNSYS	Only conduction between fluid nodes are considered

Inlet flow mode-1 [-]	1	Default value TRNSYS	User provides locations of inlet and outlet ports
Entry node-1 [-]	1	See *Figure 24* for illustration	-
Exit node-1 [-]	5	See *Figure 24* for illustration	-
Inlet flow mode-2 [-]	1	Default value TRNSYS	User provides locations of inlet and outlet ports
Entry node-2 [-]	2	See *Figure 24* for illustration	-
Exit node-2 [-]	4	See *Figure 24* for illustration	-
Inlet flow mode-3 [-]	1	Default value TRNSYS	User provides locations of inlet and outlet ports
Entry node-3 [-]	3	See *Figure 24* for illustration	-
Exit node-3 [-]	3	See *Figure 24* for illustration	-
Inlet flow mode-4 [-]	1	Default value TRNSYS	User provides locations of inlet and outlet ports
Entry node-4 [-]	4	See *Figure 24* for illustration	-
Exit node-4 [-]	2	See *Figure 24* for illustration	-
Inlet flow mode-5 [-]	1	Default value TRNSYS	User provides locations of inlet and outlet ports
Entry node-5 [-]	5	See *Figure 24* for illustration	Not available data
Exit node-5 [-]	1	See *Figure 24* for illustration	Not available data
Flue overall loss coefficient for node-1 [kJ/hr·K]	3	Default value TRNSYS	Not available data
Flue overall loss coefficient for node-2 [kJ/hr·K]	3	Default value TRNSYS	Not available data
Flue overall loss coefficient for node-3 [kJ/hr·K]	3	Default value TRNSYS	Not available data
Flue overall loss coefficient for node-4 [kJ/hr·K]	3	Default value TRNSYS	Not available data
Flue overall loss coefficient for node-5 [kJ/hr·K]	3	Default value TRNSYS	Not available data
Input data			
Inlet temperature for port-1 [°C]	-	Jacket water outlet temperature	Variables linked in TRNSYS
Inlet flowrate for port-1 [kg/hr]	43	Jacket water flowrate	Variables linked in TRNSYS
Inlet temperature for port-2 [°C]	-	Oil cooler outlet temperature	Variables linked in TRNSYS
Inlet flowrate for port-2 [kg/hr]	9.57	Oil cooler flowrate	Variables linked in TRNSYS

Inlet temperature for port-3 [°C]	-	PV/T outlet water temperature	Variables linked in TRNSYS
Inlet flowrate for port-3 [kg/hr]	100	PV/T water flowrate (Default value in TRNSYS)	Variables linked in TRNSYS
Inlet temperature for port-4 [°C]	-	Heat pump outlet water temperature	Variables linked in TRNSYS
Inlet flowrate for port-4 [kg/hr]		Heat pump water flowrate	Variables linked in TRNSYS
Inlet temperature for port-5 [°C]	52	Return water DHW- and space heating	Variables linked in TRNSYS
Inlet flowrate for port-5 [kg/hr]	-	Load demand DWH- and space heating	Variables linked in TRNSYS
Top loss temperature [°C]	20	Default value TRNSYS	Corresponding to average indoor air temperature.
Edge loss temperature for node-1 [°C]	20	Default value TRNSYS	Corresponding to average indoor air temperature.
Edge loss temperature for node-2 [°C]	20	Default value TRNSYS	Corresponding to average indoor air temperature.
Edge loss temperature for node-3 [°C]	20	Default value TRNSYS	Corresponding to average indoor air temperature.
Edge loss temperature for node-4 [°C]	20	Default value TRNSYS	Corresponding to average indoor air temperature.
Edge loss temperature for node-5 [°C]	20	Default value TRNSYS	Corresponding to average indoor air temperature.
Bottom loss temperature [°C]	20	Default value TRNSYS	Corresponding to average indoor air temperature.
Gas flue temperature [°C]	20	Default value TRNSYS	Corresponding to average indoor air temperature.
Inversion mixing flowrate [kg/hr]	-100	Default value TRNSYS	Mixing between offending nodes
Auxiliary heat input for node-1 [kW]	0	Default value TRNSYS	Zero energy added to specific node
Auxiliary heat input for node-2 [kW]	0	Default value TRNSYS	Zero energy added to specific node
Auxiliary heat input for node-3 [kW]	0	Default value TRNSYS	Zero energy added to specific node
Auxiliary heat input for node-4 [kW]	0	Default value TRNSYS	Zero energy added to specific node
Auxiliary heat input for node-5 [kW]	0	Default value TRNSYS	Zero energy added to specific node

Appendix G – Component parameters and input data Type 90

Table 22: Component parameters and input data, wind turbine (Type 90).

Parameter / Input	Value	Based on	Comments
Parameters			
Site elevation [m]	0	Default value TRNSYS	-
Data collection height [m]	2	Reasonable assumption. Data should be collected from 2m to hub height	Not available data
Hub height [m]	53	Manufacturer data [94]	Information provided in [94]
Turbine power lost	0	Default value TRNSYS	Miscellaneous losses
Number of turbines [-]	2	Desired power generation	Customized value
Logical unit of the file containing power curve data [-]	180	Default value TRNSYS	-
Input data			
Control signal [-]	1	Default value TRNSYS	Wind turbine is on and providing power
Wind velocity [m/s]	-	Wind velocity Jiuquan (China), See *Figure 20*	Variables linked in TRNSYS
Ambient temperature [°C]	-	Dry bulb temperature Jiuquan (China). See *Figure 19.*	Variables linked in TRNSYS
Site shear exponent [-]	0.14	Default value TRNSYS	Standard profile
Barometric pressure [kPa]	101.32	Default value TRNSYS	Standard atmospheric pressure

Appendix H – Fermenter model

Table 23: Parameters, explanations, and mathematical symbols for fermenter model.

Parameter	Value	Reference / Based on	Mathematical symbol
Initial temperature of fermentation liquid [°C]	6.2	Assumed equal to T_a	$T_{f,o}$
Inlet water temperature from heat storage tank [°C]	50	Assumed equal to heat storage set-point temperature. See *Table 9*	$T_{w,in}$
Outlet water temperature from fermenter [°C]	37	Assumed equal to $T_{f,d}$	$T_{w,out}$
Outdoor average air temperature [°C]	6.2	Dry bulb temperature Jiuquan (China). See *Figure 19.*	T_a
Temperature of fermentation liquid [°C]	37	Chinese ChiNoZEN project partners [67]	$T_{f,d}$
Mass flow rate of hot water [kg/s]	0.10	Calculation. See Appendix I	$\dot{m}_{m,w}$
Mass flow rate of fresh biomass feeding [kg/s]	$1.157 \cdot 10^{-15}$	Chinese ChiNoZEN project partners [67]	$\dot{m}_{m,in}$
Mass flow rate of biogas [kg/s]	0.028	Calculation. See Equation 38	$\dot{m}_{m,g}$
Specific heat capacity of fresh water [kJ/kg·K]	4.190	Water specific heat	$C_{p,w}$
Specific heat capacity of biomass feeding [kJ/kg·K]	1.25	Chinese ChiNoZEN project partners [67]	$C_{p,d}$
Specific heat capacity of biogas [kJ/kg·K]	1.341	Chinese ChiNoZEN project partners [67]	$C_{p,g}$
Area of the top of the fermenter [m^2]	95	Calculation. See Equation 27	A_{top}
Area of the bottom of the fermenter [m^2]	95	Calculation. See Equation 27	A_{bottom}
Average heat transfer coefficient top of fermenter [$W/m^2 \cdot K$]	0.21	Calculation. See Equation 28	K_{top}
Average heat transfer coefficient bottom of fermenter [$W/m^2 \cdot K$]	0.215	Calculation. See Equation 29	K_{bottom}
Inner radius of fermenter [m]	5.5	Chinese ChiNoZEN project partners [67]	r
Heat transfer coefficient of the gas at the top of the fermenter to the fermenter wall [$W/m^2 \cdot K$]	8.7	Chinese ChiNoZEN project partners [67]	h_1
Heat transfer coefficient between the outer top surface of the insulation layer, and the environment [$W/m^2 \cdot K$]	23.2	Chinese ChiNoZEN project partners [67]	h_2
Heat transfer coefficient of the gas at the bottom of the	1800	Chinese ChiNoZEN project partners [67]	$h_{1`}$

fermenter to the fermenter wall [W/m^2·K]			
Heat transfer coefficient between the outer bottom surface of the insulation layer, and the ground [W/m^2·K]	11.6	Chinese ChiNoZEN project partners [67]	$h_{2`}$
Thickness of the polyurethane insulation layer [m]	0.016	Chinese ChiNoZEN project partners [67]	δ_1
Thickness of stainless steel on the fermenter top [m]	0.1	Chinese ChiNoZEN project partners [67]	δ_2
Thermal conductivity of stainless steel [W/m·K]	16.2	Chinese ChiNoZEN project partners [67]	λ_1
Thermal conductivity of rigid polyurethane insulation layer [W/m·K]	0.002	Chinese ChiNoZEN project partners [67]	λ_2
Height of the inside fermenter liquid [m]	11.2	Chinese ChiNoZEN project partners [67]	H_s
Heigh of inside fermenter biogas [m]	1.8	Chinese ChiNoZEN project partners [67]	H_b
Liquid fermenter volume	1032	Chinese ChiNoZEN project partners [67]	V_{Liquid}
Total fermenter volume	1200	Chinese ChiNoZEN project partners [67].	V_{Total}
Thickness of 304 stainless steel [m]	0.008	Chinese ChiNoZEN project partners [67]	$\delta_{1`}$
Heat transfer coefficient between the outside of the fermenter wall, and the environment [W/m^2·K]	32.2	Chinese ChiNoZEN project partners [67]	h_2"
Area of the biogas, in contact with tank wall [m^2]	62.2	Calculation. See Equation 31	A_{wb}
Area of the side wall of the fermenter tank. Contact with tank wall [m^2]	387	Calculation. See Equation 31	A_{ws}
Heat transfer coefficients between the inner liquid of fermenter with the sidewalls of fermenter [W/m^2·K]	0.214	Calculation. See Equation 32	K_{ws}
Heat transfer coefficients between the biogas layer in fermenter with the sidewalls of fermenter [W/m^2·K]	0.22	Calculation. See Equation 33	K_{wb}
Convective heat transfer coefficients between the inner liquid of fermenter with the sidewalls of fermenter [W/m^2·K]	1800	Chinese ChiNoZEN project partners [67]	h_s
Convective heat transfer coefficients between the biogas layer in fermenter with the sidewalls of fermenter [W/m^2·K]	8.7	Chinese ChiNoZEN project partners [67]	h_b

Density of methane [kg/m^3]	0.657	Chinese ChiNoZEN project partners [67]	ρ_{CH_4}
Mass fraction of methane in biogas [%]	0.45	Research provided by Chinese ChiNoZEN project partners [67] and [100]	x_{CH_4}
Lower heating value, biogas [MJ/kg]	11.316	Engineering ToolBox [101]	
Hydraulic retention time [/day]	4	Research provided by Chinese ChiNoZEN project partners [67] and [100]	HRT
Concentration of influent volatile solids (VS) [kg/m^3]	60	Research provided by Chinese ChiNoZEN project partners [67] and [100]	S_0
Methane production rate of the organic waste [m^3/kg·VS]	0.11	Calculation. See Equation 36	B
Limiting methane production rate of the organic waste [m^3/kg·VS]	0.33	Chinese ChiNoZEN project partners [67]	B_0
Dimensionless dynamic parameter	0.8156	Calculation. See Equation 39	K
Maximum growth rate of microorganisms [/day]	0.352	Calculation. See Equation 40	u_m
Biogas production rate [m^3/kg·VS]	1.65	Calculation. See Equation 37	Y_v

Appendix I – Calculation of required hot water to fermenter

Heat loss to the environment, $Q_{f,loss}$:

$$Q_{f,r} = A_r \cdot K_r(T_{f,d} - T_a)$$

$$Q_{f,r} = 95m^2 \cdot 0.21\frac{W}{m^2K} \cdot (37 - 6.2)K = 0.62kW$$

$$Q_{f,f} = A_f \cdot K_f(T_{f,d} - T_a)$$

$$Q_{f,f} = 95m^2 \cdot 0.215\frac{W}{m^2K} \cdot (37 - 6.2)\mathrm{K} = 0.63kW$$

$$Q_{f,w} = A_{ws}K_{ws}(T_{f,d} - T_a) + A_{wb}K_{wb}(T_{f,d} - T_a)$$

$$Q_{f,w} = 387m^2 \cdot 0.22\frac{W}{m^2K} \cdot (37 - 6.2)K + 62.2m^2 \cdot 0.214\frac{W}{m^2K} \cdot (37 - 6.2)K = 3.0kW$$

Total heat loss to the environment, $Q_{f,loss}$:

$$Q_{f,loss} = (Q_{f,r} + Q_{f,f} + Q_{f,w})$$

$$Q_{f,loss} = (0.62 + 0.63 + 3.0)kW$$

$$Q_{f,loss} = 4.3kW$$

The heat extracted by biogas (methane), $Q_{f,g}$:

$$Q_{f,g} = \dot{m}_{m,g}C_{p,g}(T_{f,d} - T_a)$$

$$Q_{f,g} = \frac{0.028kg}{s} \cdot \frac{1.341kJ}{kgK} \cdot (37 - 6.2)K$$

$$Q_{f,g} = 1.2kW$$

Heat supplied by fresh biomass feeding, $Q_{m,in}$:

$$Q_{m,in} = \dot{m}_{m,in}C_{p,d}(T_{f,o} - T_{f,d})$$

$$Q_{m,in} = 1.15 \cdot 10^{-5}\frac{kg}{s} \cdot \frac{1.25kJ}{kgK} \cdot (37 - 6.2)K$$

$$Q_{m,in} = 0.0004kW$$

Results give the following required mass flow rate [kg/s] of hot water from the heat storage tank:

$$\dot{m}_{m,w} = \frac{Q_{w,req}}{C_{p,w} \cdot (T_{w,in} - T_{w,out})}$$

$$\dot{m}_{m,w} = \frac{Q_{f,loss} + Q_{f,g} - Q_{m,in}}{C_{p,w} \cdot (T_{w,in} - T_{w,out})}$$

$$\dot{m}_{m,w} = \frac{5.5kW}{4.19kJ/kgK \cdot (50 - 37)K}$$

$$\dot{m}_{m,w} = 0.10kg/s$$

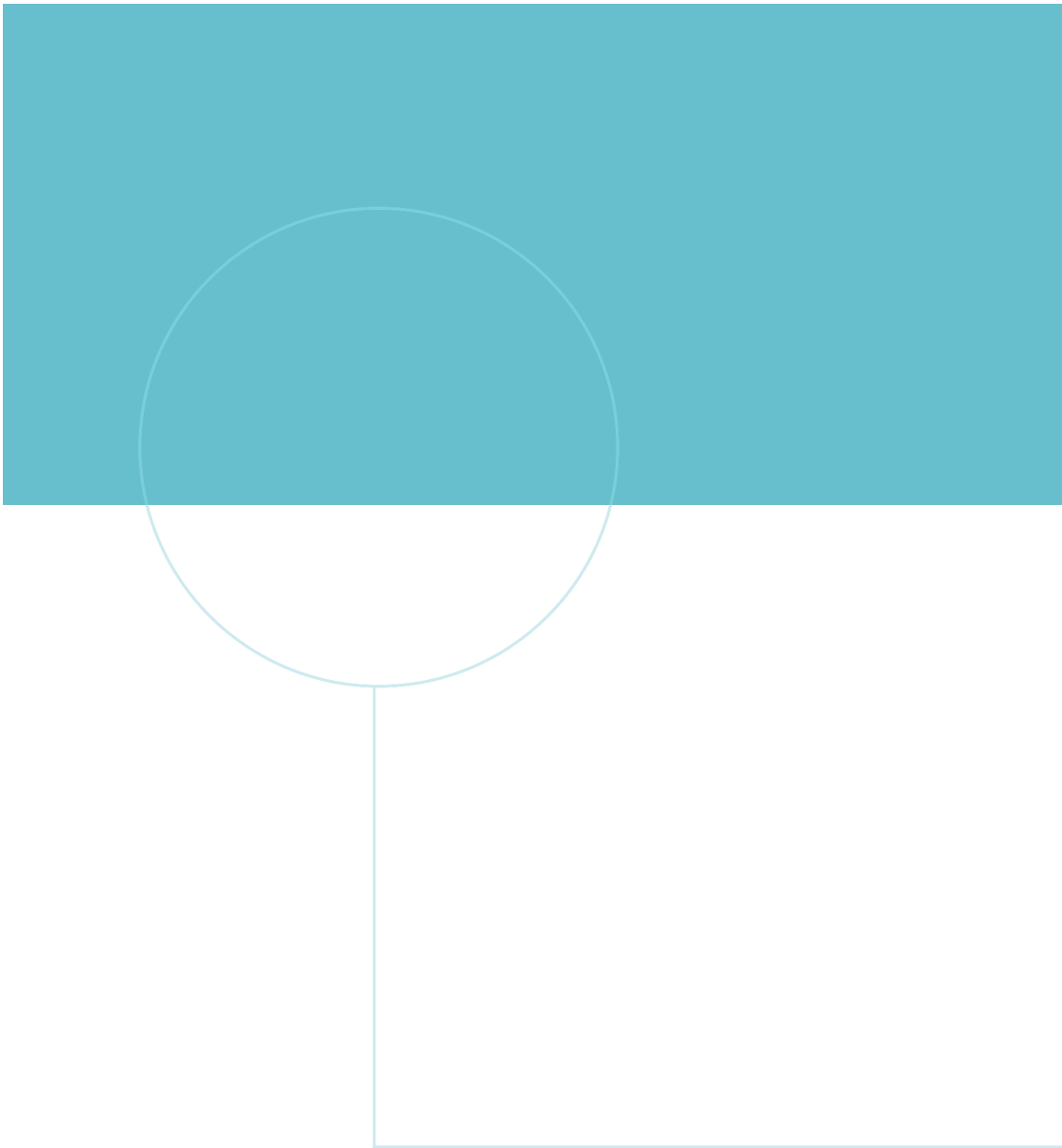

NTNU

Kunnskap for en bedre verden